Band 51

Schriftenreihe des Lehrstuhls für Wasserchemie und
der DVGW-Forschungsstelle am Engler-Bunte-Institut
des Karlsruher Instituts für Technologie (KIT)

Heterogeneous photocatalysis with titanium dioxide suspensions containing bromide and dissolved organic carbon

Luis Alberto Tercero Espinoza

Herausgeber
Fritz H. Frimmel

Karlsruhe 2010

Luis Alberto Tercero Espinoza
Heterogeneous photocatalysis with titanium dioxide suspensions containing bromide and dissolved organic carbon
Herausgeber: Fritz H. Frimmel
Band 51
Schriftenreihe des Lehrstuhls für Wasserchemie und der DVGW-Forschungsstelle am Engler-Bunte-Institut des Karlsruher Instituts für Technologie (KIT)
Karlsruhe 2010

ISSN: 1612-118X
Lehrstuhl für Wasserchemie und DVGW-Forschungsstelle
am Engler-Bunte-Institut des Karlsruher Instituts für Technologie (KIT)
Engler-Bunte-Ring 1
D-76131 Karlsruhe
Tel.: +49 (0) 721/608 2580
Fax: +49 (0) 721/699 154
E-mail: fritz.frimmel@kit.edu
http://wasserchemie.ebi.kit.edu

Heterogeneous photocatalysis with titanium dioxide suspensions containing bromide and dissolved organic carbon

zur Erlangung des akademischen Grades eines
DOKTORS DER INGENIEURWISSENSCHAFTEN (Dr.-Ing.)

der Fakultät für Chemieingenieurwesen und Verfahrenstechnik des
Karlsruher Instituts für Technologie (KIT)

genehmigte
DISSERTATION

von
Luis Alberto Tercero Espinoza, M.Sc.
aus León, Nicaragua

Referent:	Prof. Dr. rer. nat. habil. F. H. Frimmel
Korreferent:	Prof. Dr.-Ing. habil. H. Nirschl
Tag der mündlichen Prüfung:	3. Mai 2010

To my family in two continents

Acknowledgements

The work presented here was done at the Division of Water Chemistry of the Engler-Bunte-Institut at the Unviersität Karlsruhe (TH) between April 2004 and March 2009. Different people and organizations contributed to the success of this thesis:

I would like to thank my advisor, Prof. Fritz Frimmel, for giving me the opportunity to work in his research group and for his trust and encouragement. Prof. Hermann Nirschl, with whom I also had the pleasure of working, was kind enough to assume the role of second corrector.

I am also grateful to Dr. Gudrun Abbt-Braun and Dr. Birgit Gordalla for their help making things happen in spite of clever bureaucratic hurdles, and to Sylvia Heck who was always willing to lend a helping hand. I am grateful also to Dunja Haak for keeping the data safe and the computers running.

To my colleagues in the *Graduiertenkolleg*, for their support and the friendly atmosphere, I can only say thank you.

My colleagues at the EBI, past and present, also have my enduring gratitude for their professional and personal support. I would like to mention Christian Zwiener and Thomas Glauner, whose suggestions pointed me in fruitful directions. Working with Mariana Neamţu, Florencia Saravia, Eike ter Haseborg, Markus Delay, Carsten Jobelius, Ulrich Metzger Markus Ziegmann, and Heiko Schwegmann in diverse tasks related and unrelated to this thesis was a great experience. To my office mates (and they were many!): thanks for the nice atmosphere.

The results presented here would have costed a lot more pain and time were it not for the support of the technical staff. Matthias Weber was behind the many measurements with size exclusion chromatography. Axel Heidt invested numerous hours not only with trihalomethane measurements but keeping a safe working environment. Rafael Peschke and Elly Karle were responsible for the HPLC analyses and the measurement of small organic acids by ion chromatography. Domnic Bandara was perseverant in the often capricious AOX measurements. Finally, Reinhard Sembritzki performed the measurements of metal ion concentrations.

I would like to thank Marta López Furelos, Clara Arribas Matesanz, Eike Ziegler, Lei Gao, María Jesús Rubio, Raquel Malerba and Maximilian Rembor for trusting me to guide their student projects and for contributing to this thesis.

The German Research Foundation (DFG) and the German Technical and Scientific Association for Gas and Water (DVGW) provided financial support for this work. Especially, the DFG Graduate Training Program on Surface Phenomena in Aquatic Systems and Aqueous Phases (*Graduiertenkolleg* 366) was what originally attracted me to this institute and ultimately to this work.

A Travel Bursary and the Malcolm Award of the International Humic Substances Society (IHSS) allowed to me travel to Russia and present a part of the results in this thesis at the 14th Meeting of the IHSS, held in September of 2008. A travel stipend of the German Research Foundation allowed me to present a wider selection of results immediately after at the 13th International Conference on TiO_2 Photocatalysis held in San Diego, USA.

Karlsruhe, May 2010

LATE

Contents

Zusammenfassung

Die heterogene Photokatalyse mit Titandioxid (TiO_2) ist eine Methode zur Entfernung von Wasserinhaltstoffen aus unterschiedlichen Wässern. Diese Methode gehört zu den sog. *advanced oxidation processes* (AOP), deren Effektivität auf der oxidativen Wirkung von OH-Radikalen basiert. Die Bildung von OH-Radikalen und ihre schnellen Reaktionen mit fast allen organischen Belastungsstoffen stellen die Grundlage für eine effektive Oxidationsstufe in der Wasseraufbereitung dar. Ein wesentlicher Vorteil der AOPs gegenüber der Ozonung ist das höhere Oxidationspotential von OH-Radikalen. Dieses führt z.T. zu deutlich höheren Reaktionsgeschwindigkeiten. In diesem Kontext wird die heterogene Photokatalyse mit TiO_2 (immobilisiert oder in Suspension) seit mehr als 25 Jahren untersucht (Fujishima et al., 1999; Kaneko and Okura, 2002; Oppenländer, 2003).

Obwohl es bereits eine Vielzahl von Arbeiten gibt, die den Abbau von umweltrelevanten Testsubstanzen unter verschiedenen Bedingungen beschreiben, sind Studien zur Bildung von Nebenprodukten in der heterogenen Photokatalyse bisher rar (z.B. Richardson et al., 1996). Die Untersuchung der Nebenproduktbildung ist jedoch eine Vorbedingung für die Weiterentwicklung der heterogenen Photokatalyse im Bereich der Wasseraufbereitung für den menschlichen Gebrauch.

Ziel der hier beschriebenen Arbeiten war die Untersuchung der Bildung bromierter Nebenprodukte in der heterogenen Photokatalyse mit TiO_2-Suspensionen. Dies wurde über zwei Stufen verfolgt:

1. Untersuchung des photokatalytischen Abbaus von natürlicher organischer Materie, die ubiquitär in der Umwelt vorliegt und die Hauptquelle für Desinfektionsnebenprodukte (DNP) in der Chlorung und Ozonung darstellt (Zwiener, 2006); und
2. Untersuchung der Bildung von Bromat, bromierten organischen Verbindungen (als an Aktivkohle adsorbierbare organisch gebundene Halogene –AOX– quantifiziert) und Bromoform (eins der vier gesetzlich regulierten Trihalogenmethane).

Photokatalytischer Abbau natürlicher organischer Materie

Experimentelle Untersuchung des Abbaus natürlicher organischer Materie

Der photokatalytische Abbau natürlicher organischer Materie (NOM) wurde am Beispiel eines Braunwassersees (Hohlohsee, Scharzwald) untersucht. Wasser aus dem Hohlohsee als Modellsystem zu verwenden, bringt einige Vorteile mit sich:

- der See wird seit vielen Jahren untersucht, so dass auf eine gute Datenbasis zurückgegriffen werden konnte
- die Qualität des Wassers ist hervorragend für die Untersuchung natürlicher organischer Materie geeignet, denn
  - es hat eine sehr geringe Leitfähigkeit;
  - ist weitgehend frei von anthropogenen Einflüssen; und
  - es besitzt eine hohe NOM-Konzentration (als gelöster organischer Kohlenstoff –DOC– quantifiziert).

Zur Untersuchung der NOM wurde hautpsächlich die Größenausschlusschromatographie mit Detektion von gelöstem organischem Kohlenstoff (SEC-DOC) eingesetzt. In Abb. 0.1 werden Größenausschlusschromatogramme für Wasserproben aus dem Hohlohsee vor und nach der Adsorption an TiO_2 gezeigt. Die Chromatogramme zeigen die DOC-Verteilung als Funktion der Retentionszeit, t_r, in der Größenausschlusssäule; t_r ist in erster Näherung invers proportional zum Logarithmus der Molekülgröße. Für eine spätere Quantifizierung wurden drei Fraktionen operationell definiert:

F1 (28.0 min $< t_r <$ 45.8 min) — hier befinden sich vor allem hochmolekulare Substanzen des Huminstoff-Typs (Huber et al., 1994);

F2 (45.8 min $< t_r <$ 50.7 min) — dieser Bereich wird oft als "building blocks" bezeichnet (Frimmel, 1998; Huber et al., 1994);

F3 (50.7 min $< t_r <$ 56.5 min) — diese Fraktion umfasst vor allem kleine Moleküle (Huber et al., 1994; Specht and Frimmel, 2000).

Abb. 0.1 zeigt auch, dass NOM in Abhängigkeit von der Molekülgröße unterschiedlich an die TiO_2-Partikelagglomerate adsorbiert. Da die Reaktionen mit OH-Radikalen nur an oder in unmittelbarer Nähe der Oberfläche stattfinden können, lässt dieses Ergebnis einen größenselektiven Abbau erwarten. Diese Erwartung wurde in Versuchen mit simulierter solarer UV-Bestrahlung der TiO_2-Suspensionen bestätigt (Abb. 0.2). Hierbei ist ein Abbau von größeren (links) zu kleineren Molekülen (rechts)

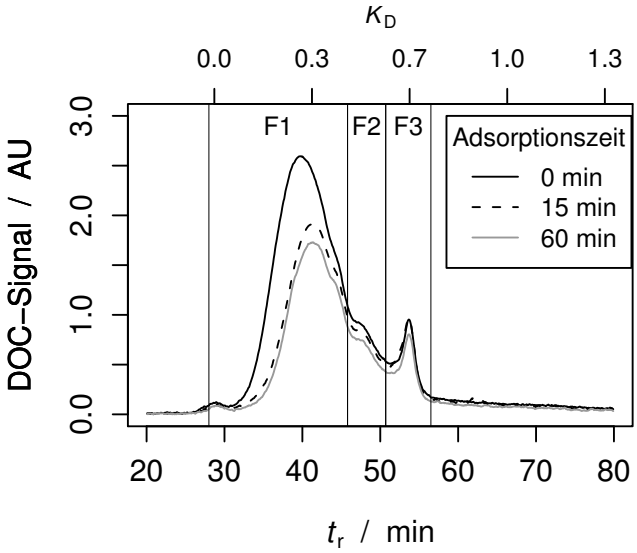

Abb. 0.1: SEC-DOC Chromatogramme von Hohlohseewasser vor und nach der Adsorption an TiO_2. Es konnte keine signifikante Änderung nach Kontaktzeiten von mehr als 60 min festgestellt werden. $\rho(TiO_2)$ = 0.5 g L^{-1}.

deutlich zu erkennen. Dieser Abbau lässt sich mit Hilfe der definierten Fraktionen quantifizieren. So nahm der DOC-Gehalt in F1 vom Beginn der Bestrahlung stetig ab. Gleichzeitig nahm der DOC-Gehalt von F2 und F3 gleichermaßen zu. Dabei blieb die Summe der drei Fraktionen in der ersten Stunde fast unverändert. Das heißt, am Anfang des Abbauprozesses ließen sich "innere" Veränderungen in den DOC-Chromatogrammen nachweisen, die mit dem Summenparameter DOC nicht zugänglich wären. Diese Ergebnisse stimmen mit denen von Wiszniowski et al. (2002), Kerc et al. (2004), Uyguner and Bekbölet (2005) und Liu et al. (2008a) überein und ergänzen sie.

Simulation des Abbaus von NOM durch OH-Radikale

Die Beobachtung einer sequentiellen Abnahme des DOCs in Abb. 0.2 muss jedoch kein Hinweis auf einen selektiven Abbau der NOM sein. Da die Moleküle in F2 und F3 sowohl abgebaut als auch aus Bruchstücken von F1 gebildet werden, während F1 nur abgebaut werden kann, ist eine sequentielle Abnahme des DOCs auch mit einem nicht-selektiven Prozess vereinbar. Es wurden z.B. ähnliche Ergebnisse für den H_2O_2/UV-Prozess beobachtet (Sarathy and Mohseni, 2007). Um dieses zu überprüfen wurden beide Prozesse –die heterogene Photokatalyse mit TiO_2 und der H_2O_2/UV-Prozess als Beispiel für einen homogenen Abbauprozess– unter Berücksichtigung einiger Annahmen simuliert.

Für die Simulation wurde vor allem die chemische Struktur der NOM erheblich vereinfacht angenommen und die Moleküle als lineare Ketten betrachtet. Es wurden

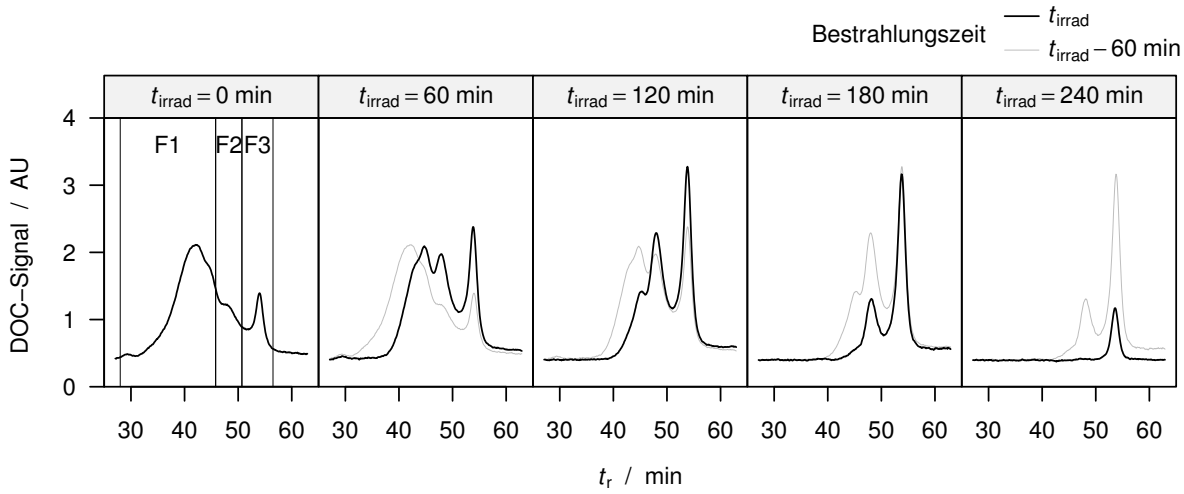

Abb. 0.2: SEC-DOC-Chromatogramme der zeitlichen Änderung von NOM ($\rho_0(\mathrm{DOC}) = 21$ mg L^{-1}) in bestrahlten TiO_2-Suspensionen. $\rho(TiO_2) = 0.5$ g L^{-1}.

des Weiteren nur Spaltungsreaktionen berücksichtigt –die als völlig unselektiv angesehen werden. Durch Auswahl eines geeigneten Reaktionsraumes konnten dann beide Prozesse simuliert werden. Im Falle des heterogenen Prozesses (Photokatalyse mit TiO_2), in dem die OH-Radikale sich nur an oder in unmittelbarer Nähe der Oberfläche befinden, wurden nur adsorbierte Moleküle in jedem Reaktionsschritt berücksichtigt. Der Anteil der adsorbierten Moleküle wurde mit Hilfe der Daten von Abb. 0.1 festgelegt. Im Falle des homogenen Prozesses (H_2O_2/UV), in dem die OH-Radikale in dem gesamten Reaktionsgefäß erzeugt werden können, wurden alle Moleküle berücksichtigt.

Die Ergebnisse der Simulation sind in Abb. 0.3 dargestellt. Hier sind insbesondere im höheren Molekülgrößenbereich Unterschiede zwischen den zwei Ansätzen zu erkennen: während im heterogenen Prozess eine schnelle und vollständige Abnahme des DOCs für das hochmolekulare Material zu verzeichnen ist, ist diese Abnahme im homogenen Prozess langsamer und unvollständig. Dies stimmt mit den experimentellen Ergebnissen gut überein (Abb. 0.2 und Sarathy and Mohseni, 2007) und zeigt den Effekt der Oberfläche (durch größenselektive Adsorption) in den heterogenen AOPs.

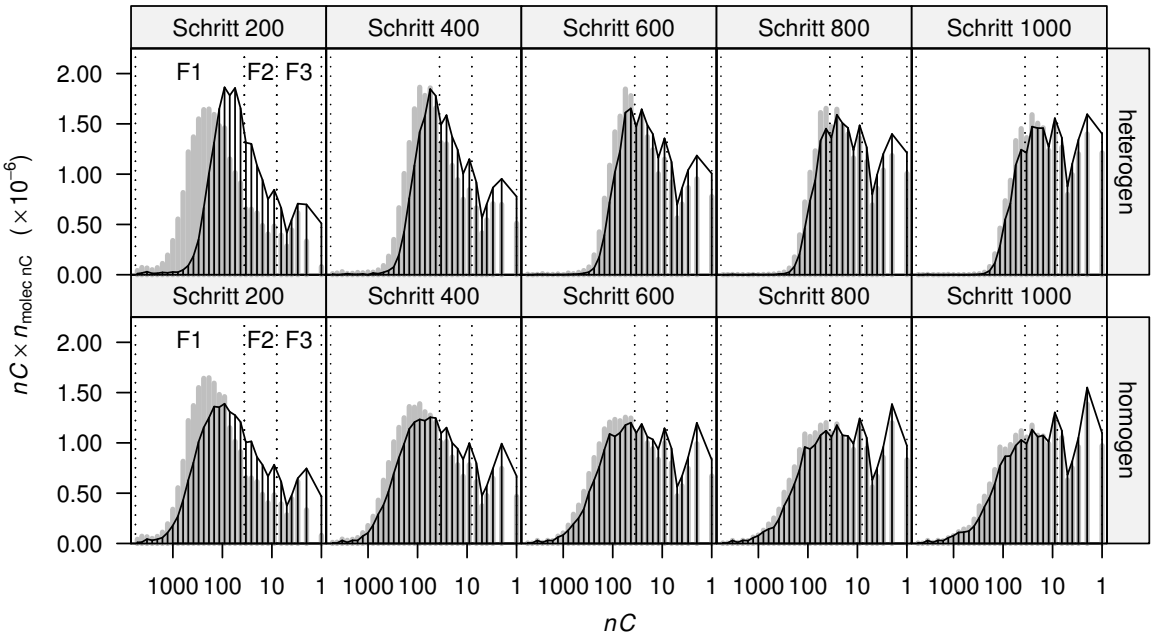

Abb. 0.3: Vergleich der simulierten heterogenen Photokatalyse mit TiO_2 (heterogen) und des H_2O_2/UV-Prozesses (homogen) unter sonst gleichen Bedingungen. $nC \times n_{molec,nC}$ ist direkt proportional zum DOC-Signal (siehe Abb. 0.2). $\sum_{nC}(n_{\text{molec},nC}) = 1 \times 10^6$ (am Anfang der Simulation); $\sum_{nC}(n_{\text{reactions},nC}) = 1 \times 10^4$ Reaktionen pro Simulationsschritt. In jeder Fläche wird das "aktuelle" Chromatogramm durch die schwarzen Linien dargestellt. Zum Vergleich ist das vorherige Chromatogramm in grau unterlegt.

Einfluss von Metallionen auf den photokatalytischen Abbau von NOM

Die Anwesenheit von Metallionen kann einen großen Einfluss auf AOPs haben (z.B. Liao et al., 2001). Es war deshalb anzunehmen, dass sich die in Abb. 0.2 und 0.3 dargestellten Veränderungen der Molekülgrößenverteilung der NOM durch die Anwesenheit von Metallionen beeinflussen lassen. Mit Hilfe der statistischen Versuchsplanung (2^4 Full Factorial Design) wurde der Einfluss von Fe^{3+}, Mn^{2+}, Cu^{2+} und Zn^{2+} auf den photokatalytischen Abbau von NOM untersucht. So konnte der Effekt aller untersuchten Metalle im Bereich von 0-10 µmol L^{-1} für jedes Metall allein und für alle Kombinationen der Metalle untersucht werden. Es stellte sich heraus, dass die Zugabe von Cu^{2+} den größten Einfluss auf den NOM-Abbauprozess ausübt. Dies ist in Abb. 0.4 für alle drei DOC-Fraktionen gezeigt.

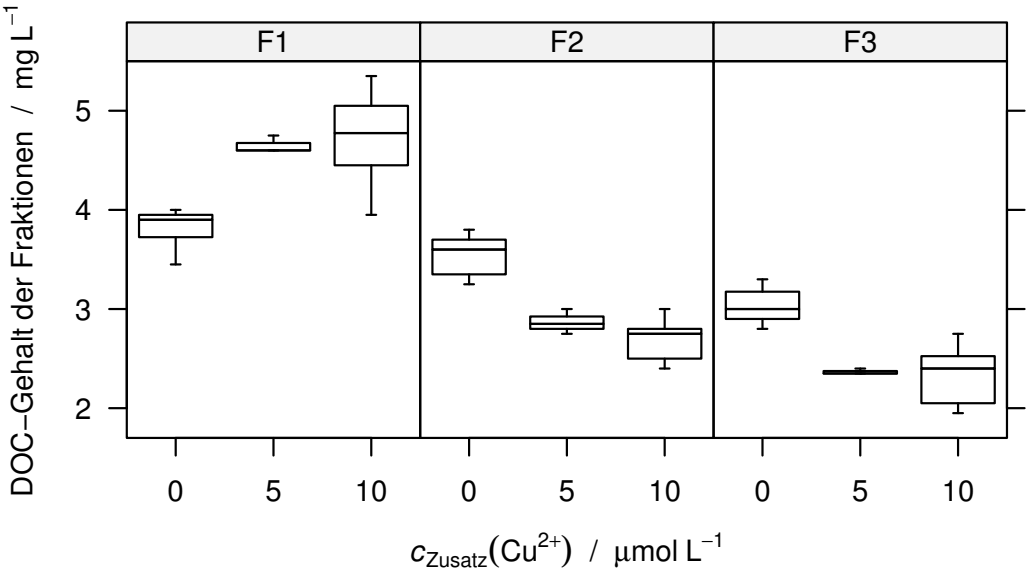

Abb. 0.4: DOC-Gehalte in F1, F2 and F3 nach $t_{\mathrm{irrad}} = 60$ min.

Für F1 ist eine Verlangsamung der Abnahme des DOC-Gehalts mit zunehmender Kupferionenkonzentration zu verzeichnen (höhere DOC-Gehalte bei steigender Zugabe von Cu^{2+}). Gleichzeitig ist eine verminderte Bildung von F2 und F3 zu beobachten. Diese Beobachtungen ergänzen einander und zeigen insgesamt eine inhibierende Rolle der Kupferionen in diesem Prozess. Die Größe des Effekts von Kupfer korreliert allerdings auch mit der gleichzeitigen Anwesenheit von Manganionen. Die Zugabe von Manganionen allein hatte jedoch keinen signifikanten Einfluss.

Bildung kleiner organischer Säuren beim Abbau von NOM

Parallel zu den "inneren" Veränderungen der Größenverteilung der NOM-Moleküle lässt sich die Bildung von kleinen organischen Säuren nachweisen. Mit Hilfe der Ionenchromatografie wurden Ameisen-, Essig-, Oxal-, Malon-, Bernstein- und Glutarsäure gemessen. Davon konnte die Konzentration von Ameisen-, Oxal-, Bernstein- und Glutarsäure quantitativ bestimmt werden. Diese Ergebnisse sind in Abb. 0.5 dargestellt. Hier ist die stetige Bildung der kleinen organischen Säuren als Resultat des Abbaus von NOM deutlich zu erkennen. Ameisen- und Oxalsäure stellen die mengenmäßig wichtigsten kleinen organischen Säuren dar. Die Bildung dieser kleinen organischen Säuren wurde durch Zugabe von Kupferionen verlangsamt.

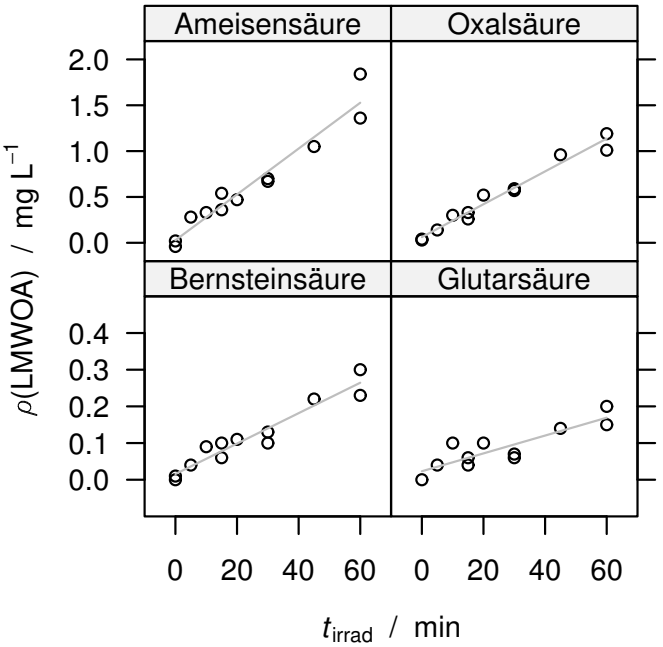

Abb. 0.5: Bildung kleiner organischer Säuren beim Abbau von NOM in mit simuliertem Sonnenlicht (UV-Bereich) bestrahlten TiO_2-Suspensionen (kein Zusatz von Metallionen).

Bildung von bromierten Nebenprodukten

Die Bildung von Bromat (BrO_3^-), bromorganischen Verbindungen (als AOX quantifiziert) und Bromoform ($CHBr_3$) wurde in einer Screening-Studie für kurze Bestrahlungszeiten ($\leq$ 45 min) untersucht. Dabei wurde die Bildung von bromorganischen Verbindungen, jedoch keine messbare Bildung weder von Bromat noch von Bromoform festgestellt. Bromoform wurde allerdings bei längeren Bestrahlungszeiten nach einer Zeitverzögerung festgestellt (Abb. 0.6).

Einflussgrößen bei der Bildung von Bromoform

Für die Bildung von Bromoform wurde eine vereinfachte Reaktionsskizze postuliert (Abb. 0.7), die auf konkurrierenden Abbauprozessen der organischen Verbindungen durch OH-Radikale mit nachfolgender Bromierung beruht. Dabei wird das Brom durch Oxidation von Bromid (Herrmann and Pichat, 1980) bereitgestellt.

Anhand dieser Skizze wurden die Konzentrationen des Photokatalysators, der Bromidionen und des gelösten organischen Kohlenstoffs als Variablen, die die Bildung von Bromoform beeinflussen könnten, identifiziert. Um dies zu überprüfen und mögliche Einflüsse quantitativ zu erfassen, wurde eine Parameterstudie mit Hilfe eines

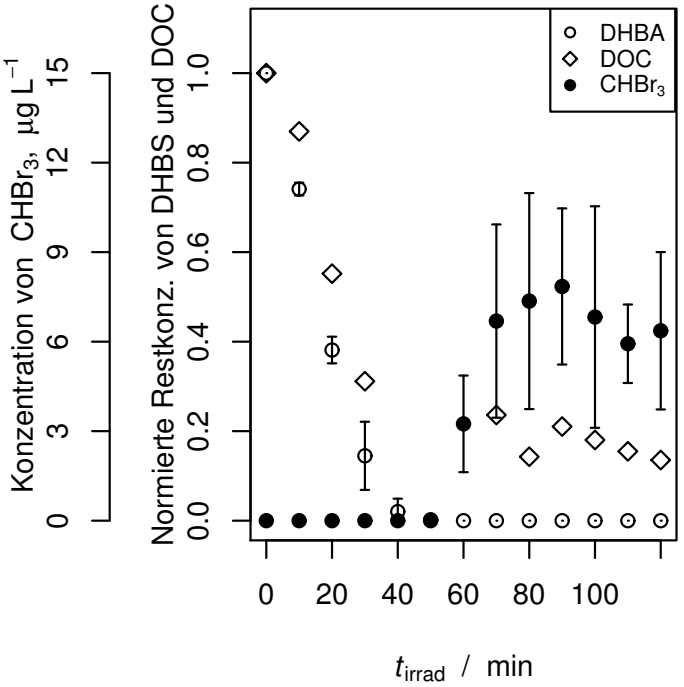

Abb. 0.6: Abbau von DHBS (10 mg L^{-1}) und Bildung von Bromoform in bestrahlten ($\lambda = 254$ nm) TiO_2-Dispersionen in Anwesenheit von $\rho_0(Br^-) = 3$ mg L^{-1} und $\rho(TiO_2) = 1$ g L^{-1}.

Box-Behnken-Designs (Box et al., 2005) durchgeführt. Dabei wurde die Bromoformkonzentration für eine Bestrahlungsdauer von 180 min gemessen.

Folgende Vergleichsgrößen wurden erfasst:

1. Der Mittelwert der drei höchsten gemessenen Bromoformkonzentrationen eines Bestrahlungsversuchs, $max_3(CHBr_3)$, und
2. die Länge der Zeitverzögerung bis zur messbaren Bromoformbildung, t_{lag}.

Die Versuchsparameter wurden in folgenden Bereichen variiert:

$$\begin{array}{rcccl} 0.5\ \text{g L}^{-1} & < & \rho(TiO_2) & < & 1.5\ \text{g L}^{-1} \\ 1\ \text{mg L}^{-1} & < & \rho(Br^-) & < & 3\ \text{mg L}^{-1} \\ 2\ \text{mg L}^{-1} & < & \rho(\text{DHBA}) & < & 10\ \text{mg L}^{-1} \end{array}$$

Die Ergebnisse der Parameterstudie sind in Abb. 0.8 zusammenfassend dargestellt. Die Werte für $max_3(CHBr_3)$ lagen im Bereich von 3-17 µg L^{-1}. In diesem Bereich konnten die Einflüsse aller drei Variablen festgestellt werden. Diese Einflüsse lassen sich wie folgt zusammenfassen:

- Je höher die TiO_2-Konzentration und die Anfangskonzentration von Bromid, desto mehr Bromoform wurde gebildet,
- je höher die DOC-Anfangskonzentration, desto weniger Bromoform wurde gebildet.

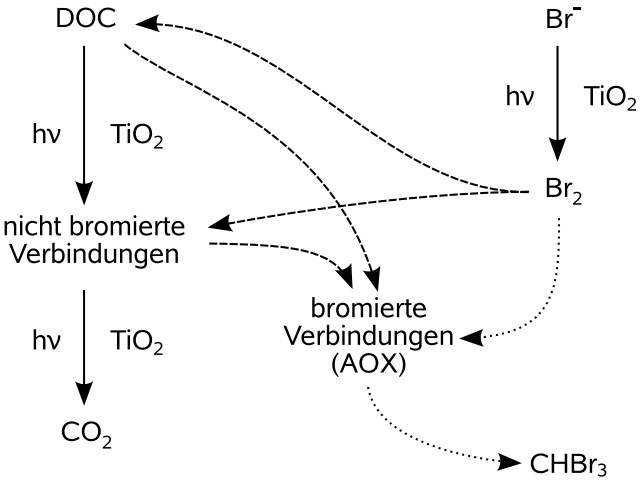

Abb. 0.7: Schematische Darstellung der postulierten Reaktionswege für die Bromoformbildung in bestrahlten TiO_2-Dispersionen.

Der Effekt einer erhöhten TiO_2-Konzentration wurde größer, je mehr Bromid in der Suspension vorhanden war (Synergismus). Im Gegensatz dazu war der Effekt einer erhöhten Bromid-Konzentration mit steigender DOC-Konzentration kleiner (Antagonismus).

Die Länge der "Lag-Phase" lag im Bereich von 10 min $< t_{\mathrm{lag}} <$ 90 min. Innerhalb dieses Bereiches konnten folgende Einflüsse als ausschlaggebend identifiziert werden:

- Je höher die TiO_2-Konzentration, desto kürzer die Lag-Phase
- je höher die DHBS-Konzentration, desto länger die Lag-Phase
- der verkürzende Effekt einer erhöhten TiO_2-Konzentration ist verstärkt bei höheren Anfangskonzentrationen von Bromid zu verzeichnen.

Zuletzt wurden drei weitere Einflussgrößen untersucht. Der Referenzwert bei diesen Versuchen war die Bromoformbildung mit P25 bei $\rho(\mathrm{TiO_2}) = 1.5\ \mathrm{g\ L^{-1}}$, $\rho_0(\mathrm{Br^-}) = 3\ \mathrm{mg\ L^{-1}}$ und $\rho_0(\mathrm{DHBA}) = 2\ \mathrm{mg\ L^{-1}}$. Bei der Bestrahlung mit einer Quecksilberniederdrucklampe wurden 15-20 µg $\mathrm{L^{-1}}$ Bromoform gebildet.

Art des Photokatalysators: Es wurden die zwei meistbenutzten Photokatalysatoren (P25 und Hombikat UV100) miteinander verglichen. Dabei stellte sich heraus, dass die Bromoformbildung unter Verwendung von Hombikat UV100 sehr gering war (< 3 µg $\mathrm{L^{-1}}$). Dies könnte eine Folge des schnelleren Bromoform-*Abbaus* in Hombikat UV100-Dispersionen sein.

DOC-Quelle: Es wurde auch die Bromoformbildung aus der Modellverbindung 2,4-Dihydroxybenzoesäure mit der Bromoformbildung aus Hohlohseewasser als

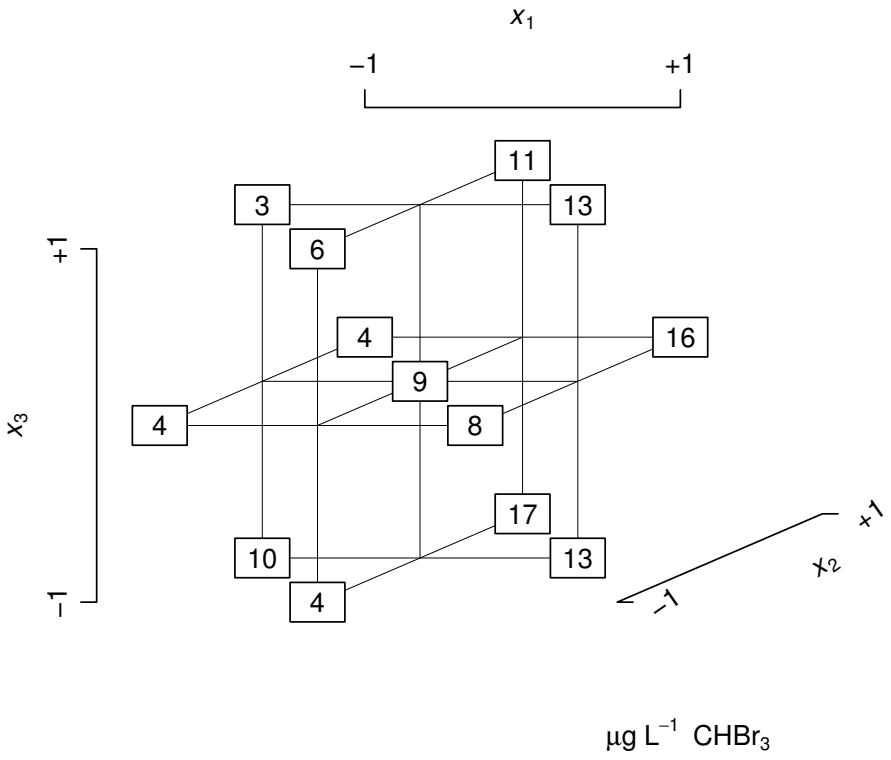

Abb. 0.8: Zusammenfassende Darstellung der Werte für $max_3(CHBr_3)$ in Abhängigkeit von der Konzentration von TiO_2 (x_1), Br^- (x_2) und DHBS (x_3). Die Standardabweichung für diese Werte wurde aus Wiederholungen ($n = 4$) des Mittelpunktes der Versuchsmatrix als ± 1.6 µg L^{-1} $CHBr_3$ ermittelt.

DOC-Quelle verglichen. Die Bildung von Bromoform verlief qualitativ bei beiden Ansätzen gleich. Auch die quantitative Übereinstimmung war gut.

Anwesenheit von Kupferionen: Bei Zugabe von $c_{added}(Cu^{2+}) = 10$ µmol L^{-1} wurden < 5 µg L^{-1} Bromoform gebildet. Dies könnte eine Konsequenz des verlangsamten DOC-Abbaus in Anwesenheit von Cu^{2+} sein.

Zusammenfassend lässt sich feststellen, dass die heterogene Photokatalyse mit TiO_2 als Photokatalysator ein relativ niedriges Potenzial für die Bildung unerwünschter bromierter Nebenprodukte aufweist. Der Einsatz dieses Verfahrens für die oxidative Behandlung von Wasser für den menschlichen Gebrauch bietet somit einen klaren Vorteil.

Chapter 1

Introduction

Heterogeneous photocatalysis with titanium dioxide, both immobilized and in suspension, has been the subject of intensive research in the past decades. This technique is one of the so-called advanced oxidation processes (AOP), which are based on the reactivity of OH radicals and can be used for both air and water treatment. Heterogeneous photocatalysis offers the advantages of high oxidation power on the basis of OH radicals, a low cost, reusable, chemically and biologically stable catalyst, and the potential for using solar irradiation for the energy intensive excitation of the photocatalyst (e.g. Fernández-Ibáñez et al., 2003; Kaneko and Okura, 2002; Oppenländer, 2003).

The presence of TiO_2 in a UV-irradiated aqueous system considerably accelerates photoinitiated degradation reactions. For example, in the case of the photoinitiated degradation of the X-ray contrast medium iomeprol, shown in Figure 1.1, the time scale for the degradation is reduced from hours to minutes by the presence of TiO_2 (Doll, 2004). Here it is worth noting that Iomeprol, like other X-ray contrast media, is by design a very poorly bioavailable compound which is also insufficiently removed or degraded in wastewater treatment facilities (Ternes and Hirsch, 2000).

While ozone is able to degrade many persistent organic pollutants, including pharmaceuticals in water, the reaction rates are in some cases fairly slow and some compounds (e.g. the lipid regulator clofibric acid and the antibiotic ciprofloxacin) are essentially non-degradable by ozonation (Ternes et al., 2002; Vieno et al., 2007). The use of OH radicals leads in many cases to substantially faster reaction rates, as shown in Table 1.1. In addition, OH radicals are able to degrade organic pollutants that are not degraded by ozone (Doll and Frimmel, 2004; Ternes et al., 2002).

Because of the high redox potential of the electron-hole (e^--h^+) pairs generated by UV-irradiation of TiO_2, the reactions initiated by this method are essentially non-selective. This has the advantage of high reaction rates with most target compounds.

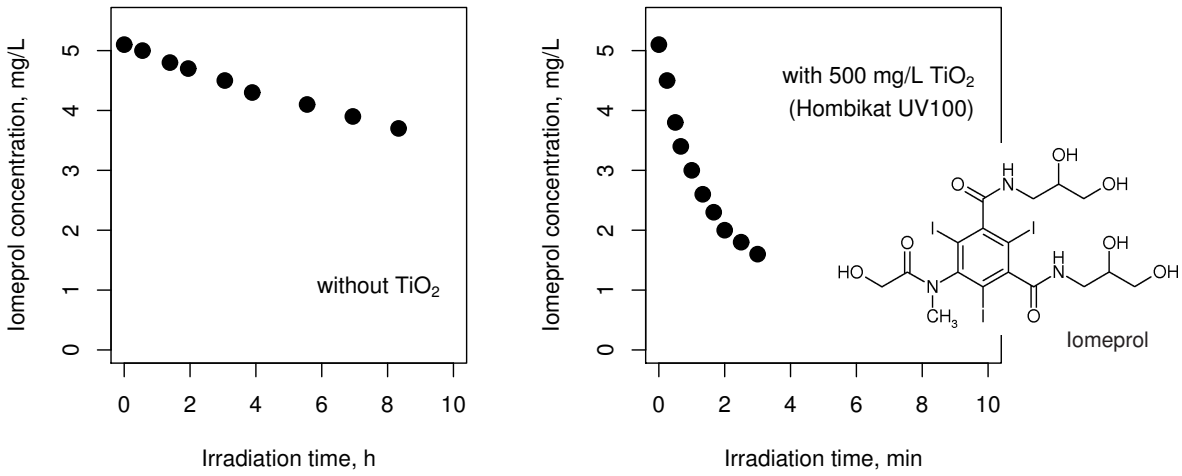

Figure 1.1: Degradation of the X-ray contrast medium Iomeprol by simulated solar UV-radiation in the absence (left) and in the presence (right) of titanium dioxide (Doll, 2004). *Note that the time scale on the left plot is 60× larger than on the right plot.*

Table 1.1: Second order reaction rates for the reaction of ozone and OH radicals ($^{\bullet}$OH) with selected pharmaceuticals (values from Huber et al., 2003).

Substance	k_{O_3} L mol^{-1} s^{-1}	$k_{OH^{\bullet}}$ L mol^{-1} s^{-1}
17α-ethinylestradiol (estrogen)	$\approx 7 \times 10^9$	$(9.8 \pm 1.2) \times 10^9$
Diazepam (sedative)	0.75 ± 0.15	$(7.2 \pm 1.0) \times 10^9$
Diclofenac (anti-inflammatory)	$\approx 1 \times 10^6$	$(7.5 \pm 1.5) \times 10^9$
Ibuprofen (pain killer)	9.6 ± 1	$(7.4 \pm 1.2) \times 10^9$
Iopromid (X-ray contrast medium)	< 0.8	$(3.3 \pm 0.3) \times 10^9$
Sulfamethoxazol (antibiotic)	$\approx 2.5 \times 10^6$	$(5.5 \pm 0.7) \times 10^9$

However, the non-selectivity of the process could also lead to the formation of unwanted byproducts. The formation of disinfection byproducts (DBPs) is a common problem in the oxidative treatment of water for human consumption. In particular, in water containing bromide ions (Br^-), the formation of brominated organic products during chlorination and the formation of bromate (BrO_3^-) during both chlorination and ozonation are of concern (Richardson et al., 1999; von Gunten, 2003). High concentrations of Br^- (low mg L^{-1} range) in surface waters can be found in arid and coastal areas, for example around the Mediterranean sea and in the middle east. These areas often have abundant solar energy at their disposal, rendering them potentially attractive locations for the application of (solar) heterogeneous photocatalysis.

Herrmann and Pichat (1980) have reported that Br^- can be oxidized in irradiated TiO_2 suspensions under both acidic and basic conditions. The oxidation of Br^- to Br_2 opens the door for the formation of BrO_3^- in the presence of OH radicals (von Gunten and Oliveras, 1998) and bromoorganic byproducts in the presence of the ubiquitous natural organic matter (Zwiener, 2006). Although there are many studies on the photocatalytic oxidation of a large variety of substances in irradiated TiO_2 suspensions, studies dealing with the formation of undesirable byproducts in this process are rare (i.e. Richardson et al., 1996).

The characterization of the formation of such byproducts is, however, a prerequisite for the further development of this technology in the field of water treatment for human consumption. Filling this knowledge gap for the case of bromide-containing raw water was what motivated the work presented in this thesis. A schematic of the process and the open questions is shown in Figure 1.2. In the worst case, unacceptable levels of regulated brominated byproducts may be formed in heterogeneous photocatalysis, though this is considered unlikely based on the results of Richardson et al. (1996). In the best case, the use of heterogeneous photocatalysis for the oxidative treatment of bromide containing water yields little or no formation of regulated brominated byproducts. This would be a very desirable outcome and give this technique a further advantage over currently established oxidation processes.

We approached the question of brominated byproducts by first studying the photocatalytic degradation of natural organic matter (NOM). This type of investigation is relevant to the study of byproduct formation for two reasons:

1. NOM is present in varying concentrations in all raw waters, and
2. NOM is an important carbon source (and the most important natural one) in the formation of unwanted byproducts.

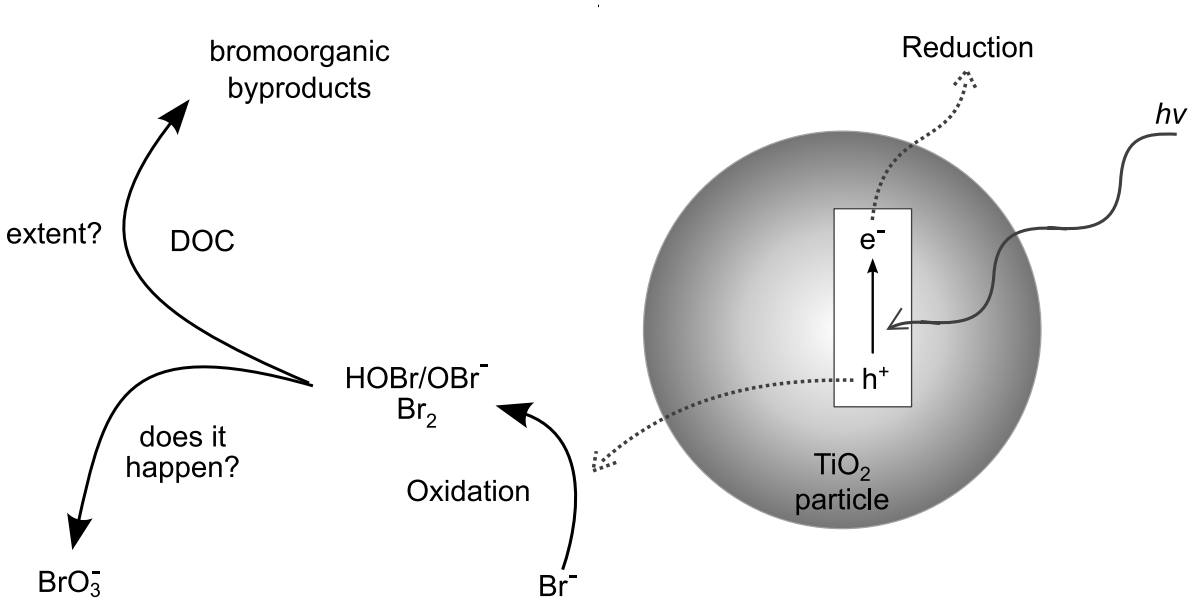

Figure 1.2: Schematic representation of the questions that motivated this work.

Both points are of practical consequence: a reduction of the incoming DOC concentration into an oxidation/disinfection reactor is a widely employed and very effective way of reducing byproduct formation. However, the DOC content in raw waters entering chemical oxidation steps cannot feasibly be completely eliminated. It is, therefore, necessary to understand the behavior of NOM during water treatment, especially in those steps that induce chemical transformations in the NOM like advanced oxidation processes.

There are several published studies dealing with the photocatalytic degradation of NOM (e.g. Bekbölet et al., 2002; Eggins et al., 1997; Palmer et al., 2002). However, most of them share at least one of two disadvantages:

1. the use of humic material from peat or coal extracts redissolved in water instead of aquatic natural organic matter, and
2. a focus on the bleaching of NOM and/or the overall reduction in DOC concentration.

Thus, the greater part of the current literature ignores the transformations (molecular size, chemical functionality, etc.) occurring to the NOM which cannot be quantified by using only summary parameters like UV absorbance and DOC measurements.

Some studies, however, have sought to address these deficiencies by fractionating the organic material before and after irradiation according to their hydrophilicity (Bekbölet et al., 1996), by chemically classifying the degradation products of NOM (Liu

et al., 2008b), by using ultrafiltration followed by DOC measurements (Uyguner and Bekbölet, 2005), or by using size exclusion chromatography with UV absorption detection (Liu et al., 2008a). From these studies, only that of (Liu et al., 2008b) used real surface water.

Our own efforts focused on the elucidation of the changes in molecular size of NOM as it undergoes photocatalytic degradation. We used size exclusion chromatography to fractionate the NOM at different stages of the photocatalytic degradation process to gain insights into the time evolution of its molecular size distribution. The use of DOC detection in addition to UV absorbance detection gives a further dimension to the data compared to that presented by Liu et al. (2008a,b), and the level of detail and time resolution is improved compared to the results of Uyguner and Bekbölet (2005).

The results present in the literature for the degradation of NOM in both homogeneous and heterogeneous AOP indicate that the large molecular weight portion of NOM disappears first or at least faster than the lower molecular weight portion. This has led to claims of selectivity in advanced oxidation processes (e.g. Liu et al., 2008b; Sarathy and Mohseni, 2007). However, this selectivity appears unlikely considering the high oxidation potential of OH radicals, as mentioned above. Rather, we hypothesized that the observed "preferential" disappearance of the large molecular weight portion of NOM in AOP is simply the result of a random process because the degradation products of large molecules are themselves smaller molecules. This should mask the disappearance of the lower molecular weight material and, because the higher molecular weight material is not replaced, should lead to an apparent selectivity.

Unfortunately, these two possibilities cannot be readily tested experimentally because of the difficulty in establishing similar conditions and the impossibility of tracking each C atom during degradation. While a radiolabeling approach would give insights into the process, it is in practice difficult to physically isolate sharp fractions out of a chromatogram for testing (Lankes et al., 2009; Müller, 2004). In order to answer this question, we designed and implemented a computer simulation, which, greatly simplifying the chemical and structural identity of NOM, is able to model the totally random degradation of NOM in the presence and absence of an adsorptive and reactive surface. Thus, we are able to make a fair comparison of the degradation of NOM in both homogeneous and heterogeneous AOP.

A further important characteristic of NOM is its ability to complex metal ions. This has implications e.g. for the solubility and transport of metals and metalloids in

water, which is of environmental relevance (Metreveli, 2008). In our case, the focus was on the possible changes in the degradation kinetics of NOM if metal ions are present. There is a small body of literature dealing with the effect of dissolved metal ions on the reaction kinetics in irradiated TiO_2 suspensions (e.g. Aarthi and Madras, 2007; Bideau et al., 1991; Cai et al., 2003; Chen et al., 2002; Lindner et al., 1997; Litter, 1999). Most work has concentrated in the doping of the photocatalyst itself instead of looking at the effect of dissolved metal ions. Studies dealing with dissolved metal ions in heterogeneous photocatalysis tend to use concentrations well beyond what may be expected in surface water and have to date not included NOM.

We wanted to characterize the effect of the presence of metal ions on the degradation kinetics of NOM. Our approach extends the current knowledge in three ways:

1. we considered a lower concentration range more reflective of the conditions in natural waters,
2. we examined the changes in molecular size distribution, not only the overall bleaching and mineralization, and
3. we systematically studied the effects of four metal ions (Cu^{2+}, Fe^{3+}, Mn^{2+}, Zn^{2+}) present simultaneously at different concentrations; that is, we are able to compare the effect of the metal ions not only in isolation but also in direct competition with each other, and to quantify their interactions.

The questions regarding the photocatalytic degradation of NOM are graphically summarized in Figure 1.3. The answers to these questions, while important for themselves, also provide a good basis for the study of brominated byproduct formation in irradiated TiO_2 suspensions because it is the bromination of organic material that leads to brominated byproducts.

The first questions to ask, as depicted in Figure 1.2, was whether BrO_3^- (carcinogenic) and brominated organic byproducts (precursors of bromoform) are formed in irradiated TiO_2 suspensions in the presence and absence of a DOC source. We focused on brominated byproducts because Br^- is oxidized to HOBr and Br_2 to a much greater extent than Cl^- is oxidized to HOCl and Cl_2 in irradiated TiO_2 suspensions (Herrmann and Pichat, 1980). Moreover, because hypobromous acid (HOBr) is a more potent halogenating agent than hypochlorous acid (HOCl) (Zwiener, 2006), we expect brominated byproducts to dominate if bromide ions are present in the suspension.

Having answered these preliminary questions, the formation of bromoform had to be studied in more detail. Because of the complexity of NOM and because of its source and seasonal variability, much of the work pertaining to the formation of bromoform

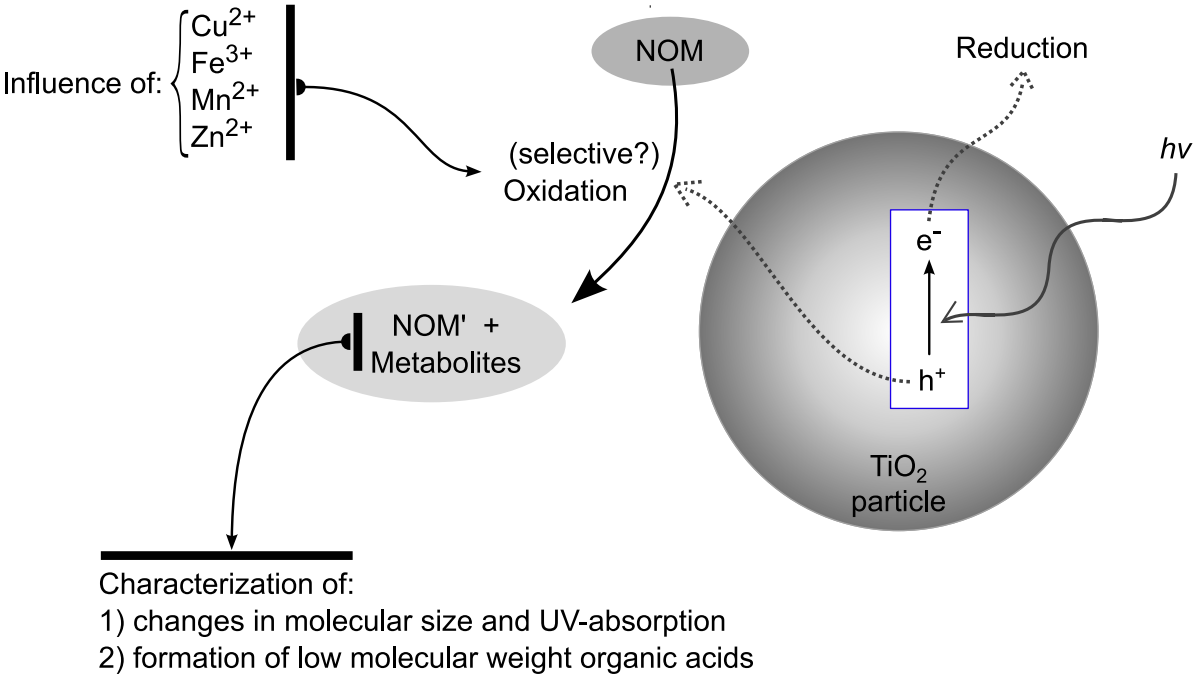

Figure 1.3: Schematic representation of the questions relating to the photocatalytic degradation of natural organic matter.

was performed using a model source of DOC alone, or in parallel with "real" NOM. For a systematic study of the main quantitative factors affecting the formation of bromoform, we resorted to the response surface methodology as outlined in Box and Draper (1987) and Box et al. (2005).

Overall, the work presented here aimed to bring together a better understanding of the transformations of natural organic matter in heterogeneous photocatalysis with an assessment of the formation of brominated byproducts, especially bromoform, in irradiated TiO_2 suspensions containing dissolved organic carbon and bromide ions. In particular, this thesis

- qualitatively and quantitatively describes the changes in the apparent molecular size distribution of NOM in irradiated TiO_2 suspensions as a function of irradiation time
- clearly answers the question of selective degradation of NOM in homogeneous and heterogeneous AOP
- gives a systematic and fair comparison of the effects of the presence of selected metal ions on the degradation kinetics of NOM
- explores the formation of inorganic and organic brominated byproducts

- presents a simple and plausible reaction scheme for the formation of bromoform in irradiated TiO_2 suspensions
- gives insights into the formation of bromoform on the basis of a parameter study covering the main variables identified from the proposed reaction scheme
- explores the effect of qualitative variables such as photocatalyst identity and DOC source, and
- tentatively ties the kinetics of formation of bromoform to those of degradation of NOM.

Chapter 2

Background

2.1 Electronic properties of semiconductors

2.1.1 Band gap structure of semiconductors

An atom in isolation exhibits discrete electronic energy states characterized by the quantum numbers n (shells), l (subshells), m_l (number of states in each subshell) and m_s (spin moment, $+1/2$ and $-1/2$). As these atoms are brought together to form molecules or a solid, the electrons surrounding each atom start to interfere with each other, starting with the electrons of the outer shell (Callister, 1997; Serway, 1996). The energetic states in each atom, in molecules and in the solid as a whole are filled following the Pauli exclusion principle, which states that each electron should have a unique combination of quantum numbers (same energy state) at any given time. As a consequence, when N atoms are brought close together, the energy levels that were identical in isolation split into N closely spaced but distinct energy levels (Callister, 1997; Laidler and Meiser, 1995). Since the maximum and minimum energy allowed for each orbital is not dependent on the number of atoms but on nearest-neighbor interactions, the energy "width" over which these levels can split is limited. When N becomes large (on the order of 10^{23} atoms cm^{-3}), the levels are so closely spaced that it is possible to consider them a continuum of energetic states forming an "electronic energy band". These "allowed" energy bands are separated by energy gaps, termed "forbidden" energy bands because electrons are not allowed to enter them (Laidler and Meiser, 1995; Serway, 1996).

Although there are as many bands as there are orbitals in the atoms conforming the solid, two bands are of interest in the ensuing discussion: the "valence band" and the "conduction band". The valence band is the highest energy band that is completely filled with electrons. These electrons are not mobile because they are involved in

chemical bonding. The conduction band is the lowest lying band which is empty or partially filled. These electrons are able to move throughout the solid with approximately zero activation energy (Laidler and Meiser, 1995).

In a conductor, there is no separation between the valence band and the conduction band, allowing electrons to become free by using only the available thermal energy ($k_bT \approx 0.025$ eV at 300 K). Only at absolute zero is the conduction band completely empty. Insulators have a large energy gap between their valence and conduction bands (≈ 10 eV) such that their conduction band remains essentially empty (Serway, 1996).

Semiconductors have a similar structure as insulators, exhibiting a filled valence band separated from an empty conduction band by an energy band gap, E_g. However, the energy gap is much smaller in semiconductors than in insulators, typically in the range of 1-2 eV. Nevertheless, there are semiconducting materials with $E_g > 2$ eV (Fujishima et al., 1999). These semiconductors are sometimes called "wide band gap semiconductors" or "photosemiconductors" because the energy required to promote an electron from the valence band to the conduction band is on the order of the energies of visible light or near ultraviolet radiation (Doll, 2004). Some examples are shown in Table 2.1.

Table 2.1: Energy band gaps and corresponding photon wavelengths required for excitation of an electron from the valence to the conduction band for selected semiconductors (Fujishima et al., 1999; Serway, 1996)

		Wavelength	
Semiconductor	E_g (eV) at 300 K	λ, nm	range
Si	1.1	1127	infrared
Ge	0.7	1771	infrared
GaAs	1.4	886	infrared
TiO_2 (anatase)	3.2	387	ultraviolet
TiO_2 (rutile)	3.0	413	visible (violet)
ZnO	3.2	387	ultraviolet
ZnS	3.6	344	ultraviolet

The relation between the energy needed to promote an electron from the valence to the conduction band, E_g, and the corresponding wavelength of a photon is given

by

$$E = h\nu = \frac{hc}{\lambda}$$

where E is the energy of a photon of frequency ν and corresponding wavelength λ, h is Planck's constant, and c is the speed of light (Serway, 1996).

2.2 Semiconductor photocatalysis

When a semiconductor (e.g. TiO_2, ZnO, Fe_2O_3, CdS, and ZnS) is impacted by a photon of energy $h\nu$ matching or exceeding its band gap energy, an electron is promoted from the filled valence band into the conduction band. The promoted electron leaves behind an electronic vacancy or hole, h^+, in the valence band. The electrons excited to the conduction band and the valence band holes can either recombine, get trapped in metastable surface states, or react with electron donors or acceptors at or in the immediate vicinity of the semiconductor surface (Fox and Dulay, 1993; Hoffmann et al., 1995; Kabra et al., 2004; Linsebigler et al., 1995). This ability to donate and accept electrons, that is, to initiate redox processes at a surface upon absorption of an adequate photon, is the basis of heterogeneous photocatalysis.

Of the semiconductors mentioned above, TiO_2 has been favored for work focusing on the degradation of persistent pollutants in both gaseous and aqueous phases because of the size and position of its band gap, and because of its physical and chemical robustness (Fujishima et al., 1999; Hoffmann et al., 1995). In the following Sections, some fundamental aspects of heterogeneous photocatalysis using semiconductor particles in suspension will be discussed, giving especial consideration to TiO_2.

2.2.1 Titanium dioxide

By far the most commonly used TiO_2 powder is P25 (Degussa/Evonik). Another widely used photocatalyst material is UV100 (Sachtleben Chemie). Transmission electron microscopy (TEM) images of these two powders are shown in Figure 2.1 and some of their characteristics are given in Table 2.2.

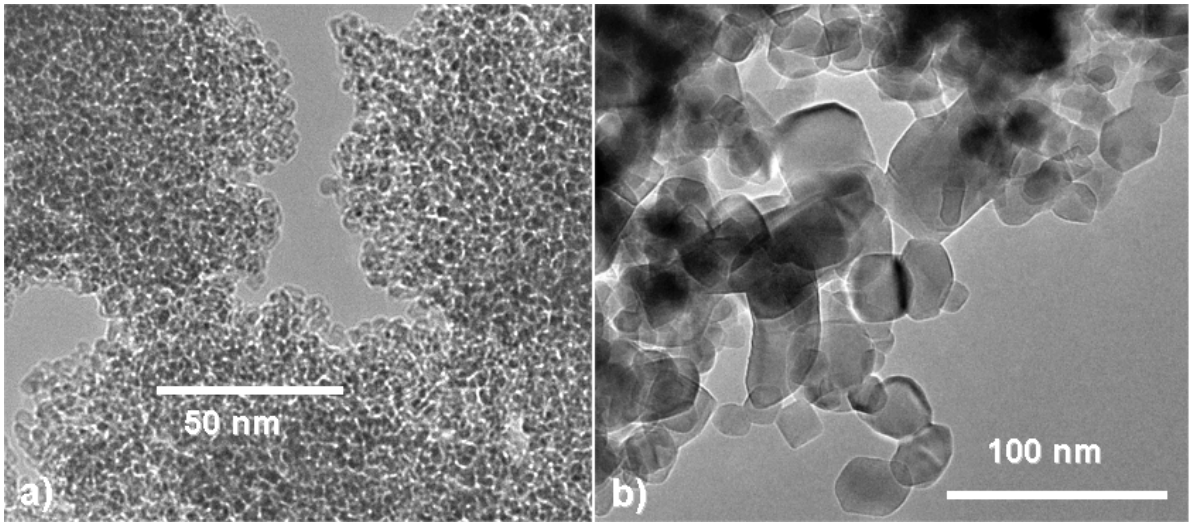

Figure 2.1: Transmission electron micrographs of the commercially available (a) Hombikat UV100 and (b) P25 TiO_2 powders (Doll and Frimmel, 2005).

Table 2.2: Some characteristics of the commercially available P25 and Hombikat UV100 powders (Doll and Frimmel, 2005, and manufacturer's specifications).

	P25	Hombikat UV100
Average particle diameter	20-30 nm	≈ 8 nm
BET surface area	50 ± 15 m^2 g^{-1}	> 250 m^2 g^{-1}
Crystal structure	approx. $\frac{3}{4}$ anatase and $\frac{1}{4}$ rutile	anatase

2.2.2 Photogeneration and reactions of electron/hole pairs

Generation of electron/hole pairs (Equation 2.1) happens within a few femtoseconds after the absorption of a photon (Fox and Dulay, 1993; Hoffmann et al., 1995; Hufschmidt et al., 2004).

$$TiO_2 + h\nu \longrightarrow TiO_2(e^-_{cb} + h^+_{vb}) \tag{2.1}$$

After generation, the electrons and holes rapidly diffuse to the surface of the TiO_2 particle, where they are trapped in subsurface and surface states (Hufschmidt et al., 2004). Because trapping and the presence of the band gap delay the recombination of the electron-hole pairs, a sufficiently long lifetime is assured to allow electrons and holes to participate in interfacial electron transfer (Fox and Dulay, 1993; Hoffmann

et al., 1995). A schematic summary of the main pathways available to e^-_{cb} and h^+_{vb} is shown in Figure 2.2. Additionally, Table 2.3 shows characteristic lifetimes for the main processes involved in heterogeneous photocatalysis. Inspection of these values reveals the interfacial electron transfer step to be rate-limiting.

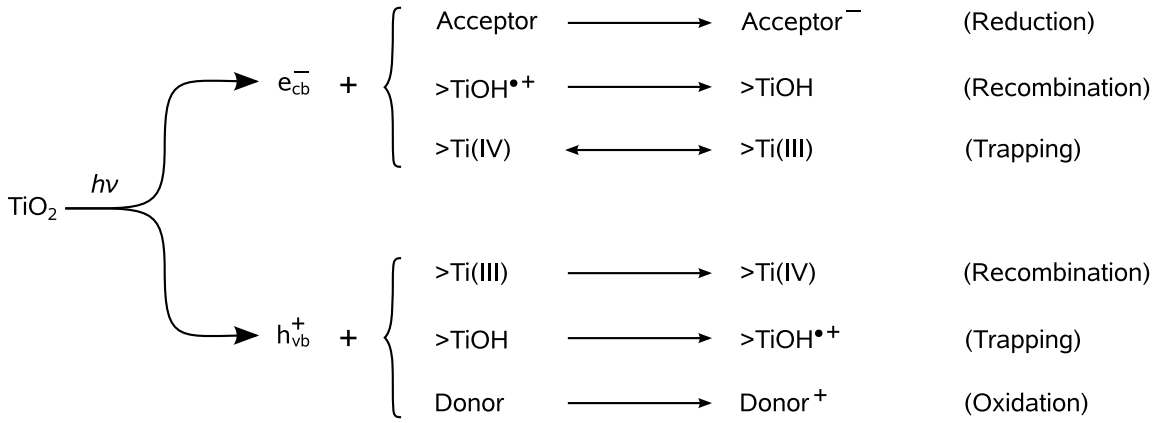

Figure 2.2: Primary steps in the photoelectrochemical mechanism (after Hoffmann et al., 1995). A preceeding ">" denotes a surface species.

Table 2.3: Characteristic times for the primary processes involved in heterogeneous photocatalysis (Hoffmann et al., 1995).

Primary process	**Characteristic time**
Charge carrier generation (eq. 2.1)	fs
Charge carrier trapping	
holes	10 ns
electrons	0.1-10 ns
Charge carrier recombination	10-100 ns
Interfacial charge transfer	
holes	100 ns
electrons	ms

2.3 Photocatalytic degradation of humic material

According to the International Humic Substances Society, humic substances (HS) are "complex and heterogeneous mixtures of polydispersed materials formed by biochemical and chemical reactions during the decay and transformation of plant and microbial remains" (International Humic Substances Society, 2007).

HS make up an important part of natural organic matter (NOM), the naturally occurring (i.e. not anthropogeneous) organic compounds found in all natural waters and which play a fundamental role in the aquatic environment. However, in water treatment, NOM is also the main natural precursor of unwanted haloorganic disinfection byproducts (DBPs), of which trihalomethanes (THMs) are the most prominent example (Frimmel et al., 2002; Zwiener, 2006). Because of this, the photocatalytic degradation of humic material has been studied mainly as a way of decolorizing raw water for drinking water production, though some studies have considered the reduction of the trihalomethane formation potential (THM-FP).

2.3.1 Reduction of the trihalomethane formation potential

The first studies in this direction were those of Hand et al. (1991) and Ogawa et al. (1995). Hand et al. (1991) reported that trihalomethane formation potential (THM-FP) could be reduced by 40-80 % with irradiation times between 15-60 min, and that sunlight can be used to activate the photocatalyst. Ogawa et al. (1995) also reported a decrease in the chloroform formation potential of a humic acid (HA) solution (9.8 mg L^{-1} DOC) after irradiation in the presence of titanium dioxide. The reduction in chloroform formation potential correlated with the decolorization of the water and a reduction in total organic carbon.

Bekbölet et al. (2005) studied the formation of trihalomethanes (THMs) and haloacetic acids (HAAs) after chlorination of three natural water samples as a function of different pre-treatment options, one of them being heterogeneous photocatalysis. However, because of the very low TiO_2 concentrations (0.1 g L^{-1}) and short irradiation times (30 min) used, no appreciable differences could be established between the formation potential in the raw water and that in the water treated by heterogeneous photocatalysis.

Following a similar approach, Liu et al. (2008a,b) found a reduction of the specific THM formation potential from $\approx$ 50 μg THM per mg^{-1} DOC to $\approx$ 10-20 μg mg^{-1} using 0.1 g L^{-1} TiO_2 (P25) over a period of 240 min for both model (Fluka humic acid) and natural (Myponga Reservoir, Australia) DOC. However, they found no significant change in the haloacetic acid formation potential (30-50 mg mg^{-1}; Liu et al., 2008b).

2.3.2 Decolorization of humic-rich waters

Far more studied is the bleaching of humic-rich waters in the presence of TiO_2 and ultraviolet irradiation.

Bekbölet and Balcioglu (1996) reported reaction kinetics for the degradation of humic acid (Aldrich) solutions at concentrations ranging from 50 to 500 mg L^{-1} (one to two orders of magnitude higher than those usually found in the environment) and followed by means of total organic carbon and UV-absorption measurements. They reported that the addition of H_2O_2 could at best enhance the rate of reaction by a factor of 1.6-1.8. The enhancement they observe is most likely due to the presence of more $^{\bullet}OH$ generated through the photolysis of H_2O_2 (Braun et al., 1991; Oppenländer, 2003). A similar increase in reaction rates was observed by Liu et al. (2008b). The rate of reaction was reduced by the presence of HCO_3^- ions, a known $^{\bullet}OH$ scavenger (Bekbölet and Balcioglu, 1996).

Portjanskaja et al. (2006) also reported an increase in reaction rates with added H_2O_2. However, the increase in reaction rate is smaller than when H_2O_2 is added to the humic acid solution in the absence of photocatalyst. Thus, although the reaction proceeds faster, the efficiency of the combination is lower than that for either of the separated elements. Efficiency was lower for higher added H_2O_2 concentrations.

A decrease in reaction rates with increasing pH (pH values tested: 3, 6, and 11) using TiO_2 suspensions and Aldrich humic acid was reported by Bekbölet and Balcioglu (1996). In contrast, Portjanskaja et al. (2006) report increasing reaction rates and energy efficiency of the process with increasing pH, also using Aldrich humic acid but with immobilized TiO_2. Minero et al. (1999) and Wiszniowski et al. (2002) both report little changes in degradation rates with pH. It is not clear what leads to these contrasting results.

Bekbölet et al. (1996) reported an increase in biodegradability (measured as biological oxygen demand after 5 days, BOD_5) and a decrease in the adsorption of Roth humic acid onto activated carbon after photocatalytic treatment over several hours. By comparing absorption at 254 nm, 280 nm and 400 nm, they conclude that the aromatic content in the humic material is reduced at a faster rate than the rate of mineralization. The gains in biodegradability were modest ($\leq$ 20%) for up to 50% organic carbon removal, increasing rapidly after that (up to $BOD_5/COD \approx 0.8$ for approx. 90% TOC elimination). In a separate study, Bekbölet et al. (1998) report that the addition of chloride, nitrate, sulfate or phosphate (all 0.04 mol L^{-1}) reduces the rate of bleaching (400 nm and 436 nm), with phosphate having by far the largest effect

(one order of magnitude in rate constant, all others less than factor 2). Addition of higher concentrations of chloride ions ($\approx$ 70 mmol L^{-1}) led to essentially no reduction in the rates of mineralization of Aldrich humic acid. In the case of sulfate ions, $\approx$ 10 mmol L^{-1} showed no influence in the mineralization rate, but a concentration of $\approx$ 80 mmol L^{-1}, there was a reduction in the mineralization rates (Wiszniowski et al., 2003).

Eggins et al. (1997) report the degradation of Aldrich humic acid by photocatalysis. Starting with a 100 mg L^{-1} humic acid solution, they observed $\approx$ 50% mineralization of the DOC content in 60 min using their particular experimental setup. In addition, they found very little degradation in the absence of oxygen. Similar results were obtained by Minero et al. (1999) and Selçuk et al. (2004).

A comparison of the efficiencies of two commercially available and widely used TiO_2 powders (Hombikat UV100 and P25) in relation to the decolorization of humic acids was carried out by Bekbölet et al. (2002). In this study, the authors conclude that P25 is the better adsorbent and photocatalyst for this reaction despite the higher BET surface area of Hombikat UV100 (cf. Table 2.2). However, the degradation curves run essentially parallel to each other at different levels, and the level is determined by the initial adsorption of the humic acids onto the TiO_2 surface.

2.3.3 Open questions

There are two main weaknesses common to most of the studies cited above:

1. they use almost exclusively commercial humic acids, which are extracts from either peat or coal, neither of which reflects well the properties of aquatic humic substances, and
2. most authors have followed the progress of the reaction by summary parameters, e.g. DOC and $UV_{\lambda=254\ nm}$, which only give information on mineralization and overall loss of UV absorbing moieties. Thus, there is a lack of information on the internal transformations occurring to humic substances in irradiated TiO_2 suspensions.

From these two weaknesses, two questions regarding the photocatalytic degradation of NOM may be asked:

1. how does *aquatic* NOM behave in irradiated TiO_2 suspensions?
2. what transformations does NOM undergo prior to mineralization in irradiated TiO_2 suspensions?

2.4 Harmful byproducts in disinfection and oxidation processes

Microbiological safety is the most important goal of drinking water treatment. Attainment of this goal is in fact one of the main factors behind the improved quality of life achieved in the past century. A variety of disinfection techniques can be used to insure microbiological safety (e.g. chlorination, ozonation, irradiation), each of which led to different amounts and compositions of undesired byproducts (disinfection byproducts, DBPs). In the case of chlorination, the formation of trihalomethanes (THM) and haloacetic acids (organic) as well as bromate (inorganic) are of concern. While yielding considerably lower quantities of THM, ozonation easily gives rise to unacceptably high concentrations of bromate (> 10 μg L^{-1} BrO_3^-) if bromide ions are present in the raw water (> 100 μg L^{-1}; von Gunten, 2003; Zwiener, 2006). Here we focus on brominated instead of chlorinated DBPs because bromide ions are more easily oxidized in heterogeneous photocatalysis, giving rise to a higher probability of brominated byproducts (Herrmann and Pichat, 1980). In addition, brominated byproducts are generally more toxic than the corresponding chlorinated compounds.

2.4.1 Sources of bromide in natural waters

The main sources of bromide in natural waters are sea water and rock salt deposits. In both cases, bromide ions are present as accompanying ions to chloride. In sea water, the molar ratio of chloride to bromide ions is $> 600 : 1$ (Gros et al., 2008). Inland, increased bromide concentrations can arise when water contacts rock salt deposits, where Br^- is present as an impurity (as NaBr and $MgBr_2$; Botsch et al., 1977).

2.4.2 Brominated trihalomethanes

Toxicological relevance

Trihalomethanes (Figure 2.3) have been shown to be cytotoxic in the liver and kidneys of rodents, but the vehicle of administration has a very strong impact on the effects observed. Chloroform and bromodichloromethane (BDCM) induce cancer in liver and kidney after lifetime exposures at high doses. BDCM and bromoform can also induce tumors in the large intestine in rats (Amy et al., 2000).

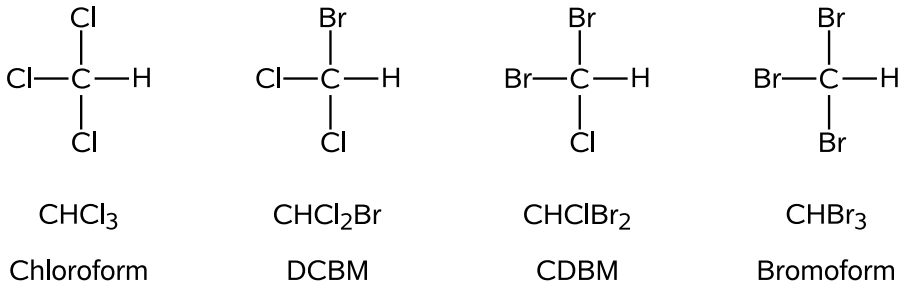

Figure 2.3: Chlorinated and brominated trihalomethanes.

Bromoform is the least toxic of all THM in terms of acute toxicity and was used in the 19th and early 20th century as a sedative for children with whooping cough. Bromoform cannot be classified carcinogenic to humans because of inadequate evidence. However, there are a variety of studies showing chronic toxicity and mutagenicity (Amy et al., 2000).

The drinking water limit for the sum of all four chlorinated and brominated THM is 50 $\mu g\ L^{-1}$ in Germany and 80 $\mu g\ L^{-1}$ in the USA (Zwiener, 2006).

Formation

Bromoform is formed by reaction of hypobromous acid (HOBr) with dissolved organic carbon (Boyce and Hornig, 1983). HOBr is in turn formed from bromine (Br_2) by disproportionation (Riedel, 1990):

$$Br_2 + H_2O \rightleftarrows HBr + HOBr \tag{2.2}$$

In chlorination, HOBr is formed by the reaction sequence (Riedel, 1990; Zwiener, 2006)

$$Cl_2 + H_2O \rightarrow HOCl + H^+ + Cl^- \tag{2.3}$$

$$HOCl + Br^- \rightarrow Cl^- + HOBr \tag{2.4}$$

$$HOBr \rightleftarrows H^+ + OBr^- \qquad pK_a = 8.7 \tag{2.5}$$

In the presence of OH-radicals ($^{\bullet}OH$), HOBr may be formed by the following sequence (von Gunten and Oliveras, 1998):

$$Br^- + {}^\bullet OH \rightleftarrows BrOH^- \tag{2.6}$$
$$BrOH^- + Br^- \rightarrow Br_2^- + OH^- \tag{2.7}$$
$$BrOH^- + H^+ \rightarrow Br^\bullet + H_2O \tag{2.8}$$
$$Br^\bullet + Br^- \rightleftarrows Br_2^- \tag{2.9}$$
$$Br_2^- + Br_2^- \rightarrow Br_3^- + Br^- \tag{2.10}$$
$$Br_3^- \rightleftarrows Br_2 + Br^- \tag{2.11}$$

Br_2 in turn disproportionates following Equation 2.2. The oxidation of Br^- in titanium dioxide suspensions, presumably through this or a similar mechanism, was observed by Herrmann and Pichat (1980).

Finally, reaction of HOBr with dissolved organic carbon leads to the formation of bromoorganic byproducts, including bromoform (Boyce and Hornig, 1983).

HOBr itself is a more potent halogenating agent than hypochlorous acid (HOCl) (Zwiener, 2006). This leads to a dominance or at least to disproportionately high concentrations of brominated trihalomethanes ($CHBr_3$, $CHClBr_2$, $CHCl_2Br$, with bromoform being the most abundant) despite the excess of HOCl compared to HOBr under normal conditions (vide supra). For example, a study found 70-90% of total THM were brominated in water from the Mediterranean coast of Spain (Villanueva et al., 2003). Similar results have been reported in Saudi Arabia (Amy et al., 2000).

2.4.3 Bromate

Toxicological relevance

Bromate causes damage to rat kidneys at high doses. In chronic studies, tumors in the kidneys, peritoneum and thyroid have been observed. Carcinogenicity appears to be secondary to oxidative stress. In humans, bromate poisoning is accompanied by anaemia, haemolysis, hearing loss and renal failure. Poisoning is frequently fatal if the dosis exceeds 6 g for an individual (Amy et al., 2000).

Formation

Bromate is of concern mainly in ozonation, where it is formed either by a direct mechanism involving ozone or by a direct-indirect mechanism involving ozone and $^\bullet OH$.

Formation of BrO_3^- through a purely $^\bullet$OH-mediated mechanism is also possible (von Gunten and Oliveras, 1998).

2.4.4 Semiconductor photocatalysis and disinfection byproducts

Byproduct formation has not been a central question in past studies of heterogeneous photocatalysis. Worth noting is the study of Richardson et al. (1996), who examined ultrafiltered raw water after photocatalytic treatment and compared it to ultrafiltered water after photocatalysis and chlorination. They found only one DBP after photocatalysis, compared to 35 after a subsequent chlorination, with the cautionary note that some highly polar as well as thermally labile compounds may have escaped detection. To our knowledge, no other authors have reported on the formation of halogenated organic byproducts in heterogeneous photocatalysis.

Studies regarding the reduction in trihalomethane (THM) formation potential are found in Section 2.3.1.

2.5 Design of experiments (DoE)

Statistical experimental design, also known as design of experiments (DoE) refers to a set of statistical tools that are particularly valuable for assessing the effect several variables acting simultaneously have on one or more responses of interest (Lapin, 1997). These techniques are especially useful when the underlying physical relationship between independent and dependent variables is not exactly known, i.e. when there is a lack of a physical model. Such systems can nonetheless be experimentally explored and useful conclusions may be drawn if the relationship between independent and dependent variables is known or may be reasonably assumed to be smooth apart from experimental error. In this case, it may be possible to fit some simple smooth functions (e.g. linear or quadratic) to the data yielding an empirical model of the system (Box and Draper, 1987).

2.5.1 Factorial designs

Factorial designs are useful for efficiently exploring an experimental region. The most common type of factorial design is that carried out at two levels (coded ± 1), and can

be used to study main (one-variable) and interaction (two or more variables together) effects of selected variables (factors) on one or more responses of interest. These designs include all possible combinations of the two levels for each variable and thus require 2^k experimental runs, where k is the number of factors to be studied (Box et al., 2005; Lapin, 1997). In addition to the 2^k runs, runs performed at the center of the experimental region are added to the design ("center points"). These center points have two main functions:

1. they provide an estimate of the experimental error for unreplicated factorials, i.e. when only the center points are repeated as genuine replicate runs
2. they provide a way of testing the adequacy of the fitted linear models (see below)

Two-level full factorial designs for $k = 2$, 3, and 4 are presented in Table 2.4.

An important feature of factorial designs in two levels is the ease with which they can be analyzed by using common sense, graphical procedures and elementary arithmetic (Box and Draper, 1987; Box et al., 2005). Because the data are uniformly distributed over the entire experimental region, the results are useful even in the absence of an adequate fit of the selected model. However, it is advantageous to use an empirical model to approximate the data, especially when more than two variables are considered. In general, a 2^k full factorial design can be used to fit a linear model including main and interaction effects of all variables. In the simplest case (two variables), this is

$$\underbrace{y}_{\text{response}} = \underbrace{\beta_0}_{\text{mean response}} + \underbrace{\beta_1 x_1 + \beta_2 x_2}_{\text{main effects}} + \underbrace{\beta_{12} x_1 x_2}_{\text{interaction effect}} \tag{2.12}$$

and for the case of $k = 4$ this becomes

$$\begin{aligned} \underbrace{y}_{\text{response}} = \underbrace{\beta_0}_{\text{mean response}} &+ \underbrace{\beta_1 x_1 + \beta_2 x_2 + \beta_3 x_3 + \beta_4 x_4}_{\text{main effects}} \\ &+ \underbrace{\beta_{12} x_1 x_2 + \beta_{13} x_1 x_3 + \beta_{23} x_2 x_3 + \beta_{14} x_1 x_4 + \beta_{24} x_2 x_4 + \beta_{34} x_3 x_4}_{\text{first-order or two-way interaction effects}} \\ &+ \underbrace{\beta_{123} x_1 x_2 x_3 + \beta_{124} x_1 x_2 x_4 + \beta_{134} x_1 x_3 x_4 + \beta_{234} x_2 x_3 x_4}_{\text{second-order or three-way interaction effects}} \\ &+ \underbrace{\beta_{1234} x_1 x_2 x_3 x_4}_{\text{third-order or four-way interaction effect}} \end{aligned} \tag{2.13}$$

Thus, the observed response is fitted in terms of deviations from the mean response owing to changes in the variables of interest (x_k, scaled and centered, ± 1). The regression coefficients (β) can be easily obtained through least-squares regression. Notice

Table 2.4: Experimental matrix for a 2^2 (left), 2^3 (center), and 2^4 (right) full factorial designs.

x_1	x_2
$+1$	$+1$
$+1$	-1
-1	$+1$
-1	-1
0	0

x_1	x_2	x_3
-1	-1	-1
-1	-1	$+1$
-1	$+1$	-1
-1	$+1$	$+1$
$+1$	-1	-1
$+1$	-1	$+1$
$+1$	$+1$	-1
$+1$	$+1$	$+1$
0	0	0

x_1	x_2	x_3	x_4
-1	-1	-1	-1
-1	-1	-1	$+1$
-1	-1	$+1$	-1
-1	-1	$+1$	$+1$
-1	$+1$	-1	-1
-1	$+1$	-1	$+1$
-1	$+1$	$+1$	-1
-1	$+1$	$+1$	$+1$
$+1$	-1	-1	-1
$+1$	-1	-1	$+1$
$+1$	-1	$+1$	-1
$+1$	-1	$+1$	$+1$
$+1$	$+1$	-1	-1
$+1$	$+1$	-1	$+1$
$+1$	$+1$	$+1$	-1
$+1$	$+1$	$+1$	$+1$
0	0	0	0

that the coefficients obtained in this way are independent of each other as a consequence of the orthogonality of the full factorial design (Box et al., 2005).

Because the center points are excluded from the calculation of the regression coefficients, a comparison of β_0 with the mean response obtained at the center point provides a simple goodness-of-fit test: if β_0 is significantly different (in the statistical sense) from the mean response at the center point, this is a strong indication that the assumed linear model does not adequately describe the data (Box and Draper, 1987).

The magnitude of the coefficients (β_i) is a direct measure of the influence of each variable on the chosen response. Notice that this only holds when scaling and centering the variables and that the magnitude of the coefficients reflects the mean difference in the measured variable when comparing experiments with the "high" ($+1$) and "low" (-1) setting for each variable. As a consequence, the range of the independent variable, U_i, has an effect on the magnitude of β_i and must be judiciously chosen. Equation (2.12) and 2.13 can be converted to real units by substituting

$$x_i = \frac{U_i - U_{0,i}}{\Delta U} \tag{2.14}$$

into the corresponding equation for each $i = 1, 2, 3, 4$; U_i is the "real" variable, $U_{0,i}$ is the center of the experimental range for variable i, and ΔU is the step size ($\Delta U = U_{max,i} - U_{0,i} = U_{0,i} - U_{min,i}$). Notice, however, that it is not possible to directly compare the magnitude of these "real" coefficients in the same way as those for the dimensionless variables x_i.

2.5.2 Box-Behnken designs

If there is curvature in the system, the response cannot be adequately described by a first-order model. The simplest way to account for curvature is the use of a second-order polynomial such as (Montgomery, 1997):

$$\begin{aligned} \underbrace{y}_{\text{response}} = \underbrace{\beta_0}_{\text{mean response}} &+ \underbrace{\beta_1 x_1 + \beta_2 x_2 + \beta_3 x_3}_{\text{main effects}} + \underbrace{\beta_{11} x_1^2 + \beta_{22} x_2^2 + \beta_{33} x_3^2}_{\text{quadratic terms}} \\ &+ \underbrace{\beta_{12} x_1 x_2 + \beta_{13} x_1 x_3 + \beta_{23} x_2 x_3}_{\text{first-order interaction effects}} \end{aligned} \tag{2.15}$$

on the case of three variables where only 2-way interactions are considered (cf. Equations 2.12 and 2.13). Box and Behnken (1960) introduced three-level designs that are

appropriate for fitting models such as Equation 2.15. The experimental matrix for a Box-Behnken design is given in Table 2.5 for the case of three variables. Notice that the notation ± 1 denotes the four runs of a 2^2 factorial (cf. Table 2.4). We note that the Box-Behnken design for 3 factors has a uniform distance pattern between experimental points and is equivalent to the uniform shell design later introduced by Doehlert (1970).

Table 2.5: Distribution of points for the Box-Behnken design in three variables. Each of the first three lines corresponds to a 2^2 full factorial design at the "0" level of the remaining variable. The last line is the "center point" and should be performed in triplicate.

x_1	x_2	x_3
± 1	± 1	0
± 1	0	± 1
0	± 1	± 1
0	0	0

2.5.3 Screening design

Sometimes the factors affecting a given response are not known or there are too many possibly important factors to be economically studied by using full factorial designs. Screening designs are especially crafted to address this situation. The simplest form of screening designs are fractional factorial designs (Box et al., 2005).

A very efficient type of screening design is due to Plackett and Burman (1946). These designs exist for any number of factors that is a multiple of 4 (Box et al., 2005). For example, a design including a total of 12 experimental runs is able to accommodate up to 11 variables is shown in Table 2.6. An important advantage of this design is its projectivity: if only three variables/factors are "active" then in most cases a 2^3 full factorial plus a half replicate (2^{3-1} fractional factorial) can be obtained. If only two variables are active, a 2^2 factorial is always obtained in triplicate.

2.5.4 Identification of important factors

The models fitted as described above will necessarily give a good fit to the data (fitting n points with $n-1$ coefficients). It is therefore essential to identify the factors

Table 2.6: Plackett-Burman design for up to 11 variables.

x_1	x_2	x_3	x_4	x_5	x_6	x_7	x_8
$+1$	$+1$	$+1$	$+1$	$+1$	$+1$	$+1$	$+1$
-1	-1	$+1$	-1	-1	-1	$+1$	$+1$
-1	$+1$	-1	-1	-1	$+1$	$+1$	-1
$+1$	-1	-1	-1	$+1$	$+1$	$+1$	$+1$
-1	-1	-1	$+1$	$+1$	$+1$	-1	-1
-1	-1	$+1$	$+1$	$+1$	-1	$+1$	-1
-1	$+1$	$+1$	$+1$	-1	$+1$	-1	$+1$
$+1$	$+1$	$+1$	-1	$+1$	-1	-1	-1
$+1$	$+1$	-1	$+1$	-1	-1	$+1$	-1
$+1$	-1	$+1$	-1	-1	$+1$	-1	-1
-1	$+1$	-1	-1	$+1$	-1	-1	$+1$
$+1$	-1	-1	$+1$	-1	-1	-1	$+1$

(main and interaction effects) that most influence the response of interest and discard those that are easily explained by random variation. Below, we describe three techniques that aid in this process.

Daniel plot

The first of these techniques is due to Daniel (1959) and is best described by an example, shown in Figure 2.4. The procedure consists of plotting the factor effects on normal probability paper. In this representation, points approximately falling on a straight line can be disregarded as being explainable by random variation (noise). Those points falling away from the line are not easily explained by chance and may be viewed as important (Box et al., 2005).

Lenth plot

The second technique is due to Lenth (1989) and compares the magnitude of each factor effect to the median, m, of the absolute values of k factor effects. Lenth (1989) defines

$$s_0 = 1.5 \times \text{median} \left|\text{factor effects}\right| \tag{2.16}$$

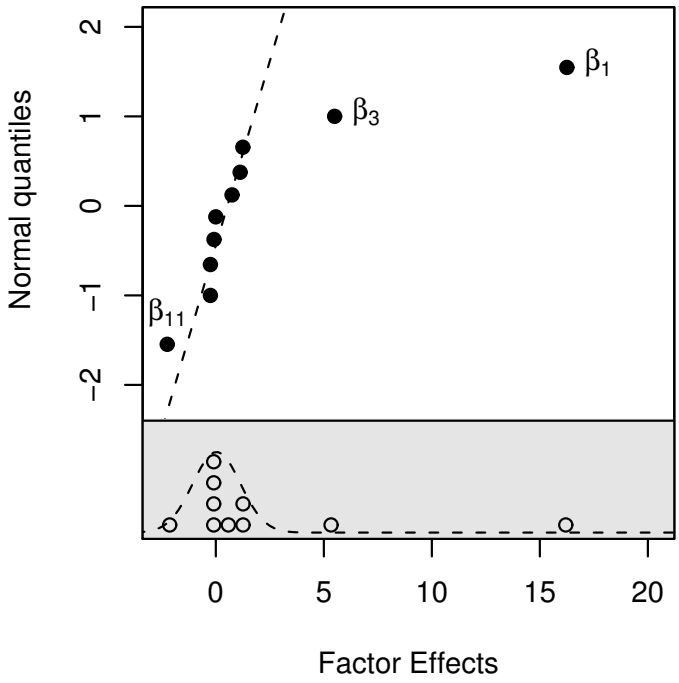

Figure 2.4: Graphical evaluation of regression coefficients. The upper part of the graph is the Daniel plot. Here, the magnitude of the factor effects is plotted on the horizontal axis against their "normal quantiles" (sometimes also referred to as "normal scores"). The vertical axis is scaled such that values derived from a normal distribution fall in a straight line (for more details see Box et al., 2005, Ch. 2 and 5). For the sample data set above, it becomes evident in this representation that all points except β_1 and β_3 approximately fall in a straight line, termed by Box et al. (2005) an "error line" since the points on it may be easily explained by noise alone. β_{11} neither completely falls on the line nor deviates clearly from it, and highlights the need for subject matter knowledge when deciding on which factors are important and which not. Projecting all points onto the horizontal axis (shaded area), we recognize that the points on the error line have a mean close to zero and are approximately normally distributed. The dashed density curve is intended as a guide to the eye. Fitted model: $y = \beta_0 + \beta_1 x_1 + \beta_2 x_2 + \beta_3 x_3 + \beta_{11} x_1^2 + \beta_{22} x_2^2 + \beta_{33} x_3^2 + \beta_{12} x_1 x_2 + \beta_{13} x_1 x_3 + \beta_{23} x_2 x_3$. Data from Tercero Espinoza et al. (2007).

and a pseudo standard error (PSE) as

$$\text{PSE} = 1.5 \times \text{median} \left| \text{factor effects} < 2.5 \times s_0 \right| \tag{2.17}$$

where all effects are included in m in equation 2.16 but only effects $< 2.5 \times s_0$ are included in m in equation 2.17. The PSE can then be used to construct an approximate 95% confidence interval ("margin of error", ME)

$$\text{ME} = t_{0.975,d} \times s_0 \tag{2.18}$$

Factors larger than ME (in absolute value) are then labeled as "significant". To minimize false positives, a "simultaneous margin of error" (SME) is defined as

$$\text{SME} = t_{\gamma,d} \times s_0 \qquad \text{with} \qquad \gamma = \frac{1 + 0.95^{1/k}}{2} \tag{2.19}$$

Factors exceeding the SME level are then considered "active" (i.e. non-zero), while those below the ME are considered "inert". A gray area remains between ME and SME, for factors considered "significant" but not "active" (Box et al., 2005; Lenth, 1989). An example of a Lenth plot is shown in Figure 2.5 using the same data as Figure 2.4.

Bayes screening and model discrimination

This procedure, introduced by Box and Meyer (1986) and discussed in Box et al. (2005), is intended for the identification of important factors in screening experiments. It fits a series of linear models including all variables (one at a time, two at a time, etc., including the possibility that no variable produces an effect) to the data and returns the probability that a given variable is "actively" involved in determining the response based on the fitted models. "Activity" is defined here as the variable producing an effect (increase or decrease in the response) on its own or in combination with any one other variable. Additionally, it is possible to compute probabilities for several competing models including a subset or all of the variables considered. There is freely-available code (Barrios, 2005) implementing this procedure for the programming environment R (R Development Core Team, 2007), making it easy to use in spite of its relative complexity.

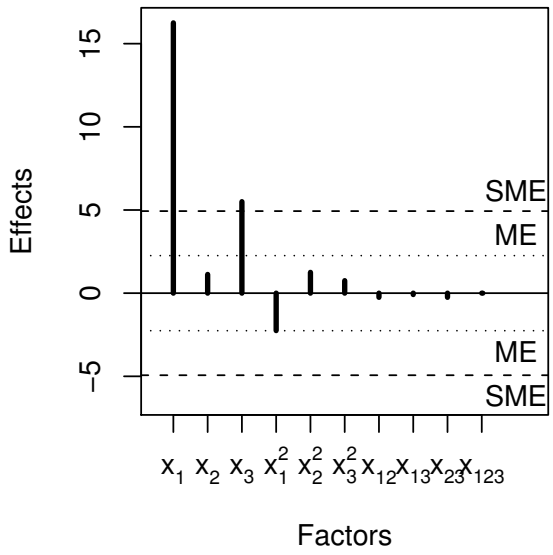

Figure 2.5: Graphical evaluation of regression coefficients with a Lenth plot (Box et al., 2005). Factors x_1 and x_3 but not x_{11} are shown as "active". x_{11} falls in the gray area where an argument can be made for and against its "importance", emphasizing that this plot is a tool to supplement but not substitute subject matter knowledge. Fitted model: $y = \beta_0 + \beta_1 x_1 + \beta_2 x_2 + \beta_3 x_3 + \beta_{11} x_1^2 + \beta_{22} x_2^2 + \beta_{33} x_3^2 + \beta_{12} x_1 x_2 + \beta_{13} x_1 x_3 + \beta_{23} x_2 x_3$. Data from Tercero Espinoza et al. (2007).

Chapter 3

Materials and Methods

3.1 Chemicals

Chemical/Material	Formula	Grade	Source
1,10-Phenanthroline	$C_{12}H_8N_2$	p.a.	Merck
2,4-dihydroxybenzoic acid (DHBA)	$C_7H_6O_4$	purum	Fluka
Copper chloride	$CuCl_2 \cdot 2H_2O$	p.a.	Merck
Copper sulfate	$CuSO_4$	98%	Aldrich
Ferric chloride	$FeCl_3 \cdot 6H_2O$	p.a.	Merck
Ferric sulfate	$Fe_2(SO_4)_3 \cdot 5H_2O$	p.a.	Fluka
Hombikat UV100	TiO_2*		Sachtleben Chemie
Manganese chloride	$MnCl_2 \cdot 4H_2O$	p.a.	Fluka
P25	TiO_2†		Degussa
Phenylglyoxilic acid	$C_8H_6O_3$	purum	Fluka
Potassium bromate (0.1 N solution)	$KBrO_3$	Titriplex	Merck
Potassium bromide	KBr	p.a.	Merck
Potassium oxalate	$K_2C_2O_4$	p.a.	Merck
Salicylic acid	$C_7H_6O_3$	ACS reagent	Sigma-Aldrich

*100% anatase, BET surface area > 250 m^2/g
†approx. 75% anatase and 25% rutile, BET surface area = 50 ± 15 m^2/g

Chemical/Material	Formula	Grade	Source
Sodium acetate	$NaC_2H_3O_2$	p.a.	Merck
Sodium bromide (std. solution, 1000 mg L^{-1})	NaBr		Merck
Sodium carbonate, anhydrous	Na_2CO_3	p.a.	Merck
Sulfuric acid (95-97%)	H_2SO_4	p.a.	Merck
Zinc chloride	$ZnCl_2$	p.a.	Merck

3.2 Analytical methods

3.2.1 Wet chemical oxidation with carbon dioxide detection

Quantification of dissolved organic carbon (DOC) was performed by a wet chemical method using a Total Organic Carbon (TOC) Analyzer 820 (Sievers Instruments, Boulder, USA). Briefly, the samples were filtered through previously rinsed 0,45 µm membrane filters and injected into the TOC analyzer using an autosampler. In the TOC analyzer, the samples are first acidified with phosphoric acid to shift the equilibrium for inorganic carbon from CO_3^{2-} and HCO_3^- to CO_2, which is removed by vacuum. Then the samples are UV-irradiated (185 and 254 nm) in the presence of an oxidizing agent ($(NH_4)_2S_2O_8$) to fully oxidize the DOC to carbon dioxide, water and inorganic acids. The formed CO_2 is quantified through electrical conductivity after separation with a semipermeable membrane. A simplified scheme of the procedure is presented in Figure 3.1 (Sievers Instruments, 1999).

3.2.2 Size exclusion chromatography with dissolved organic carbon and ultraviolet detection (SEC-DOC and SEC-UV)

Size exclusion chromatograms were recorded using the SEC-DOC/UV system described by Huber and Frimmel (1991). In this system, shown schematically in Figure 3.2, a photochemical oxidation of the sample components is carried out using a low-pressure mercury lamp in a rotating thin-film reactor. Toyopearl HW 50S resin (Tosoh Corp., Japan) packed in a Novogrom column (length: 250 mm, inner diameter: 20 mm; Alltech Grom, Germany) served as stationary phase, while phosphate eluent (1.5 g L^{-1} $Na_2HPO_4 \cdot 2H_2O$ + 2.5 g L^{-1} KH_2PO_4) flowing at a rate of 1 mL min^{-1}

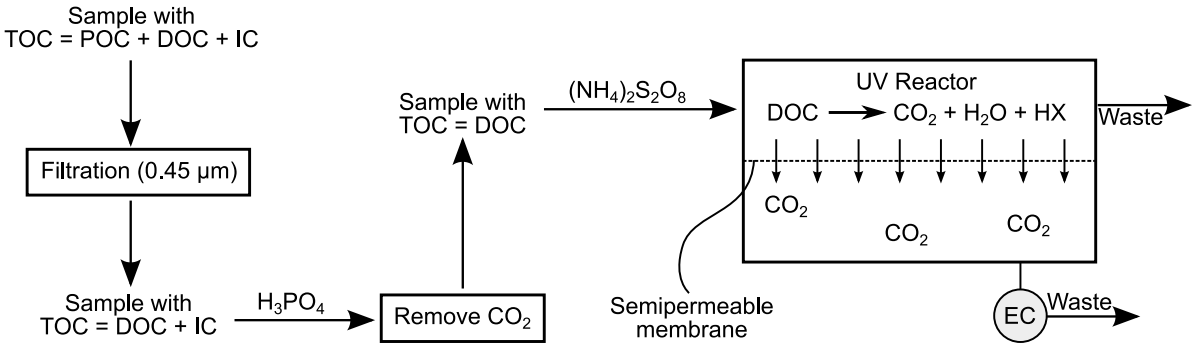

Figure 3.1: Schematic representation of the sample preparation and measurement of dissolved organic carbon (DOC). TOC = total organic carbon; POC = particular organic carbon; IC = inorganic carbon; EC = electrical conductivity.

served as the mobile phase for separation. Samples were filtered (0.45 µm) and diluted 1:5 prior to analysis. The injection volume was 1 mL and the DOC concentration of each sample was calculated on the basis of an external calibration using potassium hydrogen phthalate as a standard.

Under the conditions used, totally excluded molecules eluted after a retention time, $t_r = 28.7$ min (t_e), while totally permeating molecules eluted at $t_r = 66.3$ min (t_p). The dimensionless distribution coefficient, K_D, is often used for comparison purposes and is defined as:

$$K_D = \frac{t_r - t_e}{t_p - t_e} \tag{3.1}$$

Thus, molecules whose t_r is determined primarily through size exclusion elute with $0 < K_D < 1$. Hydrophobic interactions of the analyte molecules with the column packing material lead to longer t_r, and strongly interacting analytes may remain attached to the column material Specht and Frimmel (2000).

Ultraviolet absorption was recorded at $\lambda = 254$ nm.

3.2.3 Inductively coupled plasma-optical emission spectroscopy (ICP-OES)

Measurements of total metal concentrations were performed by means of inductively coupled plasma optical emission spectroscopy (ICP-OES) using a Vista-Pro CCD si-

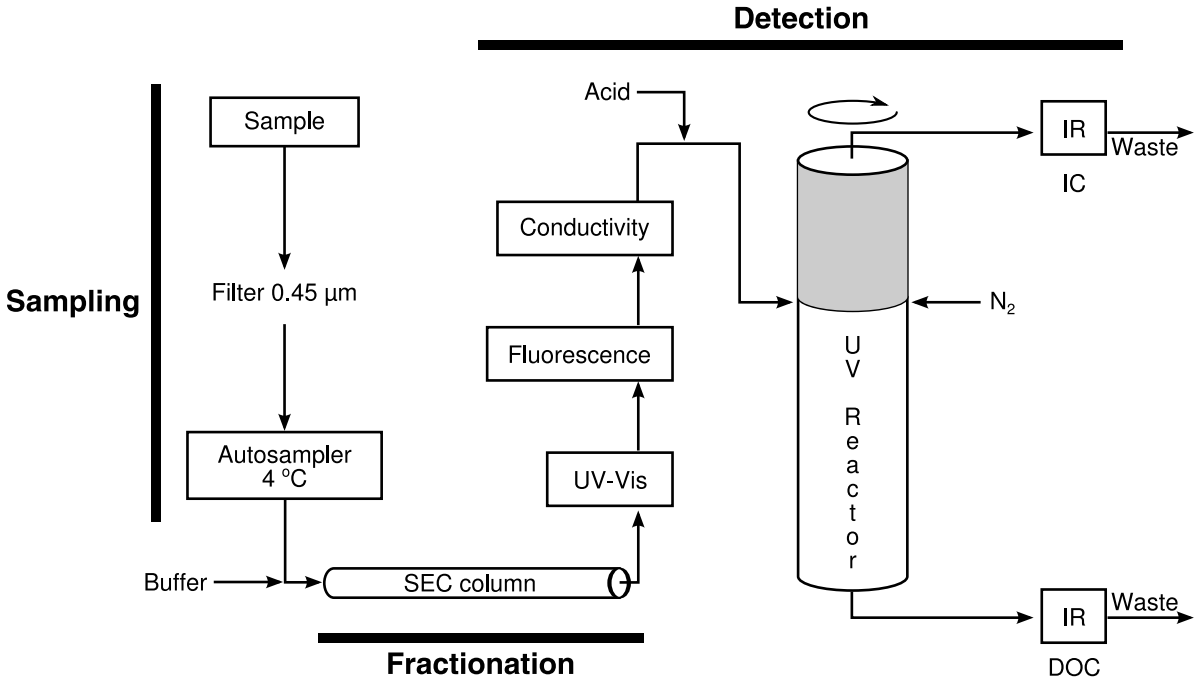

Figure 3.2: Schematic representation of the analytical setup for the quantification of UV absorption and DOC after size exclusion chromatography.

multaneous ICP-OES spectrometer (Varian). A schematic of the instrument is presented in Figure 3.3.

The wavelengths used were: $\lambda = 327.395$ nm for Cu, $\lambda = 238.204$ nm for Fe, $\lambda = 257.610$ nm for Mn, and $\lambda = 206.200$ nm for Zn. Yttrium was used as an internal standard ($\lambda = 377.433$ nm).

3.2.4 Coulometric titration

The determination of organically-bound halogens adsorbable onto activated carbon (AOX) was performed following EN 1485:1996 using an Euroglas ECS 1200 TOX analyzer (Thermo Electron GmbH, Dreieich, Germany). Briefly, 50 mg halogen-free activated carbon (LHG-Laborgeräte, Karlsruhe, Germany) were added to 100 mL samples (filtered) in Erlenmeyer flasks. 5 mL of a 0.2 M $NaNO_3$ solution were added to the mixture and the pH was adjusted to approx. 3 with HNO_3. The samples were left to shake overnight. After filtration of the samples, the halogen content of the activated carbon was measured with the TOX analyzer (combustion to generate HX, detection of HX by coulometric titration). The measurement principle for AOX is schematically shown in Figure 3.4 (Euroglas Analytical Instruments, 1995). The

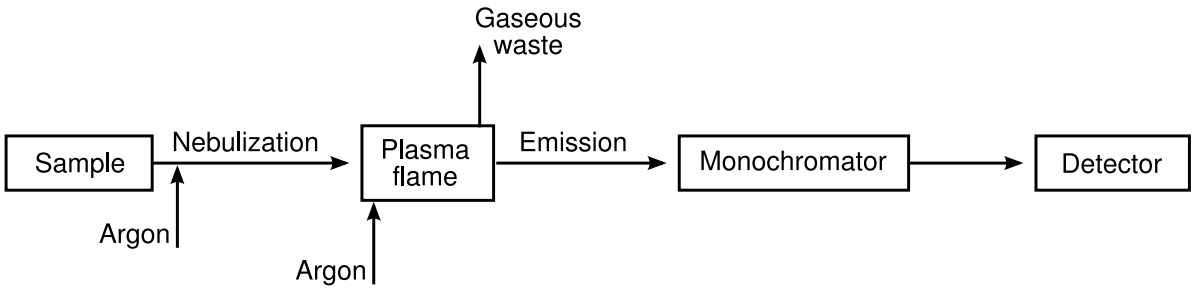

Figure 3.3: Schematic representation of the ICP-OES setup. Energy for the argon plasma is supplied by means of a magnetic field oscillating at high frequency. The temperature in the plasma is typically around 6000 K (Skoog and Leary, 1996).

detection limit (calculated as the mean of the blank measurements, $n = 16$, plus 3 standard deviations) was 7 µg/L Br^-.

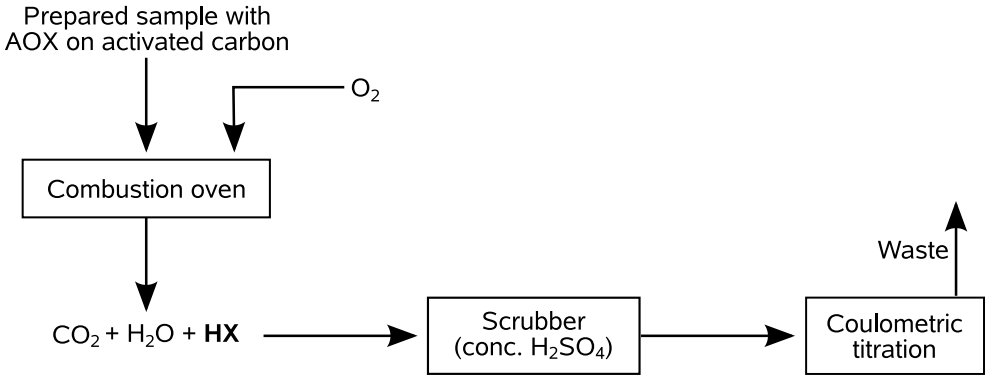

Figure 3.4: Schematic representation of the sample preparation and measurement of organically-bound halogens adsorbable onto activated carbon (AOX).

3.2.5 Ion exchange chromatography (IC)

Ion chromatography (IC) analyses were performed using a Dionex DX500 system equipped with an ASRS Ultra suppressor coupled to an ED40 conductivity detector as shown in Figure 3.5.

Determination of low molecular weight organic acids (LMWOA)

For the determination of low molecular weight organic acids in filtered samples (0.45 µm), the eluent was aqueous KOH with concentrations given in Table 3.2. The gradi-

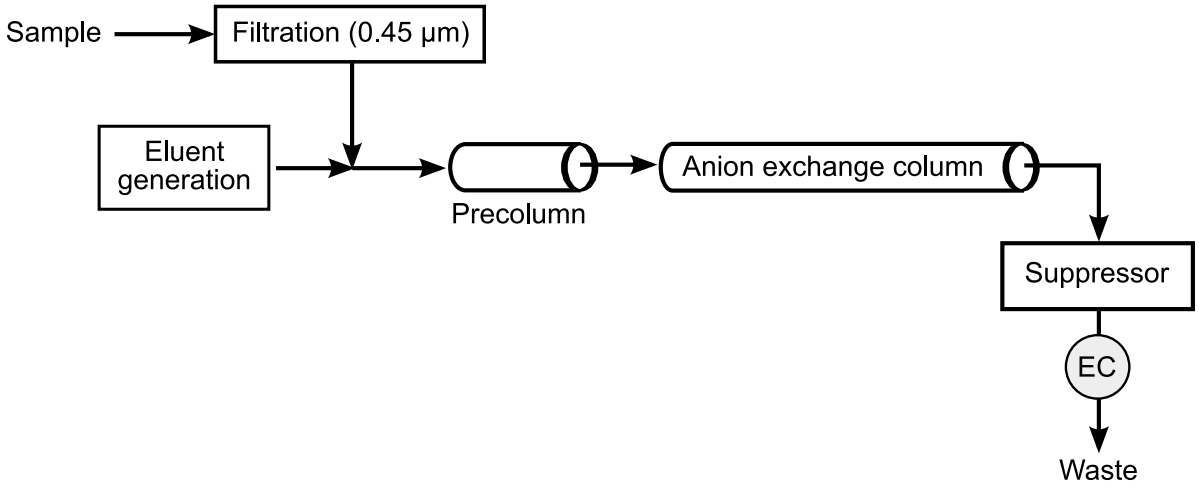

Figure 3.5: Usual setup for ion chromatography measurements. EC = electrical conductivity.

ent was prepared using Milli-Q® water previously degassed with helium (5.0). The column used was an IonPac® AS11 with AG11 pre-column.

Table 3.2: KOH gradient program used for the quantification of low molecular weight organic acids.

Duration / min	Concentration / mmol L^{-1}	Comment
10	35.0	column regeneration
5	0.2	equilibration
10	0.2 - 15.0	injection + gradient start
5	15.0 - 21.7	continue gradient, end

Determination of bromide (Br^-) and bromate (BrO_3^-)

The eluent was 9 mmol L^{-1} Na_2CO_3 (isocratic, no eluent generation). The quantification limit for BrO_3^- was 5 µg L^{-1} using an IonPac® AS9-SC column with AG9-SC pre-column. Complementary measurements were performed using the same column but 20 mmol L^{-1} $(NH_4)_2CO_3$ as eluent with ion coupled plasma-mass spectrometry (ICP-MS) detection.

3.2.6 High performance liquid chromatography (HPLC)

Measurements of 2,4-dihydroxybenzoic acid were performed by reversed-phase high performance liquid chromatography[‡] (RP-HPLC) using an HP 1100 HPLC system with Chemstation software coupled to an HP 1100 diode array detector (Agilent Technologies, Germany). Separations were carried out with a Purospher-RP18e column (dimensions 250 mm × 4 mm, 5 μm; Merck, Germany). The injection volume was 20 μL. The mobile phase was a linear gradient of phosphate buffer (A) and methanol (B) from A:B = 80:20 to A:B = 25:75 over 25 minutes at a flow rate of 1.0 mL min^{-1}.

3.2.7 Photometry

The concentration of Br_2 in solution was determined using a photometric method (Spectroquant©, Merck, Germany) calibrated in the range 0.020-1.500 mg/L Br_2. Absorption measurements (565 nm) were performed using a 5 cm quartz glass cuvette in a single beam photometer (SQ300, Merck, Germany).

3.2.8 Gas chromatography

Trihalomethanes (THMs) were analyzed using gas chromatography on an HP 6890 system equipped with a DB-5ms (J & W Scientific, Folsom, CA, USA) fused silica capillary column (length: 30 m, inner diameter: 0.25 mm, film thickness: 0.25 μm; (5% phenyl)-methoxypolysiloxane) coupled to an electron capture detector (Buffington and Wilson, 1987). The samples for THM measurements were not filtered prior to analysis.

Samples for injection into the column were drawn from the headspace of air-tight closed vessels after equilibration for 5 min at 65 °C under constant stirring (350 RPM). The injector, initially at -40 °C, is heated to 250 °C at a rate of 12 °C s^{-1} and held at this temperature for 5 min. The sample was then fractionated in the capillary column (carrier gas: N_2 flowing at 1 mL min^{-1}). The temperature in the oven was increased from initially 40 °C to 175 °C at a rate of 30 °C min^{-1}. This is shown schematically in Figure 3.6.

[‡]The measurement setup is conceptually equivalent to that shown in Figure 3.5 with different column, eluent and detector as specified in the text.

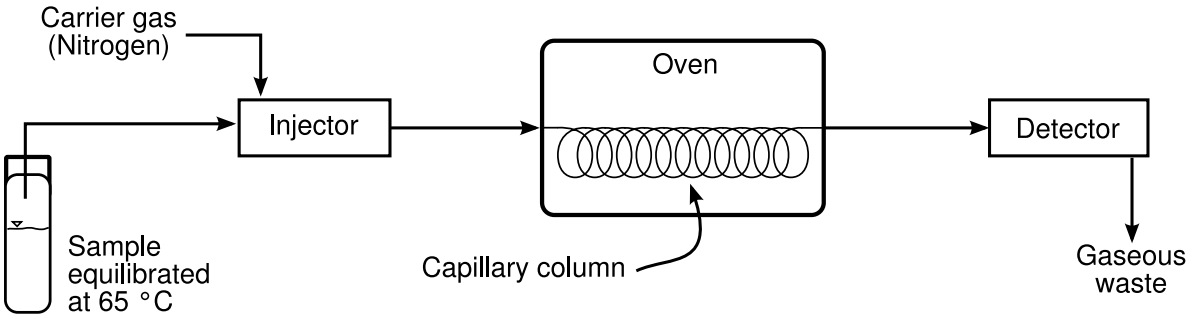

Figure 3.6: Simplified schematic representation of a gas chromatograph for analysis of headspace samples (modified from Fox and Whitesell, 1997).

Quantification was done through an external calibration using standards. The detection limits for $CHCl_3$, $CHCl_2Br$, $CHClBr_2$, and $CHBr_3$ were 0.4 µg L^{-1}, 0.2 µg L^{-1}, 0.5 µg L^{-1}, and 0.8 µg L^{-1}, respectively.

3.3 Experimental equipment and procedures

3.3.1 For Chapter 4

Irradiation procedure

20 mg TiO_2 (P25, Degussa, Germany) were suspended in 40 mL of lake Hohloh water, previously filtered through 0.45 µm cellulose acetate membrane filters (DOC = 21 mg L^{-1}). Lake Hohloh water was extensively described by Frimmel et al. (2002) among others. Samples were sonicated for 10 min prior to irradiation.

The samples were irradiated using a solar UV simulator with an atmospheric attenuation filter installed in the radiation beam (Oriel Corp., Stratford, CT, USA). The samples were stirred, open to the atmosphere, and irradiated from above by a homogeneous light field. The sample volume was 40 mL in all experiments, with an irradiation pathlength of ≈ 3.5 cm.

The incident photon flux was determined by chemical polychromatic actinometry using phenylglyoxylic acid in a mixture of acetonitrile (AcN) and ultrapure water (MilliQ) at a volume ratio 3:1 (Defoin et al., 1986). The photon flow in the UV range ($290 < \lambda < 400$ nm) of the solar UV simulator estimated by this method was 1×10^{-7} einstein s^{-1}.

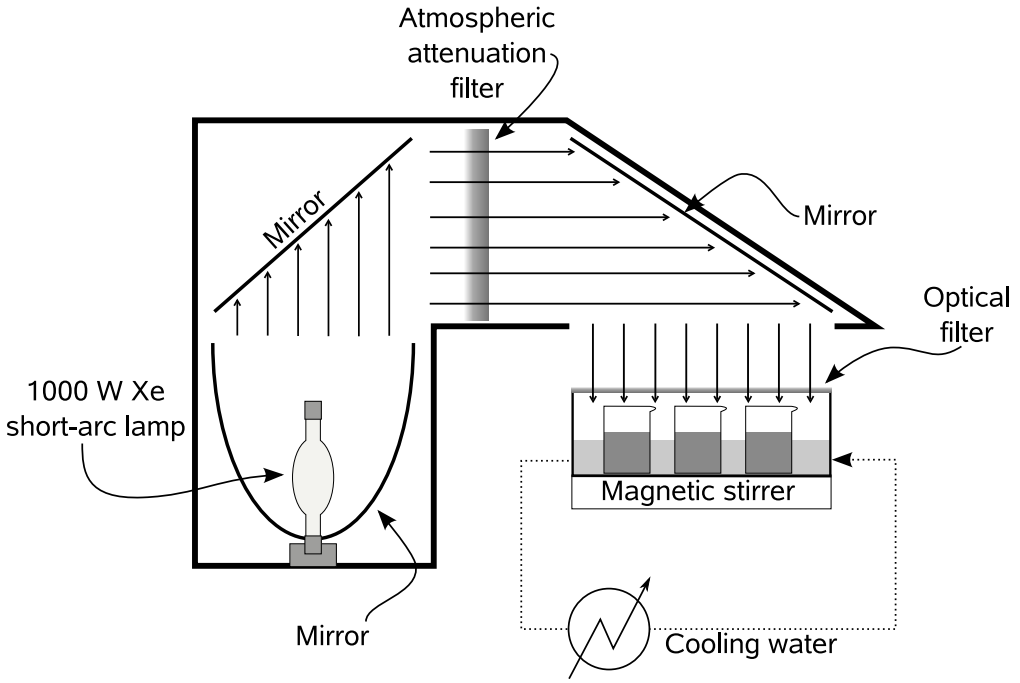

Figure 3.7: Simplified scheme of the solar simulator.

Degradation experiments with bacteria from activated sludge

4 mL of activated sludge inoculum (mixed from two wastewater treatment plants, one municipal and one industrial) were added to 50 mL of the irradiated samples (filtered 0.45 μm to remove the TiO_2 particles). The samples were then incubated on a shaker (70 RPM) kept in the dark for 48 h at 36 °C.

After incubation, the samples were filtered and characterized by means of SEC-DOC. The difference between the SEC-DOC chromatograms before and after incubation was used as an estimate of the biodegradability of the samples.

3.3.2 For Chapter 6

The irradiation procedure as well as the experiments without added metals and the biodegradation experiments were as described in Section 3.3.1.

Experiments with added metals

Lake Hohloh water was mixed with an appropriate amount of $CuSO_4$, $FeCl_3$, $ZnCl_2$, and $MnCl_2$ solutions and let stand for a minimum of 3 days in the dark. This spiked water was used instead of the original lake Hohloh water in the procedure described in Section 3.3.1. In order to systematically explore the experimental region, we turned to a full factorial design for 4 variables in 2 levels (2^4 experimental runs, see Table 2.4), which comprise all possible combinations of the $+1$ and -1 levels shown in Table 3.3, plus repetitions of the "center point" (level "0" for all variables; see Box et al., 2005).

Table 3.3: Variable settings for the 2^4 full factorial design used in Chapter 6.

		Variable setting		
Variable	Coded var.	-1	0	$+1$
$c_{\text{added}}(Cu^{2+})$	x_1	0 µmol L^{-1}	5 µmol L^{-1}	10 µmol L^{-1}
$c_{\text{added}}(Fe^{3+})$	x_2	0 µmol L^{-1}	5 µmol L^{-1}	10 µmol L^{-1}
$c_{\text{added}}(Zn^{2+})$	x_3	0 µmol L^{-1}	5 µmol L^{-1}	10 µmol L^{-1}
$c_{\text{added}}(Mn^{2+})$	x_4	0 µmol L^{-1}	5 µmol L^{-1}	10 µmol L^{-1}

3.3.3 For Chapter 7

Experimental design

The screening experiments followed a Plackett-Burman design for 11 variables as described in Section 2.5.3. The corresponding variable levels are shown in Table 3.4.

Non-thermostated reactor

The experimental arrangement for the experiments presented in Chapter 7 consisted of a 1 L glass vessel (reservoir) connected to a pump and reactor by PTFE tubing. The reactor consisted of a quartz glass tube into which a 14 W low pressure Hg lamp (Katadyn, Switzerland) was inserted. This was in turn coaxially fitted into a glass tube. The photon flux was 5.3×10^{-6} einstein $\cdot\, s^{-1}$ as determined by chemical actinometry with potassium ferrioxalate performed according to Braun et al. (1991).

The suspension was pumped into the space between the glass tubes and recycled into the reservoir. The reaction volume was $\approx$ 125 mL and the total aqueous volume of

Table 3.4: Variable settings for the screening design used in Chapter 7

		Variable setting	
Variable	Coded var.	$+1$	-1
TiO_2	x_1	P25	Hombikat UV100
$\rho(TiO_2)$	x_2	1.0 g L^{-1}	0.5 g L^{-1}
Source of DOC	x_3	Lake Hohloh water	salicylic acid
ρ_o(DOC)	x_4	10 mg L^{-1}	1 mg L^{-1}
$\rho_o(Br^-)$	x_5	3.0 mg L^{-1}	1.0 mg L^{-1}
Matrix	x_6	Karlsruhe drinking water	demineralized water
pre-heating	x_7	yes	no
Irradiation time	x_8	45 min	15 min

the system was $\approx$ 1.3 L. Because the system was not thermostated, the suspension gradually heated up during the course of irradiation (20 °C $< T <$ 45 °C), mostly due to friction from the centrifugal pump. This warming-up process was similar in all experimental runs so that the experiments are comparable among themselves. Photocatalytic reaction rates are known to be insensitive to small temperature changes (Fox and Dulay, 1993).

For the screening experiments, the "pre-heating" variable was set as follows: "+1" indicated the system was pre-heated overnight, allowing the system to equilibrate with the surrounding air. Experiments with this setting had an average temperature of 41 $\pm$ 2 °C and an average temperature change during irradiation of 3 $\pm$ 1 °C. Experiments with the setting "−1" were performed without any pre-heating, and had an average temperature of 29 $\pm$ 3 °C and an average temperature change during irradiation of 11 $\pm$ 1 °C for long irradiation times (45 min) and 3 $\pm$ 1 °C for short irradiation times (15 min). This temperature range is typical for experiments using solar irradiation (e.g. up to 45 °C, Kositzi et al., 2004).

Sample preparation

Samples of the TiO_2 suspensions in the absence of DOC were filtered through 0.22 µm polycarbonate membrane filters (Isopore, Millipore, Ireland) and immediately examined using a Spectroquant rapid Br_2 test (Merck, Germany). Screening samples were also filtered for AOX measurements but no measurements of Br_2 were performed. A portion of each sample was saved for analysis using ion chromatography (IC).

Samples from the irradiation of 2,4-dihydroxybenzoic acid were filtered (0.45 μm, PTFE, Wicom, Germany) for HPLC and DOC analysis.

Samples for THM measurements were not filtered.

3.3.4 For Chapter 8

Experimental design

Experiments were performed following a Box-Behnken design for three variables (Section 2.5.2) with variable levels as presented in Table 3.5.

Table 3.5: Variable settings for the Box-Behnken design.

		Variable setting		
Variable	Coded variable	-1	0	$+1$
$\rho(TiO_2)$	x_1	0.5 g L^{-1}	1.0 g L^{-1}	1.5 g L^{-1}
$\rho_0(Br^-)$	x_2	1 mg L^{-1}	2 mg L^{-1}	3 mg L^{-1}
ρ_0(DHBA)	x_3	2 mg L^{-1}	6 mg L^{-1}	10 mg L^{-1}

Irradiation procedure

The irradiation procedure was similar to that described in Section 3.3.1 regarding the irradiation equipment but using suspensions as specified by the Box-Behnken design using the settings in Table 3.5. The volume of the suspensions was 50 mL.

Sample preparation

The preparation of the samples for measurements of 2,4-dihydroxybenzoic acid, dissolved organic carbon and trihalomethanes was as described in Section 3.3.3.

3.3.5 For Chapter 9

Thermostated reactor

The irradiation experiments were carried out in the reactor described in Section 3.3.3 but with an added cooling coil connected to running water. The temperature in the reactor was 21 ± 1°C.

Sample preparation

Two TiO_2 powders were used: P25 and Hombikat UV100 (see Figure 2.1 and Table 2.2). Water from Lake Hohloh (northern Black Forest) and 2,4-dihydroxybenzoic acid were used as sources of dissolved organic carbon (DOC). The titanium dioxide suspensions had the following composition:

- $\rho(TiO_2) = 1.5$ g L^{-1}
- $\rho_0(Br^-) = 3$ mg L^{-1}
- $\rho_0(DOC) = 1.1$ mg L^{-1}

The samples were allowed to equilibrate for at least 15 min after contact with the TiO_2 before the start of irradiation (dark adsorption).

For the experiments with added Cu^{2+}, a spike of 10 µmol L^{-1} was used by adding an appropriate amount of $CuSO_4$ to Lake Hohloh water and let equilibrate for at least 3 days in the dark. This water was then used for the irradiation experiments.

Chapter 4

Photocatalytic degradation of natural organic matter*

Natural organic matter (NOM) is ubiquitous in natural waters and plays a fundamental role in the aquatic environment. However, in water for human consumption, NOM is also the main natural precursor of unwanted haloorganic disinfection byproducts (DBPs), of which trihalomethanes (THMs) are the most prominent example (Frimmel et al., 2002; Zwiener, 2006). Therefore, it is important to understand the behavior of NOM during water treatment both in established and alternative processes.

Owing to the importance of NOM as a DBP precursor, the study of the photocatalytic degradation of NOM, especially humic acids, in TiO_2 photocatalysis has been focused on the reduction of the THM formation potential (Ogawa et al., 1995), on the reduction of color (Bekbölet et al., 1998, 2002; Uyguner and Bekbölet, 2005), and on the different factors influencing the velocity of reaction (Al-Rasheed and Cardin, 2003; Li et al., 2002; Palmer et al., 2002; Uyguner and Bekbölet, 2004; Wiszniowski et al., 2003). The techniques used to study this process include ultraviolet-visible (UV-vis), infrared (IR) and fluorescence spectroscopies, as well as total organic carbon (TOC) measurements. However, less effort has gone into showing the changes in molecular size in a natural water rich in humic material during photocatalytic treatment (e.g. Kerc et al., 2004).

In this Chapter, we investigate the degradation of NOM in heterogeneous photocatalysis with suspended titanium dioxide (TiO_2) nanoparticle agglomerates as the photocatalyst. The focus here is the quantification of the changes in molecular size and UV absorption ($\lambda = 254$ nm), as measured by size exclusion chromatography (SEC),

*The main findings discussed here were published in *Applied Catalysis B: Environmental* by Tercero Espinoza et al. (2009b)

which occur during the course of the UV-irradiation in the presence of a TiO_2 photocatalyst. These changes are important because they can lead to different reactivity of NOM, especially towards chlorine, thus affecting the THM formation potential (Hua and Reckhow, 2007). Furthermore, changes in the molecular structure and size distribution of NOM can lead to increased bioavailability of the dissolved organic carbon (DOC), which favors bacterial regrowth (Brinkmann et al., 2003a). In order to characterize this, we examined the production of small organic acids and the bioavailability of the organic material after irradiation. NOM structure and size also play an important role in the removal of NOM by membrane filtration as shown by Saravia et al. (2006) and Saravia (2009).

As a source of NOM, we turned to humic-rich water from a bog lake (Lake Hohloh, Black Forest, Germany). This bog lake water has been extensively used as a reference material to study the characteristics and behavior of aquatic NOM (e.g. Frimmel et al., 2002, and references therein).

4.1 Results from size exclusion chromatography with dissolved organic carbon detection (SEC-DOC)

The SEC-DOC chromatograms of the samples before and after simulated solar UV irradiation were divided into three fractions for ease of analysis, as shown on the left panel of Figure 4.1. The fractions are also referred to as F1-F3 in the following presentation and discussion.

F1 was defined to lie in the interval 28.0 min $< t_r <$ 45.8 min, where t_r is the retention time (in this case numerically equal to the elution volume in mL). It appears to be composed of two overlapping peaks, the higher one with maximum at $t_r = 41.9$ min and the shorter one (shoulder) with maximum around $t_r = 43.5$ min. These two peaks are commonly attributed to humic material (Huber et al., 1994).

F2 (45.8 min $< t_r <$ 50.7 min, maximum of the underlying peak around $t_r =$ 46.8 min) constitutes a second shoulder in the chromatogram of the non-irradiated lake Hohloh water samples. This fraction becomes important upon irradiation and thus deserves separate consideration (see Figure 4.1). The DOC contained in F2 is sometimes referred to as "building blocks" and is assumed to contain aromatic and polyfunctional organic acids (Frimmel, 1998; Huber et al., 1994).

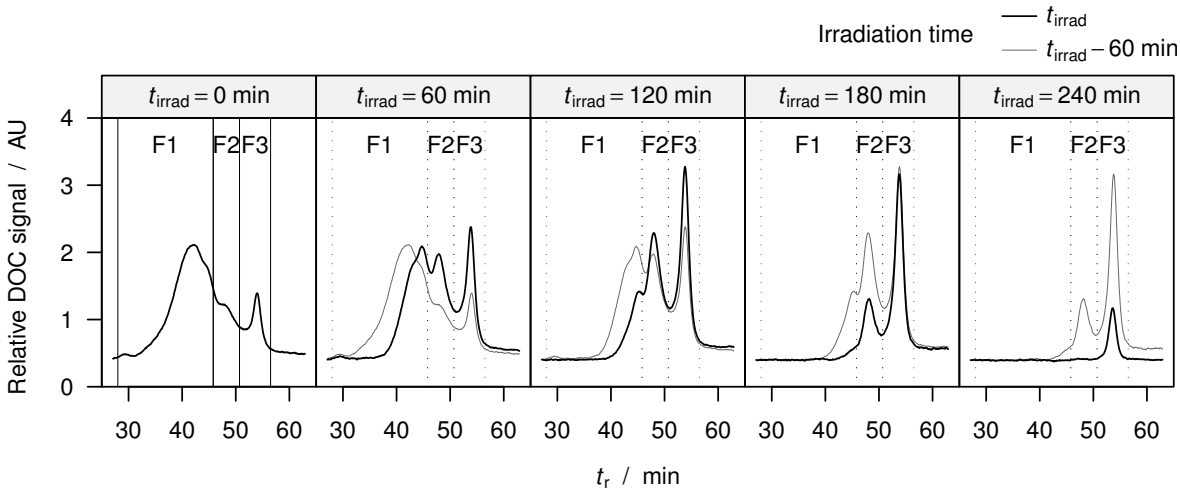

Figure 4.1: SEC-DOC chromatograms showing the defined fractions (F1-F3) and their time evolution under UV irradiation in the presence of 0.5 g L^{-1} TiO_2.

The third fraction, F3 (50.7 min $< t_r <$ 56.5 min), appears clearly as a peak with maximum at $t_r = 52.7$ min in the chromatograms of both non-irradiated and irradiated lake Hohloh samples. Because the samples were not buffered prior to injection into the SEC-DOC system, this last peak also includes molecules that elute prematurely due to the difference in ionic strength between sample and mobile phase (Huber et al., 1994; Specht and Frimmel, 2000).

Upon irradiation, we observed a rapid reduction in F1, accompanied by an increase in both F2 and F3. Assuming size exclusion to be the dominant fractionation mechanism (Brinkmann et al., 2003a), the decrease in DOC content of F1 comes from the loss of the larger portion of F1 (shorter t_r). While the maximum in F1 shifted from the larger to the smaller of the two overlapping peaks, the maxima of the peaks in F2 and F3 appeared at the same time throughout the course of irradiation. Altogether, Figure 4.1 shows a continuous shift of the SEC-DOC chromatograms towards longer retention times (t_r) with increasing irradiation time (t_{irrad}).

The decrease in DOC content of F1 was linear for $t_{irrad} \leq 120$ min, with a rate of decrease in DOC ≈ 0.05 mg L^{-1} min^{-1} (Figure 4.2). F2 and F3 increased linearly during the first hour of irradiation, each at a rate approximately half that of decrease of F1, resulting in a nearly constant sum of the DOC content in the defined fractions. F2 reached a maximum after ≈ 90 min of irradiation and decreased afterwards. F3 increased up to $t_{irrad} \approx 150$ min and also decreased afterwards. The steady decrease in F1, together with the decrease in F2 and slower increase in F3 led to an overall decrease of the DOC contained in F1-F3 starting at $t_{irrad} = 120$ min.

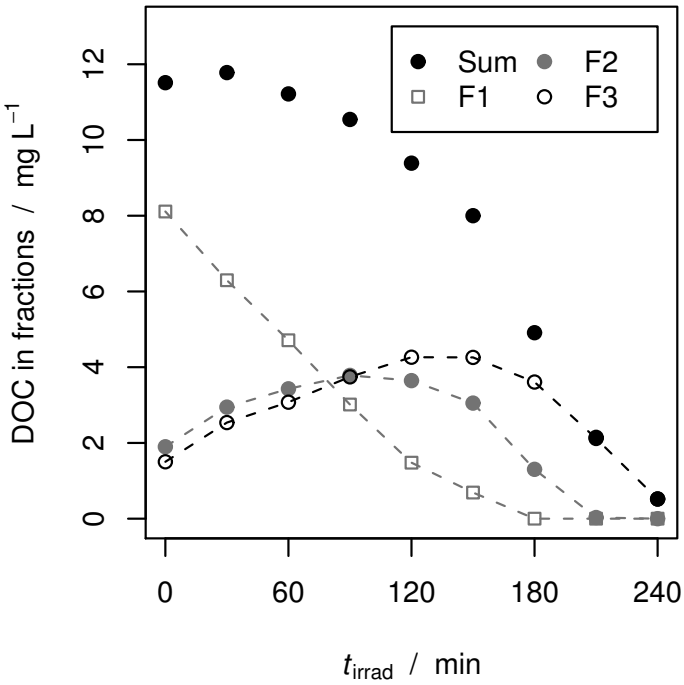

Figure 4.2: DOC content of each fraction as a function of photocatalytic irradiation time, t_{irrad}. The dashed lines are intended as a guide to the eye. The filled black dots correspond to the sum of the DOC contained in F1, F2 and F3 and therefore do not represent all DOC accessible to analysis by size exclusion chromatography (cDOC).

4.1.1 Apparent selectivity of the degradation of NOM

The degradation of NOM should proceed largely unselectively due to the dominant role of OH-radicals in heterogeneous photocatalysis (Oppenländer, 2003; Westerhoff et al., 1999). Rate constants for the reaction of $^{\bullet}$OH with NOM are typically on the order of 10^8 M^{-1} s^{-1} (Westerhoff et al., 1999). However, inspection of Figure 4.1 clearly shows the growth of the smaller fractions F2 and F3 at the cost of F1. The reason for this is that degradation of F1 does not immediately lead to mineralization but to the formation of smaller metabolites, largely contained in F2 and F3. The DOC content of F1-F3 is thus determined by its initial DOC content plus the surplus or deficit arising from differences in its rates of formation and degradation. Since there are no fractions larger than F1, it can only be degraded into smaller molecules, thus decreasing steadily throughout the course of irradiation. F2 initially grows as F1 is degraded but reaches a maximum and declines as F1 becomes smaller. F3 shows similar behavior.

The dynamics of the process thus resemble the degradation of a single parent compound over two intermediates. Inspection of Figure 4.2 reveals three stages of degradation as follows:

1. $0 < t_{\text{irrad}} \leq 60$ min — in this initial stage the degradation of F1 dominated, leading to increasing F2 and F3 such that the sum of the DOC contained in all fractions remained nearly constant;
2. $60 \leq t_{\text{irrad}} \leq 150$ min — after $t_{\text{irrad}} \approx 60$ min, the degradation of F2/F3 started to become important, leading to mineralization. The DOC content of F2 did not change considerably (3.4 ± 0.3 mg L^{-1}), indicating nearly equal rates of formation and degradation for this fraction. The DOC content of F3 continues to grow during this stage and, the rate of degradation of F1 (nearly depleted) becomes smaller towards the end;
3. $150 < t_{\text{irrad}} \leq 240$ min — because of the nearly complete disappearance of F1 after $t_{\text{irrad}} = 150$ min, the DOC content of F2 decreases more rapidly after this point (essentially no more formation of F2 from F1). At the same time, F3 reaches its maximum and decreases steadily for $t_{\text{irrad}} > 150$ min. This leads to a faster mineralization rate compared to that of the second stage. At the end of the irradiation, all remaining DOC is contained in F3 and being rapidly degraded.

4.1.2 Adsorption of NOM onto the surface of the photocatalyst

Since the photocatalyst was removed by membrane filtration before analysis, the results obtained in this study are valid only for the aqueous phase of the titanium dioxide suspensions. Moreover, we note that there is a considerable amount of DOC which adsorbs onto the surface of the photocatalyst and is not accessible to fractionation by SEC (cf. Bekbölet et al., 2002; Vermeer and Koopal, 1998; Vermeer et al., 1998). In our case, $\approx$ 37% of the DOC accessible for SEC-DOC analysis adsorbed to the photocatalyst prior to illumination. This is seen in Figure 4.3, which shows SEC-DOC chromatograms of Lake Hohloh water prior to and after 15 and 60 min of contact in the dark. These chromatograms are in good qualitative agreement with chromatograms of NOM from other natural waters (Frimmel, 1998; Hesse et al., 1997; Huber et al., 1994). No significant changes in the chromatograms could be observed after 1 h of adsorption time in the dark.

Inspection of the chromatograms shown in Figure 4.3 reveals that the DOC in F1 adsorbs to a larger extent onto the surface of TiO_2 than both F2 and F3 ($\approx$ 6.1 mg L^{-1} vs.

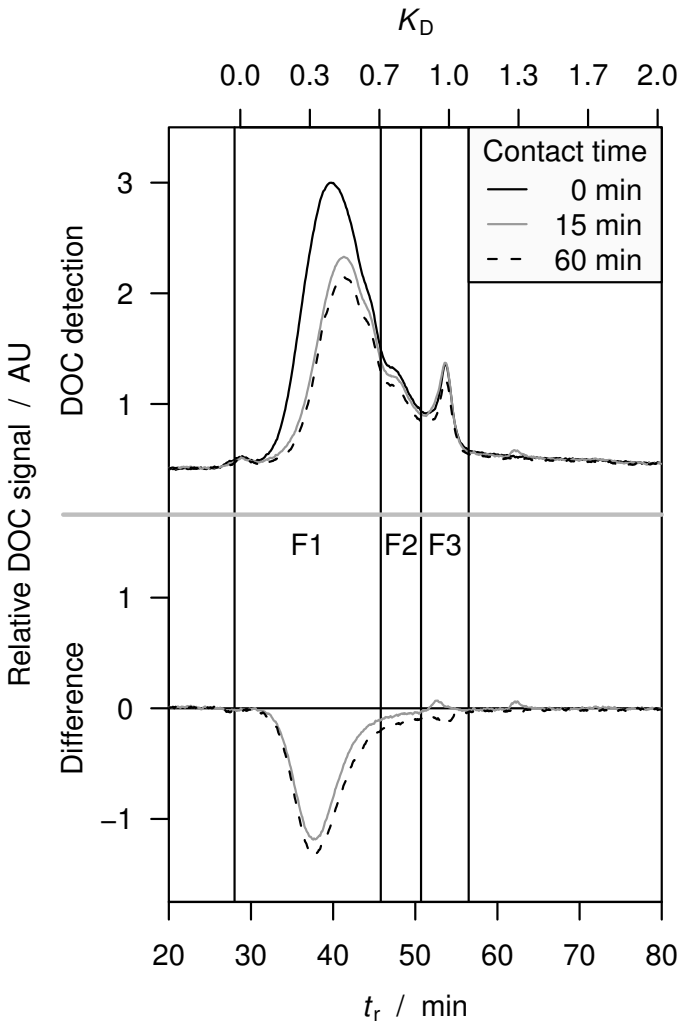

Figure 4.3: SEC-DOC chromatograms showing the adsorption of NOM onto P25 over a period of one hour. No significant change was observed in samples equilibrated for more than 60 min. $\rho(TiO_2) = 0.5$ g L^{-1}.

≈ 0.4 mg L^{-1} and ≈ 0.3 mg L^{-1} respectively for F1, F2 and F3). The preferential adsorption of the larger molecular weight fraction of humic material onto metal oxide surfaces has been reported previously (e.g. Vermeer and Koopal, 1998). Because the photoinitiated redox reactions leading to the degradation of the NOM occur at or in the immediate vicinity of the TiO_2 surface (Linsebigler et al., 1995), it follows that F1 will be preferentially degraded. Moreover, as the adsorbed portion of F1 is degraded, it is to be expected that its place on the TiO_2 surface will be preferentially occupied by F1 from solution rather than by F2 and F3 (either the product of the degradation of F1 or from the original solution). This would lead to F1 being preferentially degraded not only in the initial stages of the reaction, when the pre-adsorbed NOM dominates, but also in later stages, when transport and adsorption from solution supplies the NOM for the ongoing degradation reactions. This is indeed what we observed when the suspensions were irradiated, as shown in Figures 4.1 and 4.2. Thus, differences in the adsorption behavior of the fractions serve to introduce selectivity into an otherwise unselective system.

4.1.3 Comparison with direct photolysis

Comparing these results to those of Brinkmann et al. (2003a,b) on the photolytic degradation of NOM reveals both differences and similarities between these two processes. A key difference is the velocity of the changes observed, the photocatalytic process being much faster: the changes in the SEC-DOC chromatograms are more extensive after one hour of irradiation in the presence of TiO_2 than after 24 h in its absence.

The steady reduction in DOC content of F1 corresponds well qualitatively to the decrease in the main SEC-DOC peak in samples irradiated in the absence of TiO_2. However, Brinkmann et al. (2003a,b) observed a decrease in the height of the main peak with a slight shift of the peak maximum to longer t_r. In contrast, we observe the preferential disappearance of DOC peaks from left to right (shorter to longer t_r) with increasing t_{irrad}. In fact, while the main peak remained the largest after 24 h of irradiation without TiO_2, it clearly wandered to longer t_r before disappearing completely in the presence of TiO_2 within three hours of irradiation. The peaks constituting F2 and F3 did not change in t_r but only in area. This difference highlights that the main peak assigned to F1 is in fact the result of several overlapping peaks and that these peaks are degraded from left to right as seen in SEC-DOC chromatograms.

Brinkmann et al. (2003a,b) also observed the appearance of two additional peaks at longer retention times than the original main peak (corresponding roughly to F2 and F3), which they attributed largely to mono- and dicarboxylic acids. The formation of low molecular weight organic acids in this study is discussed later. Based on the SEC results only, we point out that the relative size of these two "new" peaks is much larger after photocatalysis with TiO_2 than after photolysis. In spite of the difference in degradation pointed out above for F1 and the different relative sizes of the fractions after irradiation, the growth of two smaller fractions at the cost of the larger fraction is common to both processes. The reasons for this, however, are different in each case: while we have given evidence that preferential adsorption of F1 onto the surface of TiO_2 accounts for the observed selectivity in photocatalysis (Section 4.1.2), it is the higher UV absorbance of the larger molecules which leads to their faster degradation in photolysis, absorption of photons of sufficient energy being the first step necessary in any photoprocess (Braun et al., 1991).

4.1.4 Formation of hydrophobic compounds

The DOC content accessible to analysis by SEC ("chromatographable" dissolved organic carbon, cDOC) is, in general, smaller than the total DOC contained in the sample. This difference is attributed to hydrophobic compounds which remain attached to the column during analysis. The difference between DOC (measured by bypassing the column) and cDOC is then an estimate of the amount of hydrophobic compounds present in the sample. Plotting this difference for the irradiated samples (Figure 4.4), we find that hydrophobic compounds are formed in the initial stages of irradiation but are later degraded.

Harmonizing this observation with Figure 4.2 is not straightforward because of the many possible underlying processes and the lack of analytical methods suitable for tracing each kind of carbon atom (whether bound in cDOC or not) during the course of irradiation. Since the carbon mass balance is essentially closed for the cDOC (Figure 4.2) in the period $0 < t_{\mathrm{irrad}} \leq 60$ min, the observed increase in hydrophobic DOC (hDOC) cannot be due to the preferential degradation of hydrophilic constituents or to the formation of hydrophobic coupling products as is often assumed in photolysis (Brinkmann et al., 2003b). A second possibility is that the hDOC still unaccounted for was initially adsorbed onto the surface of TiO_2 and desorbed upon irradiation, thus becoming available for quantification. This desorption could be due to a change in molecular size or properties as a consequence of reaction with $^{\bullet}OH$ or to the increased hydrophilic character of the surface induced by the presence of additional

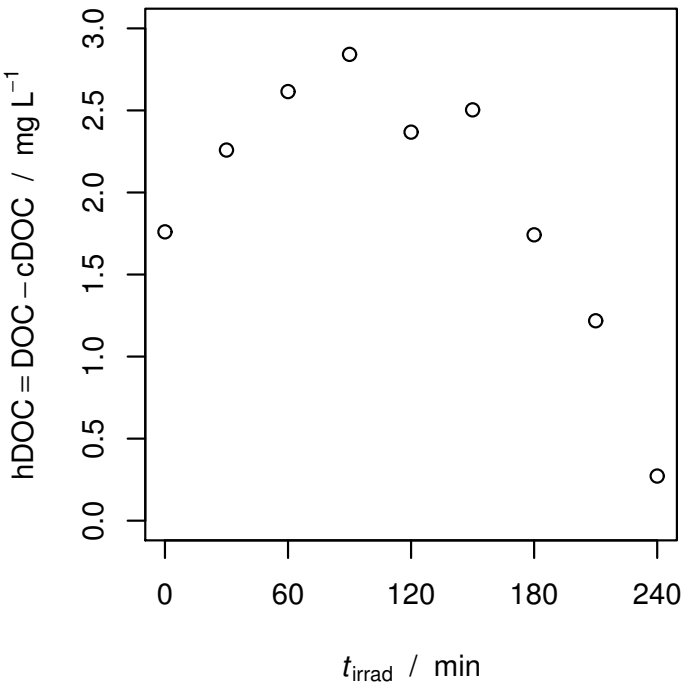

Figure 4.4: Formation of hydrophobic compounds during the course of irradiation.

charge carriers (electrons and holes) during irradiation — cf. superhydrophilic TiO_2 surfaces (Fujishima et al., 1999). Finally, this result may be due to incomplete mineralization of the DOC during the wet-chemical oxidation in our SEC-DOC setup. Moreover, it is plausible that a part of the hydrophobic compounds in the original Lake Hohloh water only becomes detectable after partial degradation in the irradiated TiO_2 suspensions.

4.2 Results from size exclusion chromatography with ultraviolet absorption detection (SEC-UV)

In the interest of a consistent description, the SEC-UV ($\lambda = 254$ nm) chromatograms were also divided into three fractions, corresponding in retention time to those defined for SEC-DOC (Figure 4.5). We point out three differences between the SEC-DOC and SEC-UV chromatograms of the original lake Hohloh water: first, the appearance of a UV peak with maximum around $t_r = 29$ min, which is very prominent in comparison to its counterpart in the SEC-DOC chromatogram, though small compared to the total area of F1. This pre-fraction corresponds to totally excluded molecules

($K_D = 0$). A second difference is that the main peak in F1 is slightly shifted to shorter t_r compared to the DOC peak. This is an indication that the higher molecular weight material possesses a higher specific UV absorbance. And third, F2 and F3 appear smaller in the SEC-UV chromatogram as compared to the SEC-DOC chromatogram. This arises from a lower specific UV absorbance of the lower molecular weight material. These last two observations are in agreement with the results of Uyguner and Bekbölet (2005) based on ultrafiltered model humic solutions.

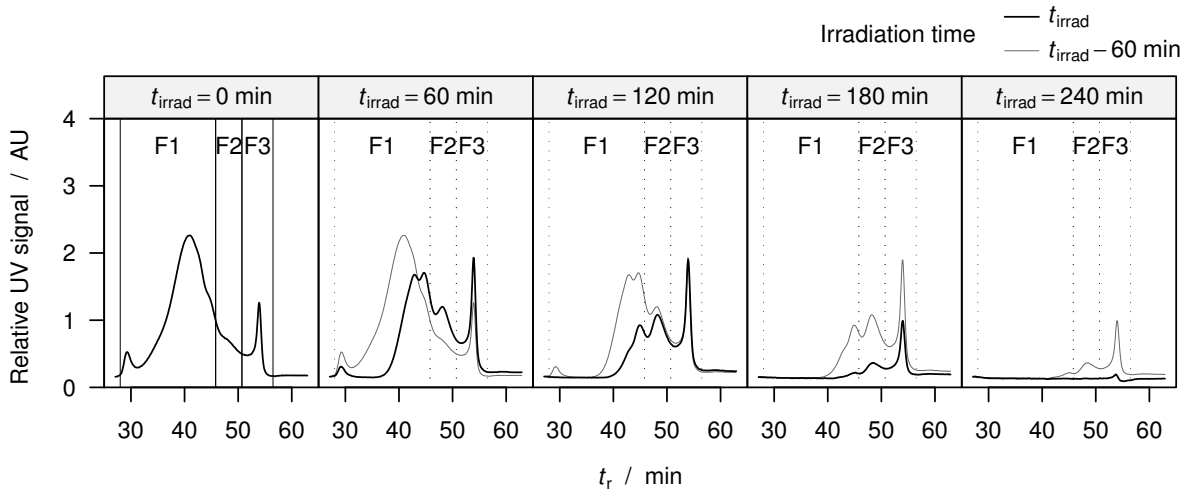

Figure 4.5: SEC-UV chromatograms showing the time evolution of F1-F3 under UV irradiation in the presence of 0.5 g L^{-1} TiO_2.

The results from SEC-UV measurements are qualitatively similar to those from SEC-DOC, but the transformations observed upon irradiation occur faster, such that at the end of the irradiation period there is no significant UV-absorption of the samples. Similarly, the SEC-UV chromatograms before and after adsorption in the dark closely resemble those from SEC-DOC (not shown).

We sought to quantify the loss of UV-absorbing moieties by integrating the SEC-UV chromatograms. These results are shown in Figure 4.6. Since NOM contains a variety of UV-absorbing groups in unknown quantity and distribution, it is not possible to directly relate UV absorption to each moiety. Therefore, the following is based on overall UV absorption.

Inspection of Figures 4.5 and 4.6 shows a steady decrease in the area corresponding to F1. This was accompanied by a slow increase of both F2 and F3 during the first 60-90 min of irradiation, followed by a slow decrease at longer t_{irrad}. As a consequence, the area under the curve corresponding to F1-F3 decreased steadily with increasing

t_{irrad}. This contrasts with the SEC-DOC results where there was no change in the sum of fractions in the first hour of irradiation. This observation is consistent with the expectation that the degradation of larger, UV-absorbing molecules leads to the formation of less UV-absorbing metabolites through the loss of double bonds, which are nonetheless still part of the DOC.

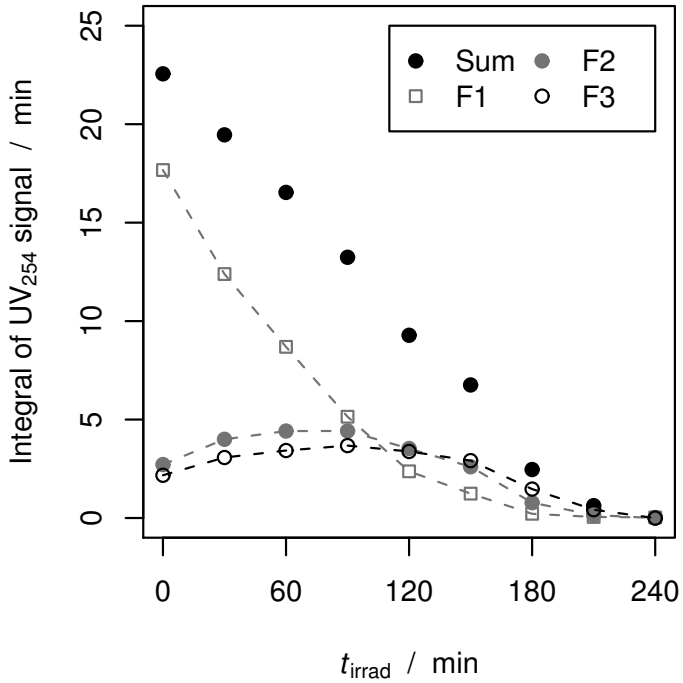

Figure 4.6: Integral of the UV_{254} signal for F1-F3 as a function of irradiation time. The dashed lines are intended as a guide to the eye.

While we observed the overall disappearance of UV-absorbing groups when considering F1, F2 and F3 together, F2 and F3 initially experienced a gentle increase in UV absorption. We attribute the increase in F2 to UV-absorbing metabolites of F1 that become part of F2 because of reduced molecular size. Similarly, we attribute the increase in UV absorption of F3 to metabolites of both F1 and F2. This contrasts with the results of Brinkmann et al. (2003a,b), who did not observe UV absorption corresponding to the peaks we have assigned to F2 and F3. These two differences, the "sequential" disappearance of F1 from shorter to longer t_r and the UV absorption of F2 and F3, indicate that the photolytic and photocatalytic processes not only proceed at different velocities but also lead to different products and size distributions of the metabolites of the original NOM.

Liu et al. (2008a,b) found a similar behavior when using SEC-UV to follow the photocatalytic degradation of a natural (Myponga Reservoir, Australia) and a model

(Fluka humic acid) DOC source. However, the TiO_2 concentration they used was low (0.1 g L^{-1} P25), such that they claim there are no adsorption effects and the "preferential" degradation of the high molecular weight DOC arises from the greater availability of reaction sites. While some differences in reactivity have indeed been reported for the reaction of $^{\bullet}OH$ with different moieties present in NOM, the reaction rate constants are typically in the range of 10^8 M^{-1} s^{-1} (Westerhoff et al., 1999). Moreover, the number of large molecules is very small when compared with the number of small molecules, leading to a very low probability of reaction in a non-selective system. This issue is discussed in detail in Chapter 5.

4.2.1 Comparison with homogeneous advanced oxidation processes

Comparing the results in Figure 4.5 with results from the reaction of $^{\bullet}OH$ (generated homogeneously through the UV/H_2O_2 process) with NOM (Sarathy and Mohseni, 2007) shows both similarities and differences. Similar is the steady breakdown of larger UV absorbing molecules to form smaller molecules, some of which retain UV absorbing properties. Different is the progression of the degradation: whereas the peak in F1 is seen to be reduced in size and to wander towards longer t_r in Figure 4.5, the corresponding peak in the case of UV/H_2O_2 (in Sarathy and Mohseni, 2007) is also reduced in size but its onset does not wander to longer t_r. We attribute this difference to differences in the localization of the reaction: in the case of the TiO_2 suspensions, the reaction occurs near the surface of the particles; thus, adsorption of NOM to the surface of TiO_2 is important as discussed in Section 4.1. In the case of the UV/H_2O_2 process, the reaction of $^{\bullet}OH$ with NOM occurs throughout the volume of the solution and the $^{\bullet}OH$ have equal access to all NOM size fractions proportional to their concentration. A comparison on the basis of DOC results is not possible because Sarathy and Mohseni (2007) only report SEC-UV data. However, the results presented here agree well with the membrane fractionation results of Wang et al. (2006) for the UV/H_2O_2 process.

4.3 Formation and low molecular weight organic acids (LMWOA)

The formation of four small organic acids, namely formic, oxalic, succinic and glutaric acids (shown in Figure 4.7) was followed by means of ion chromatography (IC). In addition to these acids, acetic and malonic acids were identified as being produced but could not be quantified due to interfering peaks and the resulting poor reproducibility in the chromatograms. Injection of the single compounds in the SEC system showed that all three dicarboxylic acids elute primarily in F2 while formic acid elutes with F3.

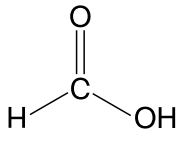

(a) Formic acid (MW = 46.03 Da)

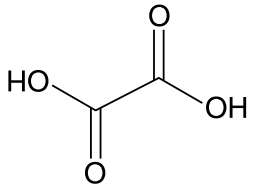

(b) Oxalic acid (MW = 90.03 Da)

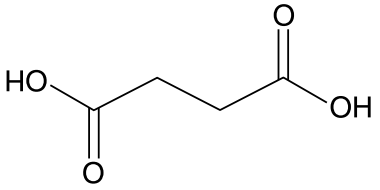

(c) Succinic acid (MW = 118.09 Da)

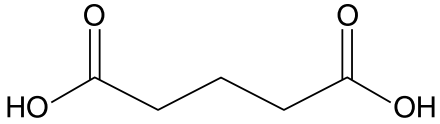

(d) Glutaric acid (MW = 132.11 Da)

Figure 4.7: Structure of formic, oxalic, succinic and glutaric acids.

In irradiation experiments with $t_{\text{irrad}} \leq 60$ min, the concentration of all four LMWOA increased linearly with t_{irrad} (Figure 4.8). The amounts of acid produced followed the order formic $>$ oxalic $\gg$ succinic $>$ glutaric. Formic acid accounted for roughly 10% of the DOC in F3 after 30 and 60 min of irradiation, with increasing tendency. The sum of the dicarboxylic acids (oxalic, succinic, glutaric) accounted for a similar proportion of the DOC in F2.

Longer irradiation experiments ($t_{\text{irrad}} \leq 240$ min) revealed that the concentration of oxalic acid plateaus between the measurements at $t_{\text{irrad}} = 90$ min and $t_{\text{irrad}} = 120$ min with a value of $\approx$ 1.5 mg L^{-1} ($\approx$ 10% of the DOC in F2) and later decreases monotonically. The concentration of formic acid showed a maximum value after $t_{\text{irrad}} = 150$ min ($\approx$ 3.2 mg L^{-1}, $\approx$ 20% of the DOC in F3). The maxima observed

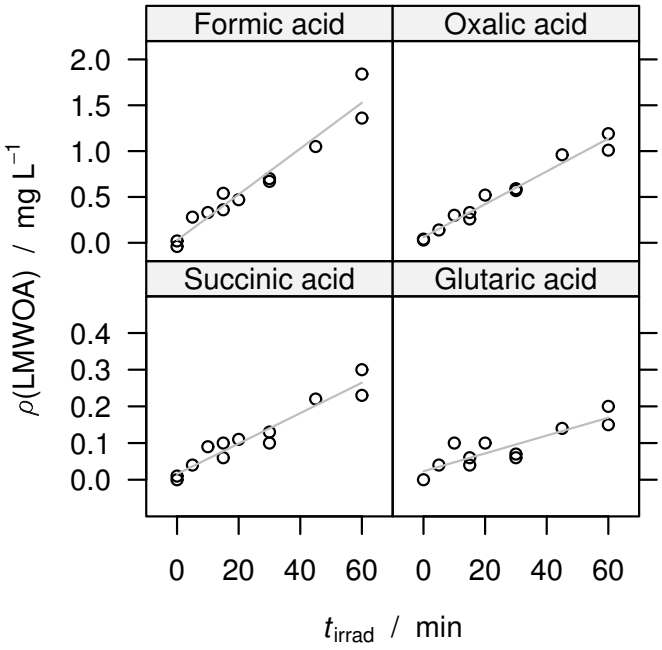

Figure 4.8: Formation of low molecular weight organic acids.

in the concentration of formic and oxalic acids correlate well with the maxima in DOC (shown in Figure 4.2).

4.4 Bioavailability of the dissolved organic carbon (DOC)

To assess the bioavailability of the DOC before and after ultraviolet irradiation in the presence of TiO_2, samples ($0 < t_{irrad} < 60$ min) were incubated with an activated sludge inoculum for two days and then examined by means of SEC-DOC. These chromatograms are shown in Figure 4.9. Addition of the inoculum was observed to bring in a significant amount of DOC, the largest part of which eluted with $K_D > 1$. These additional DOC peaks were, however, no longer present after the incubation period.

The non-irradiated sample showed little or no change in DOC content of the peaks corresponding to F2 and F3 ($|\Delta DOC_{F2}| < 0.5$ mg L^{-1}, $|\Delta DOC_{F3}| < 0.1$ mg L^{-1}). However, the range corresponding to F1 showed both an increase (peak with maximum around $t_r = 30$ min) and a decrease (starting at about $t_r = 34$ min) in DOC, for

an overall loss of $\approx$ 0.75 mg L^{-1} DOC. This was unexpected, as previous biodegradation studies had shown essentially no degradation of the region here assigned to F1 upon bacterial incubation (Brinkmann et al., 2003a). A possible reason for this are the different bacterial cultures used: whereas the inoculum used by Brinkmann et al. (2003a) was obtained from the Lake Hohloh water itself, the inoculum used in this study contained activated sludge from two different wastewater treatment plants (one industrial, one municipal). It is attractive to assume that the inoculum from activated sludge contained a larger microbial diversity with a correspondingly larger metabolic potential than the inoculum from Lake Hohloh.

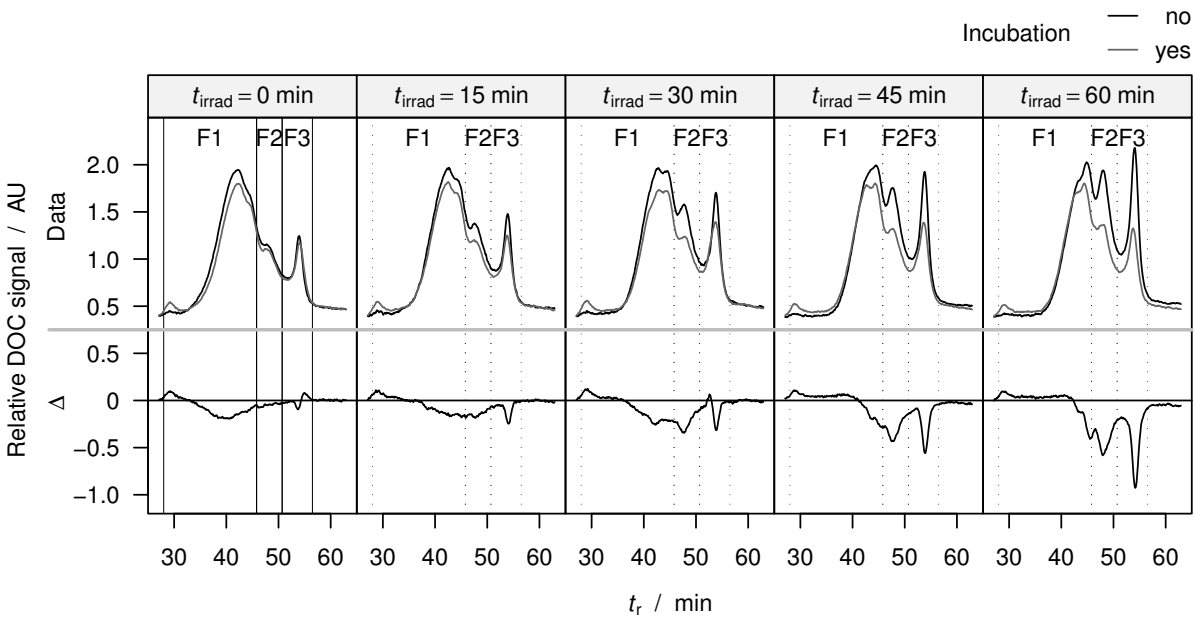

Figure 4.9: SEC-DOC chromatograms of irradiated samples ($0 < t_{irrad} < 60$ min) before and after incubation with a mixed bacterial culture for two days.

With increasing irradiation time, the net DOC decrease in F1 became smaller, while the net positive part of the difference spectrum appeared to extend to longer retention times. This points to a synthesis of higher molecular weight organic substances by the bacteria. Integrating only the net positive part of the difference spectra (bottom spectra in Figure 4.9) reveals an increasing trend in area which is nevertheless $<$ 0.1 mg L^{-1}.

The amount of bioavailable DOC contained in F2 increased from $\approx$ 0.4 mg L^{-1} for the non-irradiated sample to $\approx$ 1.6 mg L^{-1} after 60 min of irradiation. At the same time, the bioavailable DOC in F3 steadily increased from approximately zero to $\approx$ 1.7 mg L^{-1} at $t_{irrad} = 60$ min. Taking into consideration that formic acid elutes mostly

with F3 and all other acids elute largely in F2, the quantified LMWOA account for 25-30% of the bioavailable DOC in F2 and $\approx$ 20% in the case of F3. Thus, these acids, along with malonic and acetic acids which were detected but could not be quantified, form a significant part of the bioavailable DOC.

It is interesting to note that the chromatograms *after* incubation changed only minimally for the range of t_r corresponding to F2 and F3, while the range corresponding to F1 changed extensively. This further supports the notion of a sequential photocatalytic degradation of the DOC fractions in order of decreasing molecular size. Furthermore, it shows that a large fraction of the metabolites present after irradiation are bioavailable.

4.5 Interim summary

The photocatalytic degradation of humic-rich natural organic matter (NOM) from a bog lake was found to proceeded in a sequential manner, starting from the larger molecular size fraction and continuing towards smaller molecular size fractions and giving rise to the production of bioavailable products, including small molecular weight organic acids. As a result, no significant mineralization was observed in the initial stage of the reaction, followed by steady mineralization after this lag phase. This correlated well with the preferential adsorption of the larger molecular weight fraction of the NOM onto the surface of the TiO_2 photocatalyst, which favors its degradation.

Comparison of these results with the degradation of NOM through UV irradiation alone and through the homogeneous reaction of $^{\bullet}OH$ with NOM points to different molecular size distribution and chemical structure of the metabolites. This can have implications on the potential for byproduct formation during and for bacterial regrowth after water treatment.

Chapter 5

A simple simulation of the degradation of natural organic matter in advanced oxidation processes*

Because of the enormous complexity, source and seasonal variability of natural organic matter (NOM), it is necessary to use a battery of different, complementary techniques to adequately describe its behavior. Size exclusion chromatography with dissolved organic carbon and/or ultraviolet detection (SEC-DOC and SEC-UV, respectively) is increasingly taking an important place in the toolkit of NOM researchers, with more and more results (e.g. Liu et al., 2008b; Sarathy and Mohseni, 2007) being published using a system similar to that of Huber and Frimmel (1991). The application of SEC to the fractionation of humic substances goes back to the work of Gjessing (1965) and Gjessing and Lee (1967). Application and limitations of the SEC-DOC technique have been recently assessed critically by Lankes et al. (2008, 2009).

In Chapter 4 we examined the photocatalytic oxidation of natural organic matter (NOM) from a bog lake by using SEC-DOC. In the work presented in this Chapter, we sought to examine the claims made in Chapter 4 (Sections 4.1 and 4.2) and also those from others (e.g. Sarathy and Mohseni, 2007) regarding the preferential degradation of high molecular weight material and to complement those based on fractionation of NOM by ultrafiltration (e.g. Uyguner and Bekbölet, 2005; Wang et al., 2006).

The main question to answer is whether the observed changes in the apparent molecular weight distributions of NOM upon treatment with homogeneous (e.g. the H_2O_2/ UV process) and heterogeneous (photocatalysis with TiO_2) advanced oxidation processes (AOP) can be plausibly ascribed to randomness or whether there is indeed evidence of selectivity in the published results. Our approach was to simulate

*The findings discussed here were published in *Water Research* by Tercero Espinoza and Frimmel (2009).

both heterogeneous and homogeneous advanced oxidation processes (AOP) as fully random processes and compare the results of the simulation to experiment. Through this comparison, we sought to contribute to the interpretation of SEC-DOC results in AOP.

5.1 Underlying physical model

The simulation code discussed below is based on a simple physical model that seeks to represent the basic features of the *unselective* degradation of NOM. Specifically, it aims to describe the degradation by OH-radicals ($^{\bullet}$OH), the basis of AOP. The proposed model assumes that:

1. the NOM molecules are linear chains;
2. the probability of reaction for molecules of a particular chain length depends only on their relative number compared to the total number of available molecules (i.e., molecular size and chemical identity are ignored);
3. only cleavage reactions take place;
4. the linear chains can be cleaved at any point with all cleavage points being equally likely; and
5. mineralization only occurs when a C1 organic molecule (i.e. a molecule containing 1 C atom) reacts; every reaction of a C1 molecule leads to mineralization. This is the only way for organic carbon to leave the simulated system (as CO_2).

As seen from the assumptions above, this model prominently ignores the chemistry of the NOM molecules. This is because a) this information is not available in detail, and b) it simplifies the calculations enormously. This has a series of consequences which must be kept in mind when analyzing the results. Specifically, the proposed model ignores the (small) differences in reactivity of $^{\bullet}$OH with different functional groups (Westerhoff et al., 1999) and the resulting preferential degradation and/or formation of certain structures. Furthermore, because only cleavage reactions are allowed, the formation of products larger than the parent compounds (e.g., through the termination reaction between two C-centered radicals; Oppenländer, 2003) is ignored. Finally, there is no information about the NOM molecules (functional groups, double bonds, heteroatoms, C:O ratios, geometry, etc.) besides the chain length.

5.2 Simulation algorithm

Data from Section 4.1 were used as starting point for the simulation and as a base for comparing simulation and experiments. The code for the simulation was written in R (R Development Core Team, 2008).

5.2.1 Initialization

The initialization process is based on both experimental data and simplifying assumptions. The experimental basis is a representative SEC-DOC chromatogram of water from a bog lake (Lake Hohloh, discussed in Chapter 4).

SEC-DOC chromatograms give, to a first approximation, a mass distribution of organically bound carbon (DOC) according to hydrodynamic molecular size (retention time, t_r, in the SEC column). However, there are two factors which affect this ideal picture:

1. the retention time of organic molecules is affected by their functionality (Specht and Frimmel, 2000), and
2. the peaks are generally very broad.

Nevertheless, it is possible to correlate retention times with the hydrodynamic size of molecules –provided the molecules have similar structures– making it a useful tool in polymer science (Rodriguez, 1996). Thus, by ignoring the heterogeneous structure of NOM and peak spread, it is possible to assign an apparent molecular weight to each retention time (t_r) by interpolation. The calibration points for the interpolation were chosen on the basis of a calibration of the SEC column with poly(ethylene glycol) and small organic molecules (cf. Figure C.1). The relationship between apparent molecular weight and elution time is given by

$$\ln(MW_{t_r}) = a + b\,t_r \tag{5.1}$$

where MW_{t_r} denotes the molecular weight assigned to a particular t_r and a and b are fitting constants.

By assuming a constant carbon content for the NOM, we can convert the estimated MW_{t_r} into a chain length for each elution time, nC_{t_r}, as

$$nC_{t_r} = MW_{t_r} \times \frac{0.45}{MW_C} \tag{5.2}$$

where MW_C is the molar mass of carbon and the assumed carbon content of the DOC is 45% for all molecular sizes (Müller, 2004). For the initial data, this leads to $1 \leq nC \leq 5705$, with nC given in number of C atoms per chain. It is possible to estimate the number of molecules for each chain length, $n_{\text{molec},nC}$, because the DOC signal in the experimental data is directly proportional to $nC \times n_{\text{molec},nC}$. Furthermore, it is possible to scale this number to a desired total number of molecules, in this case $\sum_{n_C} n_{\text{molec},nC} = 1 \times 10^6$.

Finally, because t_r is logarithmically related to nC (Equations 5.1 and 5.2), there are 4 to 17 data points which correspond to each $nC < 10$ but this becomes ≤ 1 data point for $nC \geq 35$. We note that the experimental chromatogram contains ≈ 350 individual data points, but there are 5705 possible chain lengths considered. All chain lengths that did not correspond to one of the data points was assigned $n_{\text{molec},nC} = 0$ as an initial value. Thus, it is necessary to use binning in order to be able to reproduce a chromatogram based on nC and $n_{\text{molec},nC}$. After a process of trial and error, 33 bins were selected to reproduce the experimental chromatogram. The size of the bins (given in number of different consecutive chain lengths) is one for $1 \leq nC \leq 5$ and increases exponentially from two to ≈ 1000 for $6 \leq nC \leq 5705$.

The result of this initialization procedure can be seen in Figure 5.1. It becomes clear that, despite the shortcomings due to the assumptions made in computing the value of nC_{t_r}, the estimated initial chromatogram describes very well the main features of the experimental chromatogram. For ease of comparison with further experimental results, three fractions were defined analogous to those defined in Section 4.1 (cf. Figure 4.1).

5.2.2 Reaction step in a homogeneous system

For the case of homogeneous reaction and assuming that the degradation is unselective, the number of reacting molecules of chain length nC is simply

$$n_{\text{reactions},nC} = \frac{n_{\text{molec},nC}}{\sum_{nC} n_{\text{molec},nC}} \times \underbrace{\sum_{nC} n_{\text{reactions},nC}}_{\text{set number of reactions}} \tag{5.3}$$

where the second subscript indicates that the equation is applied to each chain length, nC. The total number of reactions can then be set to a selected number, in this case $\sum_{nC} n_{\text{reactions},nC} = 1 \times 10^4$ reactions per simulation step.

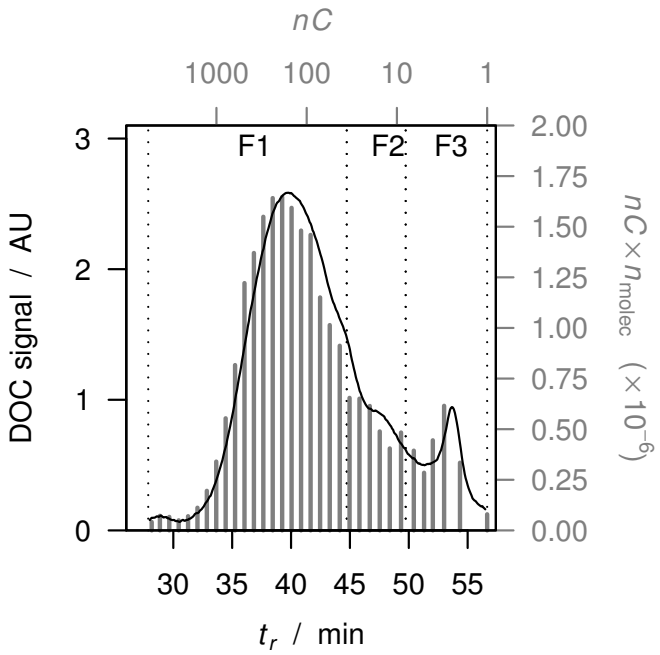

Figure 5.1: Initialization of the simulation. The continuous black curve represents the experimental SEC-DOC data used as a basis for the simulation (cf. Figure 4.3). The gray bars are the approximated chromatogram based on the procedure described in Section 5.2.1. We note that each bar corresponds to one bin, and that the bin size decreases from left to right. F1, F2 and F3 correspond to the three fractions defined in Section 4.1 (Figure 4.1) and used to follow the evolution of DOC.

Because the value of $n_{\text{reactions},nC}$ obtained from Equation 5.3 was rounded to the nearest integer, this leads to a small over- or underestimation of the number of reactions assigned to each nC. As long as $n_{\text{reactions},nC} \gg 1$, this error may be safely ignored. However, this becomes a problem especially for the case of $0 < n_{\text{reactions},nC} < 1$. This is particularly relevant for very long chains ($t_r \geq 31$ min or $nC \geq 2200$ in Figure 5.1), which have $n_{\text{molec}} \leq 2$. The approach used in this simulation is not to round if $0 < n_{\text{reactions},nC} < 1$ but to choose between 0 and 1 using weights derived from $n_{\text{reactions},nC}$ itself. So for $n_{\text{reactions},nC} = p$, 1 is selected with probability p, while 0 is selected with probability $1 - p$. This gives a more realistic estimate of $n_{\text{reactions},nC}$ for $n_{\text{molec},nC} = 1$.

5.2.3 Reaction step in a heterogeneous system

In the case of TiO_2 suspensions (heterogeneous system), the NOM adsorbs onto the surface of TiO_2 at a different rate for different molecular sizes. Because the reaction can only take place at or in the immediate vicinity of the TiO_2 surface (Oppenländer, 2003), this selective adsorption changes the effective $n_{\text{molec},nC}$ available for reaction. This is taken into account by adding a correction factor to Equation 5.3 as follows:

$$n_{\text{reactions},nC} = \frac{n_{\text{molec},nC} \times \phi_{\text{ads},nC}}{\sum_{nC}(n_{\text{molec},nC} \times \phi_{\text{ads},nC})} \times \underbrace{\sum_{nC} n_{\text{reactions},nC}}_{\text{set number of reactions}} \tag{5.4}$$

where $\phi_{\text{ads},nC}$ is the fraction of molecules adsorbed onto the surface for each chain length. This is computed from the difference between the SEC-DOC chromatograms before and after adsorption in the dark as seen in Figure 4.3 and is assumed to remain constant during the course of irradiation. As for the homogeneous case, the computations leading to $0 < n_{\text{reactions},nC} < 1$ received special treatment and $\sum_{nC} n_{\text{reactions},nC} = 1 \times 10^4$ reactions per simulation step. Thus, the computational basis for both (homogeneous and heterogeneous) cases is the same.

5.2.4 Iteration

For each reaction, a cleavage point is randomly selected, the resulting two fragments are added to the corresponding nC and the parent molecule is substracted from the corresponding $n_{\text{molec},nC}$. The exception to this is $nC = 1$, where each reaction is considered to be mineralization – this is the only way the simulation removes carbon from the system.

This reaction step is repeated $n_{\text{reactions},nC}$ times for each chain length and a cycle through all chain lengths constitutes one simulation step. The simulation was allowed to run until complete mineralization ($\approx$ 5550 steps).

5.3 Simulation of the heterogeneous system

First, we used the code described above to simulate the degradation of NOM from a bog lake in irradiated titanium dioxide suspensions. An important advantage of

this heterogeneous system is the availability of the directly comparable experimental results presented in Chapter 4 and shown again in Figure 5.2a for convenience.

5.3.1 Comparison of experimental and simulated chromatograms

Inspection of Figure 5.2 shows that the simulation results well describe the main features of the heterogeneous photocatalytic degradation of NOM, in particular:

1. the shifting of the chromatograms from left to right, i.e. from higher to lower molecular size,
2. the increase in the material corresponding to F2 and F3 at the expense of F1, and
3. the overall shape of the chromatogram, especially in the initial stages of degradation.

However, a comparison of the time evolution of the chromatograms reveals that, while the shape and the qualitative progression of the simulated degradation sequence closely follows experiment, the time scales are very different. The simulated chromatogram after 600 steps compares well with the experimental chromatogram after 60 min of irradiation. Assuming a linear relation between number of steps and irradiation time, t_{irrad}, the chromatogram after 2400 steps should correspond to $t_{\text{irrad}} = 240$ min, but this is not the case. Instead, the chromatogram after $t_{\text{irrad}} = 240$ min more closely resembles that after 5400 simulation steps. That is, although the simulation can closely reproduce the degradation sequence, the dynamic behavior is not well described or, at least does not linearly correspond to that given by the simulation.

5.3.2 Comparison of dissolved organic carbon (DOC) evolution

A further way to compare simulation and experiment is through the time evolution of the DOC. For this purpose, Figure 5.3 presents the time evolution of dissolved organic carbon corresponding to each fraction, compared to simulated values. Here, the simulation results are presented in two different diagrams: one for the total organic carbon (OC_{total}) present in the simulation and one for the organic carbon present in solution ($OC_{\text{total}} - OC_{\text{adsorbed}}$). The OC in solution corresponds conceptually to what is seen in experiment because only the OC that is not adsorbed is accessible to analysis by SEC-DOC.

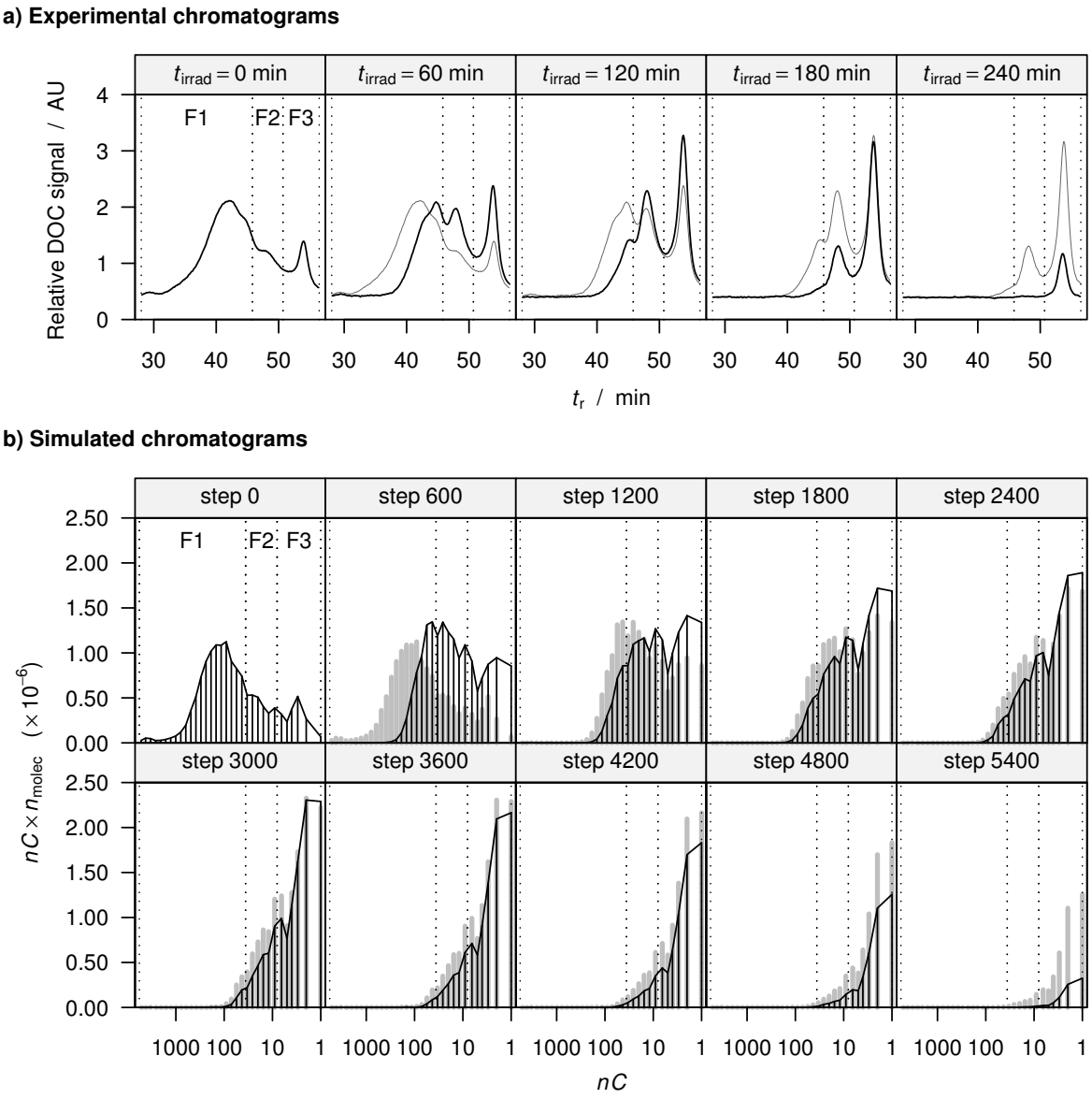

Figure 5.2: Degradation sequence for a) the photocatalytic degradation of brown water natural organic matter (cf. Figure 4.1) and b) the simulated heterogeneous system. In every panel, the black bars and lines correspond to the experimental or simulated chromatogram after a given irradiation time or number of steps, while the gray bars/lines show the chromatogram as it was in the previous panel for ease of comparison.

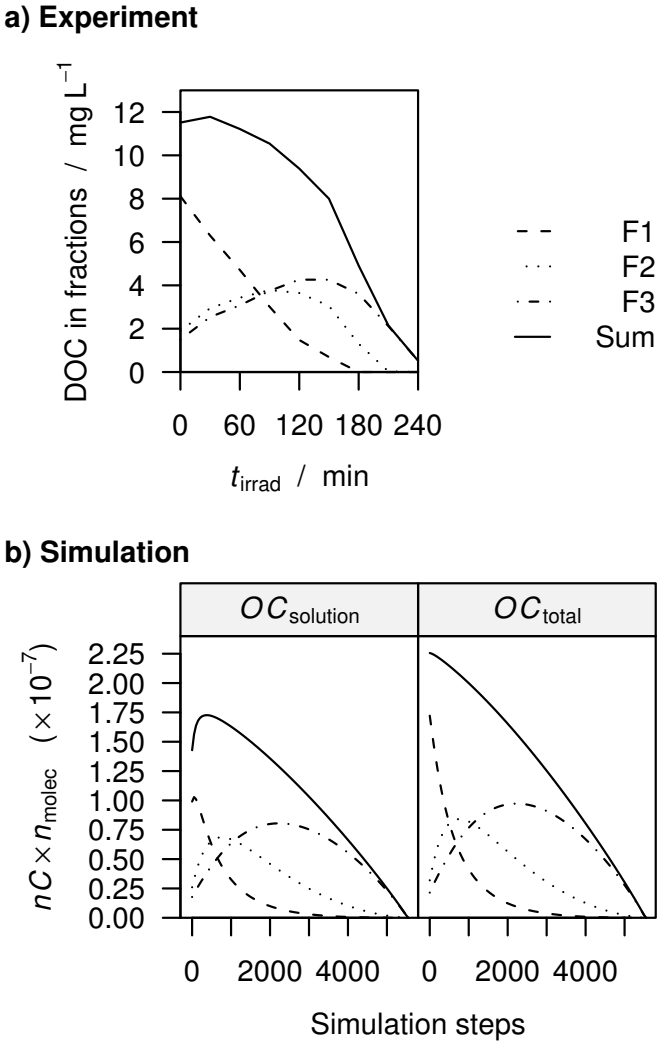

Figure 5.3: Evolution of the organic carbon (OC), expressed as the product of chain length times number of chains for the entire simulated chromatogram. OC_{total} refers to the OC present in the system; $OC_{solution}$ is the result of substracting the adsorbed portion of the OC from OC_{total}.

The simulation results compare well qualitatively to the experimental data regarding the time evolution of F1-F3. In particular, the rapid decrease in F1 and the increase in both F2 and F3 are well depicted in Figure 5.3. However, we point out three key differences between Figures 5.3a and b:

1. the experimental curve for the sum of F1-F3 does not agree with the simulated curve for OC in solution but lies mostly between the simulated curves for OC in solution and total OC;
2. the decrease in F1 and the increase in F2 and F3 is much slower in the experiment than in the simulation; and
3. the curve for F2 has a strong tailing to the right in the simulation results which is not present in the experimental results.

Difference (1) suggests that desorption of the F1 fragments after degradation is not complete. Complete and immediate desorption is the case shown in Figure 5.3b for OC_{solution}. Here, some F1 molecules are degraded to (smaller) F1, F2 and F3 molecules with less affinity for the surface, which immediately desorb. The extent of desorption observed in the experimental curve is very small. This difference implies that the adsorption-desorption kinetics play a role in the observed experimental results and underline the difficulty in making conclusions for heterogeneous systems based on data from solution only.

Regarding OC_{total} (simulation), a steady decrease with a slightly increasing degradation rate is observed and is due to mineralization of C1 compounds taking place from the start of the simulation. Furthermore, because the rate is directly proportional to the relative number of C1 chains, the rate of degradation increases with increasing simulation step number (time) for both simulated curves, giving rise to the concave down shape of the sum curve in good agreement with experiment.

Difference (2) may be the result of adsorption-desorption kinetics. While in the simulation these effects are ignored and adsorption-desorption occur instantaneously, in the real system some time is required for the desorption of product chains and the diffusion of new chains to the surface. Metabolites may also remain on the surface and react further without returning to the bulk solution. Dark adsorption experiments revealed that a contact time of > 15 min is necessary to establish conditions approaching equilibrium (cf. Figure 4.3). Thus, it is plausible that relatively slow transport of F1 molecules to the surface and F2 and F3 molecules from the surface is responsible for the observed difference.

Difference (3) results from the lack of (assumed, static) differential adsorption between F2 and F3, as discussed in Section 5.3.1.

5.4 Simulation of the homogeneous system

If all molecules are available for reaction ($\phi_{ads} = 1$ for all nC)[†], the simulated system corresponds to the homogeneous degradation of NOM, and may be simulated in a manner parallel to that of the heterogeneous system. The results of this simulation are presented in Figure 5.4.

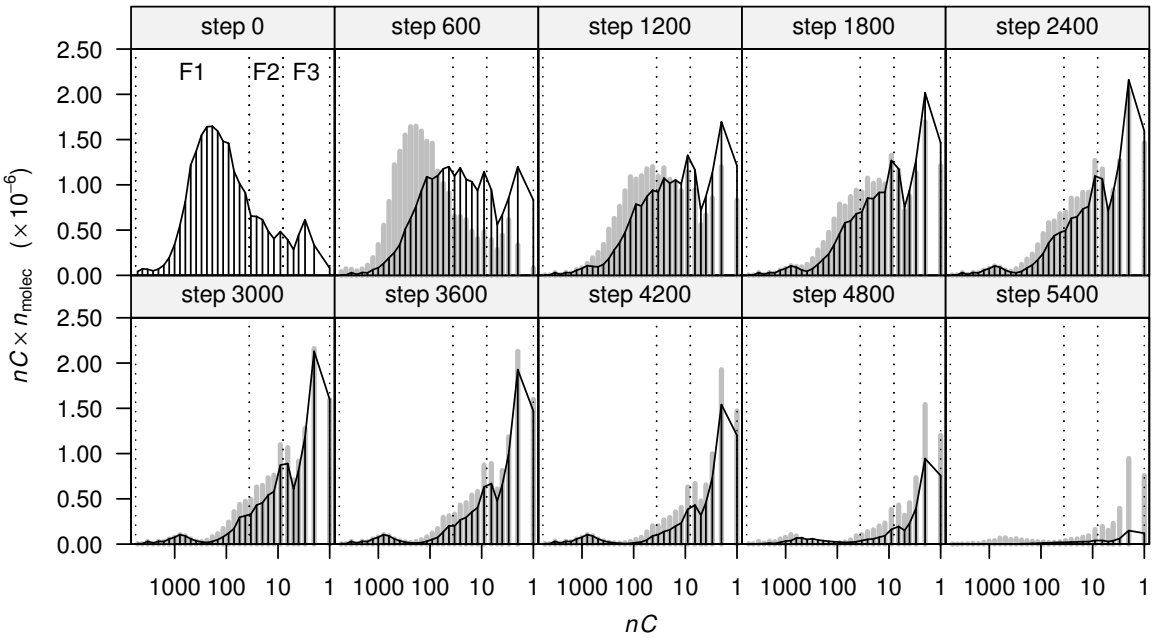

Figure 5.4: Degradation sequence for the simulated homogeneous system. Initial $\sum_{nC}(n_{molec,nC}) = 1 \times 10^6$; $\sum_{nC}(n_{reactions,nC}) = 1 \times 10^4$ reactions per simulation step. In every panel, the black bars (connected at the top by a line) correspond to the simulated chromatogram after a given number of steps, while the thicker gray bars show the chromatogram as it was in the previous panel for ease of comparison.

As was the case for the heterogeneous system, the degradation of long chains (F1) leads to the formation of medium and short chains (F2 and F3, respectively). The numbers of these medium and short chains decrease after passing though a maximum. These results agree well with membrane fractionation results by Wang et al. (2006) and the LC-DOC results of Kleiser (2000) with the UV/H_2O_2 process. In addition, there are several studies of the UV/H_2O_2 with SEC-UV (e.g. Liu et al., 2008b;

[†]Because the total number of reactions is adjusted to a stipulated number, it is sufficient if ϕ_{ads} is the same for all nC for the system to be equivalent to a homogeneous system.

Sarathy and Mohseni, 2007), which are unfortunately not comparable because of the fundamental differences between DOC and UV measurements.

It is worth noting that the high molecular weight fraction, though degraded first in both homogeneous and heterogeneous systems, exhibits a clearly different behavior in the homogeneous simulation. Namely, it is essentially persistent throughout the simulation because its molecules are present in such small numbers. This stands in contrast to the rapid and complete degradation of the large molecular weight fraction in the heterogeneous system, where a bias is introduced due to preferential adsorption of the NOM onto the surface of the photocatalyst.

5.5 Comparison of the homogeneous and heterogeneous systems

The largest changes in the apparent molecular size distribution of NOM occur in the first 1000 steps of the simulation, as seen in Figures 5.2 and 5.4. To compare the two processes in more detail, Figure 5.5 shows the progression of this initial part of the degradation sequence. Here, it becomes clear that the fully random system (homogeneous) experiences a marked decrease in long chains with an accompanying increase in medium and short chains. However, the introduction of a bias due to differential adsorption greatly accelerates the degradation of the long chain material, despite the otherwise identical conditions of the simulation.

Thus, the observation of apparently "preferential" degradation of the large molecular size fraction is observed in both the biased (heterogeneous) and unbiased (homogeneous) system. However, there is no "preference" involved in the homogeneous (unbiased) system and all results known to the authors involving homogeneous AOP (e.g. VUV, UV/H_2O_2) can plausibly be described by randomness regarding the qualitative reaction sequence.

On the other hand, imposing a selectivity (weighting) towards degradation of the large molecular size material causes the simulation to closely follow the degradation sequence observed experimentally for heterogeneous photocatalysis. Thus, the claim of selectivity on the basis of adsorption appears to be well founded on the basis of these results, where the process was otherwise allowed to proceed at random.

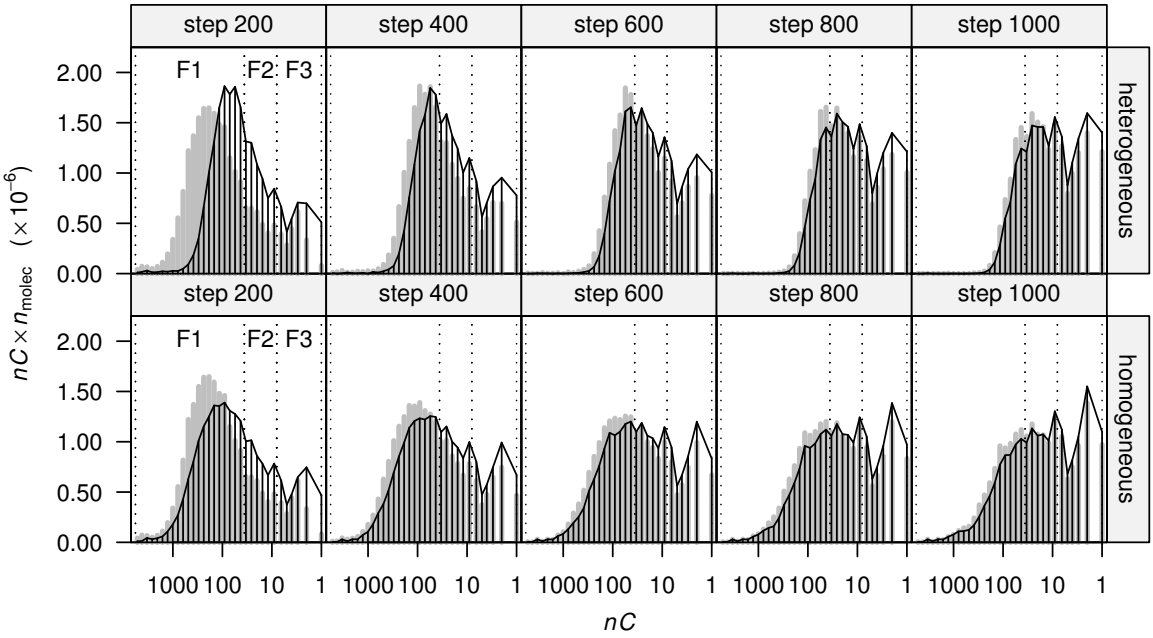

Figure 5.5: Detailed comparison of the simulation results for the heterogeneous and homogeneous systems under identical conditions. Initial $\sum_{nC}(n_{\text{molec},nC}) = 1 \times 10^6$; $\sum_{nC}(n_{\text{reactions},nC}) = 1 \times 10^4$ reactions per simulation step. In every panel, the black bars (connected at the top by a line) correspond to the simulated chromatogram after a given number of steps, while the thicker gray bars show the chromatogram as it was in the previous panel for ease of comparison.

5.6 Interim summary

In this Chapter we presented a simple simulation of the unselective degradation process of NOM in the presence and absence of a bias. In this case, the bias arises from selective adsorption of the NOM molecules onto a reactive surface.

The simulation of both biased and unbiased systems were found to be good first approximations to the experimentally observed behavior for the corresponding systems: heterogeneous photocatalysis with TiO_2 suspensions (biased) and UV/H_2O_2 (unbiased). We conclude that claims of a selectivity towards degradation of the high molecular weight material in homogeneous advanced oxidation processes (AOP) are not tenable on the basis of SEC-DOC or SEC-UV alone, since the observed results can be well described qualitatively by a fully random process.

On the other hand, based on the good agreement between simulation and experiment, we conclude that the degradation of NOM in heterogeneous photocatalysis with TiO_2 suspensions does indeed exhibit selectivity and that this selectivity is most likely due to selective adsorption of NOM onto the TiO_2 surface. This holds particularly well for the initial part of the degradation sequence, where the system most resembles the state after dark adsorption and simulation and experiment most closely agree. This result should also hold for all conceptually similar processes.

Chapter 6

Effect of selected metal ions on the photocatalytic degradation of natural organic matter

The work presented in this chapter is a continuation of our efforts to characterize the photocatalytic degradation of NOM under simulated solar ultraviolet (UV) irradiation. Here we examine the effect of the presence of selected metal ions, namely iron(III), manganese(II), copper(II) and zinc(II) on the photocatalytic degradation of NOM, taking into account changes in molecular size as measured by size exclusion chromatography with dissolved organic carbon detection (SEC-DOC), as well as the production of low molecular weight organic acids (LMWOA) and changes in the bioavailability of the dissolved organic carbon (DOC) upon irradiation.

6.1 Degradation of NOM in the absence of added metals

The experiments presented in Chapter 4 were used as a base case for experiments with added Cu^{2+}, Mn^{2+}, Zn^{2+} and Fe^{3+}. Because F2 experienced a maximum in DOC content at $t_{irrad} \approx 90$ min (cf. Figure 4.2), we chose irradiation times of 30 and 60 min for the experiments with added metals. Through this choice of t_{irrad} we aimed to avoid having to distinguish between values on either side of the UV (cf. Figure 4.6) and DOC maxima for F2.

6.2 Degradation of NOM in the presence of added metals

In order to study the influence of added metals on the photocatalytic degradation of NOM, we performed irradiation experiments with added iron(III), copper(II), manganese(II) and zinc(II) in the range 0-10 μmol L^{-1}. The original Lake Hohloh water contained $\ll$ 1 μmol L^{-1} of each Cu and Mn, approx. 2 μmol L^{-1} Zn, and approx. 6 μmol L^{-1} Fe, as measured by inductively coupled plasma optical emission spectroscopy (ICP-OES). No steps were taken to change this natural background concentration. Thus, the concentration of the spiked samples is given as $c_{\text{added}}(\text{metal ion})$ instead of total concentration.

As expected from the irradiation experiments without added metals, the DOC content of F1 decreased upon irradiation, and that of F2 and F3 increased with increasing t_{irrad}. While more than half of the DOC initially contained in F1-F3 was present as F1, this fraction was reduced to approximately half after $t_{\text{irrad}} = 30$ min and less than half after $t_{\text{irrad}} = 60$ min. The sum of F1-F3 remained nearly constant (cf. Figure 4.2).

The results for all experiments containing added metals are summarily presented in Figure 6.1. For comparison, the values corresponding to the experimental runs without added metals are given at the bottom of the histograms (gray and black stubs). After $t_{\text{irrad}} = 30$ min, the DOC content of the sample without added metals (gray stub in Figure 6.1, left panel) was close to the mean of all samples for F1 and F3. However, for F2, the DOC content of this sample was at the high end of the distribution, suggesting that the addition of metals led to a smaller F2.

After $t_{\text{irrad}} = 60$ min, the value of the DOC content of the sample without metals (black stub in Figure 6.1, left panel) was at the lower end of the distribution for F1, pointing to a retardation of the degradation of F1 in the presence of added metals. Congruently, this sample showed larger F2 and F3 (both close to the upper end of their respective distributions). Thus, addition of the selected metal ions appears to generally slow down the transformations of NOM in the direction F1 $\rightarrow$ F2 $\rightarrow$ F3 as observed after $t_{\text{irrad}} = 60$ min. This inhibitive effect may be related either to the presence of metal ions as scavengers of both electrons and OH radicals (Litter, 1999), or to the complexation of metal ions with NOM. These aspects will be discussed in more detail later.

It is interesting to note that not only the mean but also the *shape* of the histograms changes as the irradiation progresses, with peaks for the individual fractions appar-

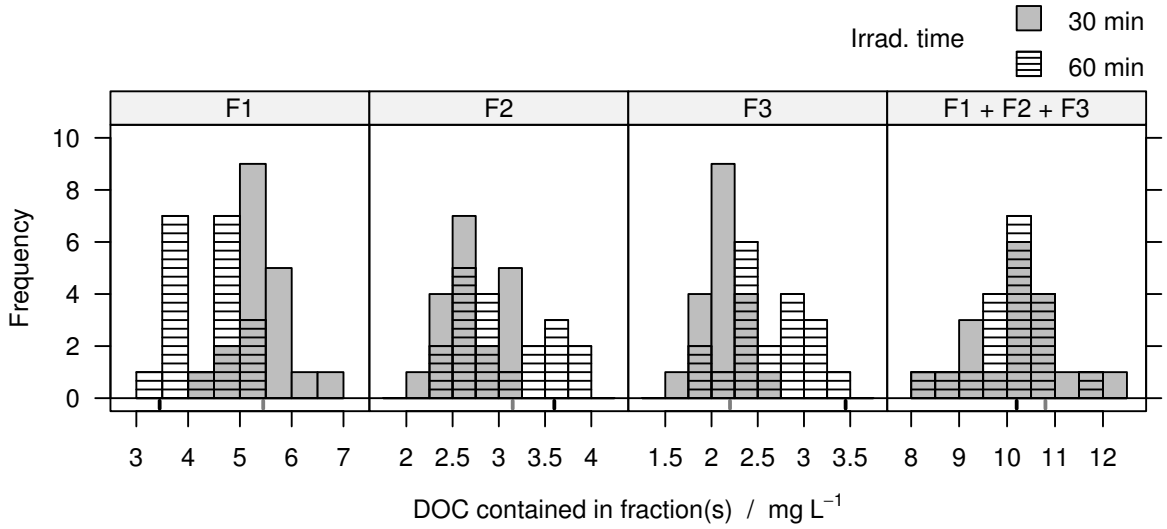

Figure 6.1: Frequency distribution of the DOC content of F1-F3 as a function of time (each data point corresponds to one experiment from a 2^4 full factorial experimental design, cf. Table 2.4 on page 22; the variable settings are shown in Table 3.3 on page 38). The gray and black stubs at the bottom of the histograms indicate the values corresponding to samples without added metals after 30 and 60 min of irradiation, respectively. Note the different bin sizes: 0.5 mg L^{-1} for F1 and F1 + F2 + F3 but 0.25 mg L^{-1} for F2 and F3.

ently acquiring a more pronounced bimodal character after 60 min of irradiation than after 30 min, as seen in Figure 6.1. For example, the mode of the DOC content of F1 after $t_{\text{irrad}} = 30$ min is between 5 and 5.5 mg L^{-1}. However, there are two modes visible after $t_{\text{irrad}} = 60$ min: one around 3.5-4.0 mg L^{-1} and one around 4.5-5.0 mg L^{-1}. This suggests that the DOC content of these fractions, originally the same regardless of the added metals, splits into two distinct "groups" during the course of irradiation. These groups may in turn result from the action of one or more of the added metals. This aspect is explored below.

6.3 DOC content of the individual fractions

In order to help quantify the effect of the added metals on the "internal" changes in the apparent molecular size distribution of the NOM samples, we fitted the polynomial model

$$y = \underbrace{\beta_0}_{\text{mean}} + \underbrace{\beta_1 x_1 + \beta_2 x_2 + \beta_3 x_3 + \beta_4 x_4}_{\text{main effects}} + \underbrace{\beta_{12} x_1 x_2 + \beta_{13} x_1 x_3 + \cdots + \beta_{34} x_3 x_4}_{\text{first-order or two-way interaction effects}} + \underbrace{\beta_{123} x_1 x_2 x_3 + \cdots + \beta_{234} x_2 x_3 x_4}_{\text{second-order or three-way interaction effects}} + \underbrace{\beta_{1234} x_1 x_2 x_3 x_4}_{\text{third-order or four-way interaction effect}} \tag{6.1}$$

to the data, where the subscripts 1-4 correspond to Cu^{2+}, Fe^{3+}, Zn^{2+} and Mn^{2+}, respectively, as defined in Table 3.3 on page 38. We then analyzed the magnitude of the coefficients by using the techniques due to Daniel (1959), Lenth (1989), and Box and Meyer (1986) to identify the most important factors influencing the DOC content of each fraction.

6.3.1 Fraction 1 (F1)

There was no clear effect of the added metals on the DOC content of F1 at $t_{\text{irrad}} = 30$ min (cf. Figure 6.1, left panel). However, evaluation of the data after $t_{\text{irrad}} = 60$ min shows an effect of added Cu^{2+}. Plotting the results only as a function of $c_{\text{added}}(Cu^{2+})$ reveals that an increasing concentration of Cu^{2+} results in a larger DOC content of F1, indicating a retardation in the degradation of this fraction as compared to samples without added Cu^{2+}. For $c_{\text{added}}(Cu^{2+})$ = 0 μmol L^{-1}, the DOC content of F1 was 3.8 ± 0.2 mg L^{-1}, while for $c_{\text{added}}(Cu^{2+})$ = 10 μmol L^{-1} it was 4.7 ± 0.5 mg L^{-1}. These data are shown as box plots* in Figure 6.2, left panel.

Note that the results in Figure 6.2 are presented as if the other metals were not present. Therefore, the variability observed for $c_{\text{added}}(Cu^{2+})$ = 0 and 10 μmol L^{-1} also includes the variations caused by the presence/absence of the other three added metals. In spite of this, the difference observed for F1 in Figure 6.2 between $c_{\text{added}}(Cu^{2+}) = 0$ and at $c_{\text{added}}(Cu^{2+}) = 10$ μmol L^{-1} is statistically significant when considering a 99% confidence interval (CI) for the difference of means. The data at $c_{\text{added}}(Cu^{2+}) = 5$ μmol L^{-1} (center point) show the variability of true replicates of the same experiment ($n = 3$). We note that the experimental error associated with a single experiment was, therefore, small when compared with the variability observed with $c_{\text{added}}(Cu^{2+}) = 0$ and 10 μmol L^{-1}, indicating that the influence of the

*Box plots (sometimes called box and whisker plots) summarily present all data in a distribution. The lower end of the bottom whisker in a box plot corresponds to the minimum of all observations while the top of the upper whisker represents the maximum. The bottom of the box represents the 25th percentile (1st quartile), the central line the median (50th percentile or 2nd quartile), and the top of the box the 75th percentile (3rd quartile) of the distribution (Lapin, 1997).

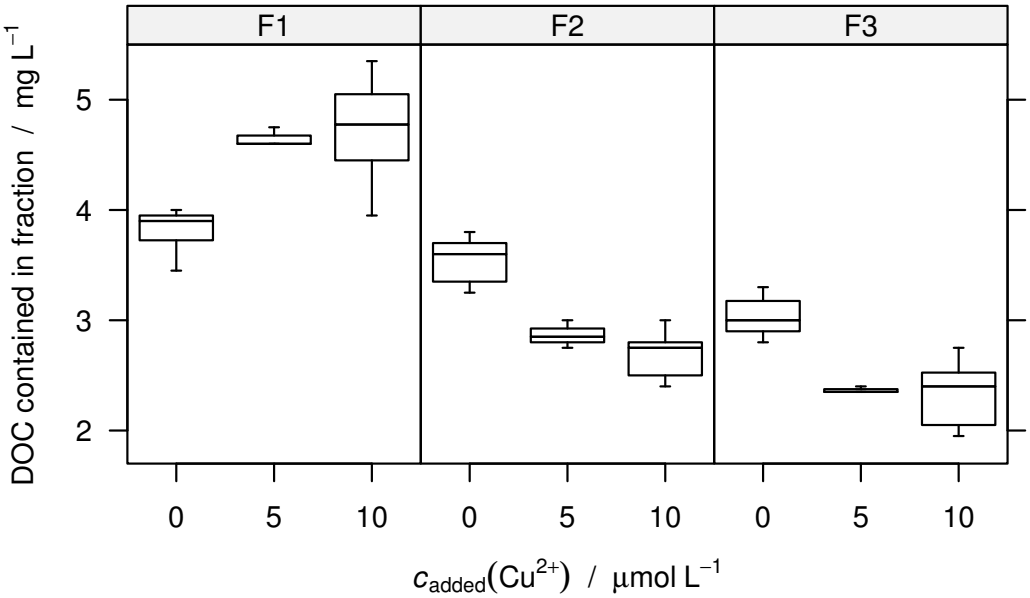

Figure 6.2: Box plots showing the DOC content of F1, F2 and F3 after 60 min of irradiation. The box at $c_{\text{added}}(\text{Cu}^{2+}) = 5$ µmol L^{-1} ($x_1 = 0$) results from the repetitions at the center point (true replicate runs, $n = 3$).

other added metals on the degradation of F1, though small compared to that of Cu^{2+}, may not be negligible.

The largest of these other influences was that of added Mn^{2+}. The change in DOC content with added Cu^{2+} was different in the absence and in the presence of added Mn^{2+}: $\rho(\text{DOC}_{\text{F1}})_{x_1=+1} - \rho(\text{DOC}_{\text{F1}})_{x_1=-1} = 1.2 \pm 0.3$ mg L^{-1} for $c_{\text{added}}(\text{Mn}^{2+}) = 0$ µmol L^{-1} but only 0.6 ± 0.4 mg L^{-1} for $c_{\text{added}}(\text{Mn}^{2+}) = 10$ µmol L^{-1}. Thus, the magnitude of the observed effect of added Cu^{2+} decreased with increasing $c_{\text{added}}(\text{Mn}^{2+})$ (first-order interaction effect). We note that the addition of Mn^{2+} alone did not have a significant effect on the DOC content of the fractions.

Figure 6.2 also reveals that the change in DOC content of F1 after 60 min of irradiation did not depend linearly on $c_{\text{added}}(\text{Cu}^{2+})$. Instead, it appears that already small amounts of added Cu^{2+} strongly retarded the degradation of F1, with the effect of $c_{\text{added}}(\text{Cu}^{2+})$ becoming smaller per µmol L^{-1} as $c_{\text{added}}(\text{Cu}^{2+})$ increased.

The presence of Cu^{2+} in NOM samples has been reported to interfere with wet chemical oxidation methods, such as the one used to quantify DOC in this study. In fact, using the same analytical system and the same water source[†], Brinkmann (2003) re-

[†]Water from Lake Hohloh exhibits moderate changes in DOC content depending on the sampling

ported reduced carbon recovery rates when adding Cu^{2+} at concentrations greater than 25 µmol L^{-1}. However, for $c(Cu^{2+}) \leq 10$ µmol L^{-1}, no detection problems were observed. Furthermore, in our experiments, added Cu^{2+} led to higher DOC content of F1, indicating a retardation in the photocatalytic degradation of F1 rather than an inhibition in DOC detection as observed by Brinkmann (2003), which would have led to an erroneously lower value. Therefore, we rule out a biasing of our results due to systematic measurement error in the presence of added Cu(II) ions. Accordingly, we conclude that the effect of added Cu(II) ions is real and requires an explanation.

Different authors have reported the acceleration and inhibition of degradation reaction kinetics when copper(II) ions are added to titanium dioxide suspensions (e.g. Aarthi and Madras, 2007; Bideau et al., 1991; Cai et al., 2003; Chen et al., 2002; Lindner et al., 1997; Wang et al., 2007). The mechanisms proposed therein are based on the electron acceptor role of copper(II) ions for the conduction band electrons from the irradiated TiO_2. This effect has been reported to be concentration dependent (Litter, 1999):

- at "low" concentrations (similar to those in the present study), the effect of added Cu(II) ions is often reported to be *accelerating*. This is explained by the ability of Cu(II) ions to accept electrons from the conduction band, thus inhibiting recombination.
- at "high" concentrations, the effect of added Cu(II) ions is generally *inhibiting*. This is attributed to the Cu(II) ions acting as scavengers for OH-radicals.

These two explanations require the Cu(II) ions to be free in solution. This is a reasonable assumption if the DOC present does not possess complexing moieties, as has been the case in most previous studies. However, NOM is known to have a high copper complexation capacity.‡ Thus, the formation of NOM-Cu^{2+} complexes may well play a key role in the inhibiting effect observed when adding Cu(II) ions to the TiO_2 suspensions.

Frimmel and Geywitz (1983) reported complexation capacities of isolated aquatic humic substances from different German lakes and rivers ranging from 1.8 to 6.8 µmol Cu per mg C, as measured by polarography. The complexation capacity of NOM is largely determined by the acidic functional groups present in it (Prado et al., 2006), although Cu^{2+} is known to be able to bind to both carboxylic and phenolic groups in humic substances (Martyniuk and Wieckowska, 2003). Lake Hohloh water has been

time and season. However, the quality of the DOC is essentially constant (Abbt-Braun and Frimmel, 2002).

‡Incidentally, the copper complexation capacity is used as an estimate of the upper bound for the metal ion complexation capacity of NOM. These complexes are considered stable (Lubal et al., 1998).

shown to possess an acidic functional group in every 4-8th carbon (based on proton titration), with approximately every 10th of these functional groups being able to form stable bivalent metal complexes. Measurements of the copper complexation capacity of Lake Hohloh water yielded a value of $\approx$ 1.9 µmol Cu per mg C (Abbt-Braun and Frimmel, 2002). Were all the added copper in our experiments bound in complexes with the NOM, this would lead to $\lessapprox$ 0.5 µmol Cu per mg C, a value well below the complexation capacity for this NOM. Thus, we expect most Cu^{2+} ions to be present as Cu^{2+}-NOM complexes.

While there is no literature information regarding the photocatalytic degradation of NOM in the presence of Cu(II) ions, indirect information on this process can be obtained from other advanced oxidation processes. Using the H_2O_2/UV process, Liao et al. (2001) report the inhibition of humic acid (HA) mineralization in the presence of added copper(II) ions, albeit at higher concentrations than those used in this study (40-60 µmol L^{-1}). They proposed that HA-copper complexes are more resistant to attack by $^{\bullet}OH$ than HA alone. This would agree with the results presented in Figure 6.2 (left panel). However, the experiments by Liao et al. (2001) are strongly convoluted with the radical scavenging effect of Cu^{2+} because the concentrations present in their experiments exceed by a factor of 5-8 the complexation capacity of the humic acid (Aldrich) ($\approx$ 1µmol per mg C; Kolokassidou et al., 2009). No other reports of the degradation of copper-NOM or copper-HA complexes by hydroxyl radicals are known to us. However, the complexing agent EDTA is known to be degraded more rapidly by $^{\bullet}OH$ (in the sonolysis process) than its copper complex (Cu-EDTA; Frim et al., 2003). Thus, it appears that a stabilization of the NOM by complexation is responsible for the inhibition in degradation observed in our experiments.

It is, however, unclear how the addition of Mn^{2+} affects the effect of added Cu^{2+}. Uyguner and Bekbolet (2007) reported that the addition of Mn^{2+} ions did not significantly alter the degradation kinetics of humic acids, in agreement with our results for the effect of added Mn^{2+} alone. However, the type of interaction described above has not yet been reported. A possibility would be, that the Cu^{2+} complexes are largely substituted by Mn^{2+} complexes. An analogous behavior was observed by Park et al. (2006) in the system EDTA-Cu^{2+}/Fe^{3+}, where the Cu^{2+} replaced the Fe^{3+} and changed the degradation kinetics accordingly. However, such a substitution is unlikely for the case NOM-Cu^{2+}/Mn^{2+} because the stability of the Cu^{2+} complexes of humic and fulvic acids is approx. one order of magnitude higher than that of the corresponding Mn^{2+} complexes (Hirata, 1981). Cu^{2+} and Fe^{3+} generally bind more strongly to humic acids than Mn^{2+} and Zn^{2+} (Van Dijk, 1971).

We stress, however, that complex stability and increased stability against attack by $^{\bullet}OH$ are not the same, as shown for example by the work of Madden et al. (1997) with EDTA complexes of several metal ions. Instead, the effect of complex formation on the degradation kinetics in irradiated TiO_2 suspensions appears to depend both on the nature of the metal ion and on the nature of the complexing partner. For example, in the case of EDTA complexes, addition of Fe^{3+} and Zn^{2+} inhibit the photocatalytic degradation of the complexes to a much larger extent than addition of Cu^{2+}, although Cu^{2+} complexes of EDTA are more stable (Madden et al., 1997; Park et al., 2006). In our experiments, the formation of Cu^{2+} complexes was the dominating factor.

6.3.2 Fraction 2 (F2)

Inspection of the fitted coefficients for Equation 6.1 applied to F2 after $t_{irrad} = 30$ min (shown in Figure D.1) showed an influence of $c_{added}(Cu^{2+})$ and suggested small interaction effects between Cu^{2+} and Zn^{2+} as well as between Fe^{3+} and Mn^{2+}. After 60 min, the effect of added Cu^{2+} became more dominant. Plotting the DOC content of F2 as a function of only $c_{added}(Cu^{2+})$ reveals a strong, non-linear dependence (Figure 6.2, center panel). This dependence closely mirrored the one shown for F1. Thus, the finding that increasing concentrations of Cu^{2+} led to a lower DOC content of F2 is complimentary to the observation that adding Cu^{2+} led to a larger F1.

6.3.3 Fraction 3 (F3)

Following the same procedure as above, we found a marked effect of added Cu^{2+} on the DOC content of F3 already after 30 min of irradiation. As already seen for F2, increasing $c_{added}(Cu^{2+})$ also led to a lower DOC content of F3. Analysis of the results after $t_{irrad} = 60$ min shows qualitatively the same results (shown in Figure 6.2, right panel). Thus, the presence of the added metals, especially of copper, slows down the degradation and mineralization of NOM apparently by stabilizing the high molecular weight material through complexation.

6.4 Formation of low molecular weight organic acids (LMWOA)

The concentration of formic, oxalic, succinic and glutaric acids (structures shown in Figure 4.7 on page 55) was quantified by using ion chromatography (IC). Acetic and malonic acids were also detected but could not be quantified (cf. Section 4.3).

The measured concentrations of all four acids after $t_{\text{irrad}} = 30$ min and $t_{\text{irrad}} = 60$ min are summarized in Table 6.1. The acids were present in concentrations following the order: formic $>$ oxalic $\gg$ succinic $\approx$ glutaric acid. It is worth pointing out that the LMWOA are not only formed during the course of irradiation but can also be degraded by $^{\bullet}$OH. Regarding the time evolution of the concentrations, we note that both the mean and the standard deviation increased with increasing irradiation time. The increase in mean concentration shows the steady production of these acids during irradiation, while the increase in standard deviation may result from an effect of the added metals.

Table 6.1: Concentration after irradiation of the quantified low molecular weight organic acids (LMWOA).

	ρ(LMWOA), mg L^{-1}		
LMWOA	0 min	30 min	60 min
Formic acid	0.3 ± 0.2	0.8 ± 0.3	1.3 ± 0.6
Oxalic acid	0.1 ± 0.1	0.4 ± 0.2	0.7 ± 0.4
Succinic acid	< 0.1	0.1 ± 0.0	0.1 ± 0.1
Glutaric acid	< 0.1	< 0.1	0.1 ± 0.1

In order to explore the effect of the added metals, we employed the same techniques as in Section 6.3. These could be applied to both formic and oxalic acids but not to succinic and glutaric acids because the absolute amounts produced were too small.

First, we note that the range of concentration of formic acid is not very large, spanning from 0.4 to 1.2 mg L^{-1} after $t_{\text{irrad}} = 30$ min. Within this range, however, there were differences between the amounts produced at different levels of added metals. The largest of these was found in experiments with $c_{\text{added}}(\text{Mn}^{2+}) = 10$ µmol L^{-1}. Here we observed a *decrease* in the concentration of formic acid with *increasing* $c_{\text{added}}(\text{Cu}^{2+})$, from 1.1 ± 0.1 mg L^{-1} at $c_{\text{added}}(\text{Cu}^{2+}) = 0$ µmol L^{-1} to 0.5 ± 0.0 mg L^{-1}

at $c_{\text{added}}(Cu^{2+})$ = 10 µmol L^{-1} (significant, 99% CI). In contrast, there was no clear effect of added Cu^{2+} in the case of no added Mn^{2+}. This type of interaction effect is similar to that described in Section 6.3.1, but the "direction" of the interaction is exactly the opposite. Unfortunately, we cannot offer a plausible explanation for this at the present time.

At $t_{\text{irrad}} = 60$ min, the same qualitative results were obtained as for $t_{\text{irrad}} = 30$ min. Quantitatively, the formic acid concentrations were approximately twice as high (0.8-2.3 mg L^{-1}) and the effect of added Cu^{2+} increased proportionately.

In the case of oxalic acid, the largest effect was that of added Cu^{2+}, as shown in Figure 6.3. After 30 min of irradiation, ρ(oxalic acid) = 0.6 ± 0.3 mg L^{-1} in the absence of added Cu^{2+} but only 0.3 ± 0.1 mg L^{-1} when $c_{\text{added}}(Cu^{2+})$ = 10 µmol L^{-1}. This difference is significant considering a 99% CI. The same trend is seen at a higher level after 60 min of irradiation. We note that the effect of added Cu^{2+} is *not* linear for both 30 and 60 min of irradiation. A small interaction effect observed for the addition of Mn^{2+} was not statistically significant.

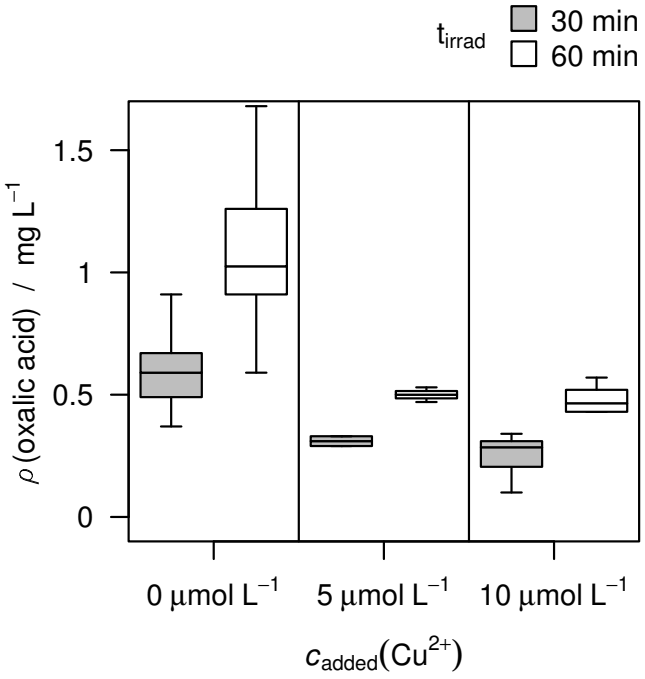

Figure 6.3: Box plots showing the concentration of oxalic acid after simulated solar irradiation of NOM in the presence of TiO_2 and of added Cu^{2+}.

Thus, it is apparent that the main influence on the formation of both formic and oxalic acids came from the addition of Cu^{2+}, and that this influence was negative with

respect to LMWOA formation. A similar behavior regarding Cu^{2+} was found by Brinkmann et al. (2003a) in bog lake water samples irradiated with simulated solar light in the absence of TiO_2 (direct photolysis), but the addition of Mn^{2+} and/or Zn^{2+} was not considered in that work. In addition, an increase in production of LMWOA in the presence of added Fe^{3+}, as was the case for the direct photolysis of Lake Hohloh water NOM (Brinkmann, 2003; Brinkmann et al., 2003a), was not observed in our experiments.

6.5 Bioavailability of DOC in F1-F3

The irradiated samples were incubated with a bacterial culture for a period of two days in order to examine the bioavailability of the DOC after partial degradation (cf. Section 4.4). SEC-DOC chromatograms revealed changes in all fractions, with F1 being larger after incubation compared to before incubation, and both F2 and F3 being smaller after incubation. These results are shown in Figure 6.4. We attribute the increase in F1 to the synthesis of high molecular weight organic compounds by the bacteria (Wingender et al., 1999), and the decrease of F2 and F3 to the biological degradation of the bioavailable components present in these two fractions (cf. Brinkmann et al., 2003a). We note that LMWOA (contained in F2 and F3) are more easily available for uptake and integration into the microbial metabolism than larger molecules.

Addition of the metal ions led to changes in the amount of DOC degraded by the bacteria, in particular, addition of Cu^{2+} was observed to lead to lower amounts of DOC being biodegraded, as shown for F2 in Figure 6.5. Although Cu^{2+} is necessary for bacterial life and growth in trace amounts, it is known to be toxic at higher concentrations (Domek et al., 1984; Lamb and Tollefson, 1973; Trevors and Cotter, 1990). Within the range of $c_{\text{added}}(Cu^{2+})$ used in this study, however, only a reversible inhibition (adaptation) of the added bacteria is to be expected (Trevors and Cotter, 1990). Furthermore, the inhibiting effect of Cu^{2+} in biological systems is observed when adding free Cu^{2+}, which then interacts with different biomolecules. In our case, the copper ions are initially complexed to the NOM, leaving a much lower effective concentration of copper ions.

Comparison of Figure 6.5 with Figure 6.2 reveals that the "inhibition" in the biodegradation mirrored the inhibition seen for the photocatalytic degradation of F1 to form F2 and F3. Thus, we are not able to discern any effect of the presence of the metals

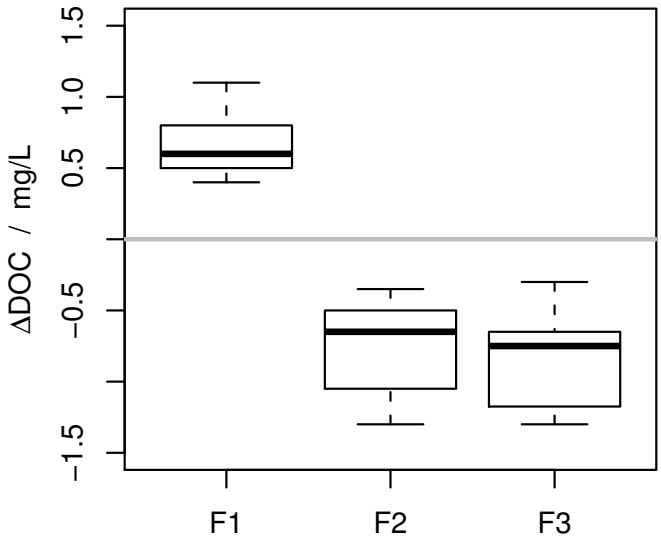

Figure 6.4: Box plots showing the change in DOC content of F1-F3 for all irradiated samples ($t_{\text{irrad}} = 60$ min) after incubation with a mixed bacterial culture. The change in DOC is defined as $\Delta\text{DOC} = \text{DOC}_{\text{after incubation}} - \text{DOC}_{\text{before incubation}}$.

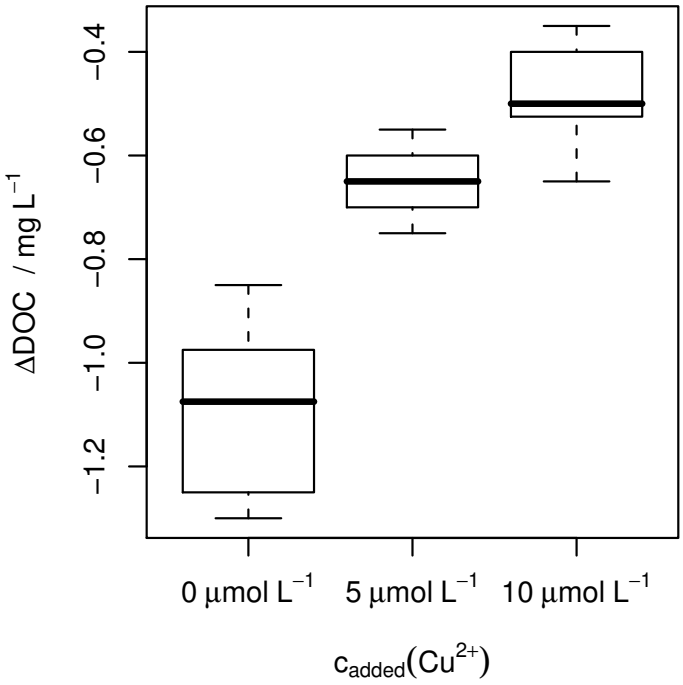

Figure 6.5: Effect of added Cu^{2+} on the bioavailability of Fraction 2 after irradiation ($t_{\text{irrad}} = 60$ min). The change in DOC is defined as $\Delta\text{DOC} = \text{DOC}_{\text{after incubation}} - \text{DOC}_{\text{before incubation}}$.

on the bioavailability/biodegradation of the DOC because the amounts degraded are closely coupled to the available amounts.

6.6 Bioavailability of low molecular weight organic acids (LMWOA)

Formic, succinic and glutaric acid were completely biodegraded after two days of incubation. The concentration of oxalic acid was reduced by $82 \pm 8\%$ for $t_{\mathrm{irrad}} = 30$ min and $87 \pm 10\%$ for $t_{\mathrm{irrad}} = 60$ min. Thus, the fraction of degraded oxalic acid was nearly constant although more oxalic acid was initially present before incubation in the case of $t_{\mathrm{irrad}} = 60$ min.

The difference in biodegradation between oxalic acid and formic, glutaric and succinic acids can be explained by their different functions in the bacterial metabolism. Formic acid is built up or utilized in several metabolic pathways present in many different microorganisms such that a direct use of formic acid is to be expected (Gräntzdörffer, 2000). Similarly, succicinic acid is used directly in the citric acid cycle (Bailey and Ollis, 1986) and glutaric acid plays an important role in the amino acid degradation. The glutaric acid is converted to acetyl coenzyme A that could be directly used in the citric acid cycle or for the build-up of fatty acids (e.g. Griffin and Trudgill, 1972).

In contrast, oxalic acid is in many organisms an end product that is secreted into the environment. Only plant cells and few bacteria (e.g. *Oxalobacter formigenes*, *Ralstonia oxalatica* or *Moorella thermoacetica*) have been shown to be able to metabolize oxalic acid. Oxalic acid is degraded by e.g. *Oxalobacter formigenes* to formic acid that can be utilized by many different microorganisms (Daniel et al., 2004).

6.7 Interim summary

We observed an inhibition of the photocatalytic degradation of NOM by the addition of up to 10 µmol L^{-1} of Cu^{2+}, also in combination with up to 10 µmol L^{-1} of Fe^{3+}, Mn^{2+} and Zn^{2+}. The addition of Mn^{2+} was observed to change the magnitude of the effect of added Cu^{2+} in two cases:

- a larger inhibiting effect of $c_{\text{added}}(Cu^{2+})$ was observed in the *absence* of added Mn^{2+} during the degradation of the DOC contained in F1 (large molecular weight material); and
- an inhibiting effect of $c_{\text{added}}(Cu^{2+})$ was only observed in the *presence* of added Mn^{2+} for the case of formic acid formation.

These two first order interaction effects between added Cu^{2+} and added Mn^{2+} have the opposite "direction" for the same combination of metals and exemplify the complexity of the system at hand. No significant effects were observed when adding Fe^{3+} and Zn^{2+} to the suspensions.

While there are several reports of metal ion addition affecting reaction kinetics in irradiated TiO_2 suspensions, the metal ion concentrations used in this study (0-10 μmol L^{-1}) are low compared to most other reported previously. This means that the influence of free metal ions (electron scavenging, radical scavenging) is expected to be negligible in our experiments due to complexation of the metal ions by the NOM. Therefore, our results point to a stabilization of the NOM against degradation by $^{\bullet}OH$ by complexation with Cu^{2+}.

By defining three fractions in the SEC-DOC chromatograms, the role of the middle fraction as a degradation intermediate was observed, in agreement with the experimental and modeling results presented in Chapter 4 and Section 5.2. The effects of added metal ions were observed most clearly and at shorter irradiation times with this middle fraction.

Addition of metal ions also affected the production of low molecular weight organic acids. The addition of Cu^{2+} led to reduced production of formic and oxalic acids. Addition of Mn^{2+} led to an interaction effect as described above. There was no evidence of the added metal ions affecting the bioavailability neither of the NOM nor of the low molecular weight organic acids.

Chapter 7

Initial evaluation of the formation of brominated byproducts in irradiated titanium dioxide suspensions*

With this chapter we leave the study of the photocatalytic degradation of natural organic matter and turn our attention to the formation of unwanted byproducts. Although there are many studies on the photocatalytic oxidation of a large variety of substances in irradiated TiO_2 suspensions, studies dealing with the formation of undesirable byproducts in this process are rare. The characterization of the formation of such byproducts is, however, a prerequisite for the further development of this technology in the field of water treatment for human consumption.

There are reports suggesting that TiO_2-photocatalysis does not lead to significant formation of disinfection byproducts (DBPs). Richardson et al. (1996) found only one DBP after photocatalytic treatment of ultrafiltered raw water, compared to 35 after a subsequent chlorination. However, in this study neither the influence of the presence of Br^- in the raw water nor the formation of BrO_3^- were considered.

The formation of brominated byproducts in the photocatalytic oxidation of bromide-containing waters is nonetheless a possibility that needs to be considered if the raw water contains elevated concentrations of bromide ions. Herrmann and Pichat (1980) have reported that Br^- can be oxidized in irradiated TiO_2 suspensions under both acidic and basic conditions to a much greater extent than Cl^-. Their experiments were performed in the absence of dissolved organic carbon (DOC). In irradiated TiO_2 suspensions containing bromide and DOC, the Br_2 that is formed should react with the available organic compounds to yield brominated products (quantified

*The main findings discussed here were published in *Water Research* by Tercero Espinoza and Frimmel (2008).

as AOX, the amount of organically-bound halogen adsorbable onto activated carbon). These halogenated products are undesirable, although their concentration is not regulated. The formation of these (by)products needs to be taken into account since DOC is present in varying concentrations in all raw waters in the form of natural organic matter (NOM). A regulated bromoorganic compound which could also be formed is bromoform ($CHBr_3$). The sum of the concentrations of bromoform, dibromochloromethane, bromodichloromethane, and chloroform (trihalomethanes, THM) has a limit of e.g. 50 $\mu g\ L^{-1}$ in drinking water under German legislation.

In the previous Chapters, we examined the photocatalytic degradation of NOM because of its role as a precursor for disinfection byproducts (DBPs). In this Chapter, we describe and discuss experiments on the irradiation of aqueous TiO_2 suspensions containing elevated but drinking water-relevant concentrations of Br^- (1-3 mg L^{-1}), in the absence and in the presence of dissolved organic carbon (DOC) in the concentration range 1-10 mg L^{-1} C. We aimed to quantify the formation of BrO_3^- and bromoorganic byproducts (AOX and THM) formed upon irradiation of these suspensions using three sources of DOC, one natural source (water from Lake Hohloh, Black Forest, Germany, described in detail in Frimmel et al., 2002) and two model sources: salicylic acid and 2,4-dihydroxybenzoic acid (shown in Figure 7.1).

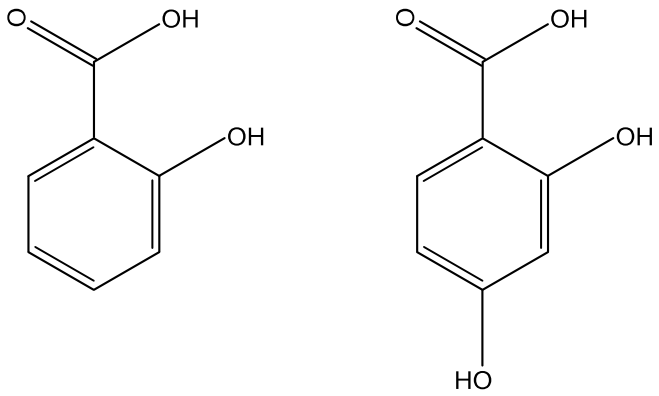

Figure 7.1: Structure of the two model compounds used as source of dissolved organic carbon in this study: (left) salicylic acid and (right) 2,4-dihydroxybenzoic acid.

7.1 Titanium dioxide suspensions containing bromide but no dissolved organic carbon

Initial experiments using 1 g L^{-1} suspensions of P25 containing 10 mg L^{-1} Br^- and irradiated in the reactor described above for a period of $\leq$ 120 min revealed no formation of Br_2. Using ion exchange chromatography (IC), we found neither a change in the concentration of Br^- nor any evidence for the formation of BrO_3^- (< 5 µg L^{-1}) during the course of irradiation.

These observations are similar to those of Selcuk et al. (2004), who studied the formation of "active bromine species" (i.e. Br_2 and HOBr) in both photocatalysis and photoelectrocatalysis. They found active bromine species in photoelectrocatalysis but not in photocatalysis using immobilized TiO_2. This would suggest that no active bromine species are formed in heterogeneous photocatalysis, implying that no bromate can be formed. However, Herrmann and Pichat (1980) reported that in TiO_2 suspensions (of TiO_2 concentration similar to ours) containing 10^{-2} mol L^{-1} Br^- and irradiated with UV, a very small fraction ($\approx$ 0.003 %) of the initial Br^- is oxidized after 6 h of irradiation under both acidic and basic conditions (pH 1 and 13.5, respectively). In our experiments, carried out at pH 6, a conversion of a similar fraction of the initial Br^- ion would lead to a change of concentration of Br^- on the order of $\approx 10^{-9}$ mol L^{-1} leading to a maximum possible generation of 10^{-9} mol L^{-1} BrO_3^- ($\approx 10^{-7}$ g L^{-1}). This amount, if formed, would be 100 times lower than the allowable maximum concentration of BrO_3^- in drinking water according to European and German legislation and approximately one order of magnitude below the detection limit of our ion chromatography setup. Furthermore, it is known that BrO_3^- can be reduced in irradiated TiO_2 suspensions (Lindner et al., 1997; Mills et al., 1996; Noguchi et al., 2002, 2003), such that any BrO_3^- formed is likely to be immediately reduced to Br^-.

7.1.1 Reduction of bromate to bromide

In experiments with irradiated TiO_2 suspensions containing BrO_3^- (2.1-4.3 mg L^{-1}) or a mixture of Br^- (10 mg L^{-1}) and BrO_3^- (2 mg L^{-1}), we observed a rapid reduction of BrO_3^- to Br^- and the formation of Br_2 as an intermediate product. The formation of Br_2 was dependent on both the concentration of TiO_2 and initial concentration of BrO_3^-, as seen in Figure 7.2 for P25. Comparison of panels a & c with b & d in Figure 7.2 reveals that increasing the concentration of TiO_2 from 0.5 to 1.0 g L^{-1} gives rise to increased production of Br_2 regardless of the initial concentration of BrO_3^-. In

turn, increasing the initial concentration of BrO_3^- gave rise to increased production of Br_2 regardless of the concentration of TiO_2.

In the case of Hombikat UV100 suspensions, no generation of Br_2 was observed. However, BrO_3^- was reduced to Br^- in suspensions of both TiO_2 materials, albeit with different velocity: the reaction proceeded faster in P25 suspensions than in Hombikat UV100 suspensions. These results are presented graphically in Figures E.1 and E.2 on pages 169-170. An increase in the concentration of TiO_2 in the range 0.5 to 1.0 g L^{-1} led to a modest acceleration of the reduction of BrO_3^- to Br^- for both materials, as seen in Figures E.3 and E.4 on pages 171-172.

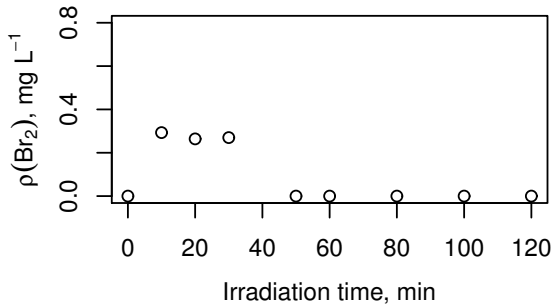

(a) $\rho(TiO_2)$= 0.5 g L^{-1}, $\rho_o(BrO_3^-)$= 4.3 mg L^{-1}

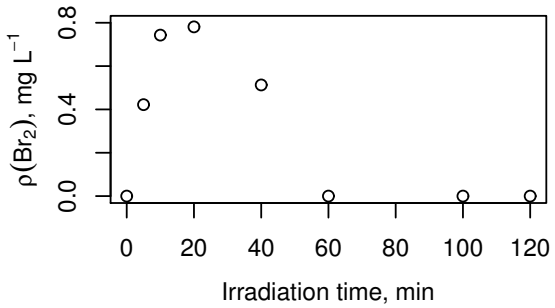

(b) $\rho(TiO_2)$= 1.0 g L^{-1}, $\rho_o(BrO_3^-)$= 4.3 mg L^{-1}

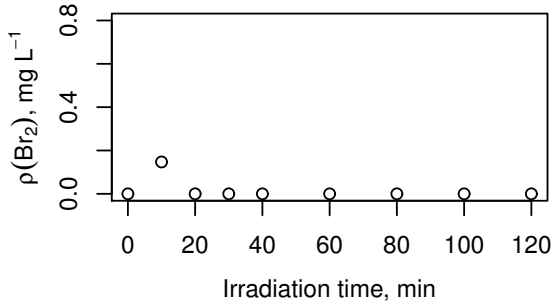

(c) $\rho(TiO_2)$= 0.5 g L^{-1}, $\rho_o(BrO_3^-)$= 2.1 mg L^{-1}

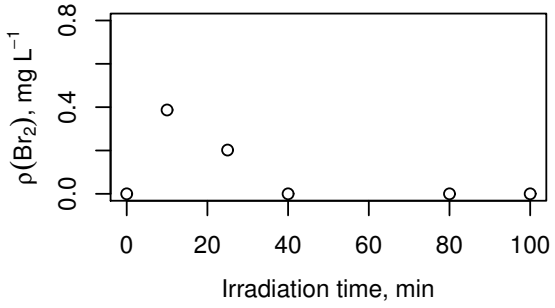

(d) $\rho(TiO_2)$= 1.0 g L^{-1}, $\rho_o(BrO_3^-)$= 2.1 mg L^{-1}

Figure 7.2: Generation of Br_2 during irradiation of bromide-containing TiO_2-suspensions under different conditions, showing the dependence on $\rho(TiO_2)$ and $\rho_0(BrO_3^-)$.

It is worth noting that BrO_3^- poses an important problem in drinking water treatment by ozonation and that its removal is difficult by conventional means (e.g. reduction on the surface of activated carbon, or by Fe(II) or UV irradiation; von Gunten, 2003).

This has led to heterogeneous photocatalysis being proposed as a possible cleanup step after ozonation (Mills et al., 1996; Noguchi et al., 2002, 2003).

7.2 Titanium dioxide suspensions containing bromide and dissolved organic carbon

The results discussed above, ours and those of Selcuk et al. (2004) and Herrmann and Pichat (1980), suggest that photocatalysis may be used in the treatment of water for human consumption without having the drawback of forming BrO_3^- in water containing Br^-. However, these experiments were conducted in the absence of dissolved organic carbon (DOC). DOC, in the form of natural organic matter (NOM) is ubiquitous in nature and always present (in varying concentrations) in raw water. The experiments of Richardson et al. (1996), mentioned above, did include NOM but did not consider the presence of bromide ions.

We sought to extend our results to conditions closer to those encountered in the treatment of natural waters for drinking purposes. To do this, we irradiated suspensions of both P25 and Hombikat UV100 TiO_2 powders of different concentrations in the presence of varying amounts of Br^- and DOC from both a natural water and a model source. In addition, we performed the experiments in both demineralized water and drinking water (Karlsruhe, Germany) and with different irradiation times. The variable ranges are presented in Table 3.4. Because of the many factors explored, we did not seek to immediately characterize in detail the influence of every factor on the (possible) formation of BrO_3^- and/or brominated byproducts (AOX and THM). Instead, we sought to ascertain: 1) whether BrO_3^- and/or brominated byproducts are formed in the given range of conditions, and 2) which factors are most likely to influence the process based on the experimental results. To do this, we turned to a Plackett-Burman screening design, as described in Section 2.5.3.

Four responses were measured for each experiment: the change in concentration of Br^- and organically-bound halogens adsorbable onto activated carbon (AOX) upon irradiation, and the concentration of bromate and trihalomethanes (THM) after irradiation. The concentration of Br^- changed only slightly between the beginning and end of irradiation and was typically within analytical error.

Further analysis of the irradiated samples by anion exchange chromatography revealed no detectable formation of BrO_3^- (< 5 μg L^{-1}). We also checked for the for-

mation of trihalomethanes (THMs) in the liquid phase but none of the samples tested positive (detection limits $CHCl_3 \leq 0.4$ µg L^{-1}, $CHCl_2Br \leq 0.2$ µg L^{-1}, $CHClBr_2 \leq 0.5$ µg L^{-1}, $CHBr_3 \leq 0.8$ µg L^{-1}). In addition, we examined the headspace of irradiated suspensions containing a high initial concentration of both Br^- (3 mg L^{-1}) and DOC (10 mg L^{-1}) and found no THMs.

Measurements of halogenated organic compounds adsorbable onto activated carbon (AOX, here expressed as adsorbable organic bromine, AOBr) revealed that the difference in AOBr content before and after irradiation of the suspensions depended on two variables, namely, the reaction time and initial concentration of Br^- (Figure 7.3a). Whereas at an initial Br^- concentration of 1 mg L^{-1} no significant formation of AOBr was measured, we observed an increase in AOBr after 15 min of irradiation when the initial concentration of bromide was 3 mg L^{-1} (Figure 7.3b). The mean AOBr content was much lower in the samples irradiated for 45 min. We note that the AOBr concentrations reported here are those in solution after separation of the titanium dioxide particles through filtration. These values do not reflect the unknown amount of AOBr which adsorbs to the titanium dioxide particles or to the membrane filter during sample preparation. Later attempts to quantify the "missing" AOBr pointed to a quantity roughly of the same magnitude as that found in solution.

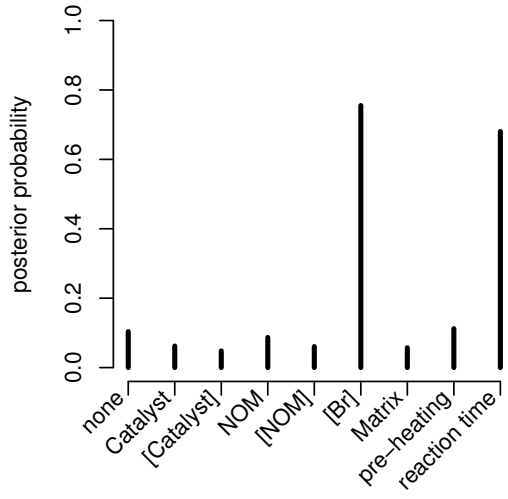

(a) Posterior probability plot for the change in AOBr (in µg L^{-1}). The bars indicate the probability that a variable is "active".

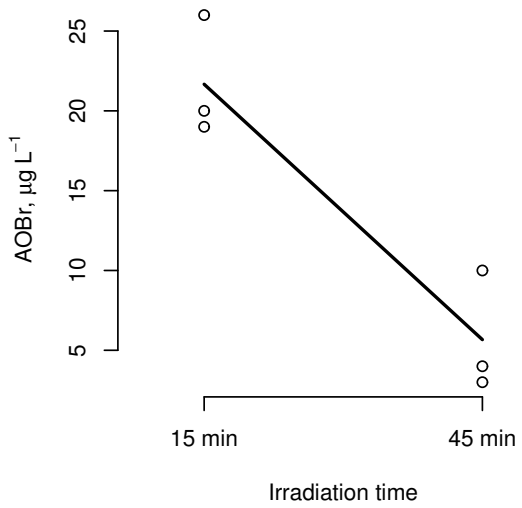

(b) Results for high initial Br^- concentration ($x_5 = +1$, $\rho_o(Br^-)$ = 3 mg L^{-1}) plotted as a function of irradiation time only.

Figure 7.3: Screening results for the change in AOBr.

Assuming a sequence of reactions as shown in Figure 7.4 (Br_2 attacks the original DOC and its metabolites yielding AOX, further attack by Br_2 can lead to bromoform), the absence of bromoform in the screening results could be due to three reasons:

1. a low concentration of Br_2 yields AOX but is insufficient to drive the reactions further, e.g. to triply-brominated carbon-compounds such as bromoform,
2. the original DOC does not easily lead to the formation of bromoform (low bromoform formation potential), and
3. not enough time was allowed for the reaction to yield measurable amounts of bromoform.

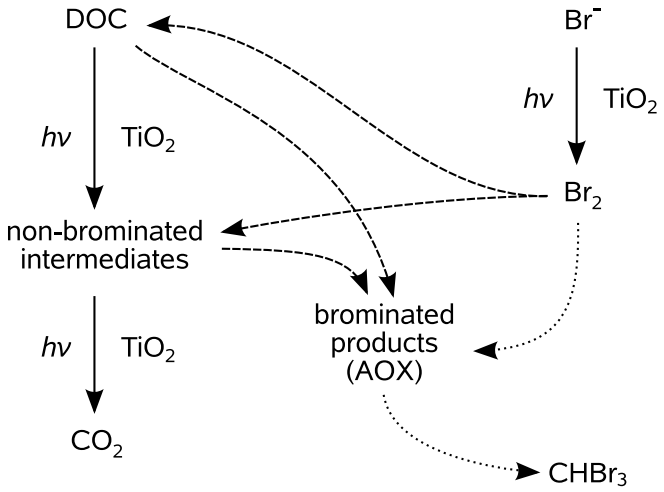

Figure 7.4: Schematic representation of the assumed steps in the formation of bromoform.

7.3 Photocatalytic oxidation of 2,4-dihydroxybenzoic acid in the presence of bromide

In order to further investigate the oxidation of organic compounds in the presence of Br^-, and especially to rule out the formation of bromoform, we prepared 1 g L^{-1} TiO_2 suspensions containing 10 mg L^{-1} 2,4-dihydroxybenzoic acid (5.5 mg L^{-1} DOC) and 3 mg L^{-1} Br^-. We chose 2,4-dihydroxybenzoic acid (DHBA) for two main reasons: 1) its functional groups make it a good model of humic substances, and 2) it has been shown to have a high yield of bromoform when reacting with Br_2 at neutral pH (0.46 mol THM per mol 2,4-dihydroxybenzoic acid when reacted with 10^{-4} mol L^{-1} Br_2; Boyce and Hornig, 1983). Furthermore, by following the reaction over longer

periods of time, it is possible to ascertain whether photocatalytic oxidation produces sufficient amounts of Br_2 to yield bromoform.

In addition to the formation of THMs, we also considered the possibility of an effect of Br^- on the reaction kinetics. Abdullah et al. (1990) have shown that the presence of some inorganic ions, including Cl^-, causes a decrease in the degradation rates of organic compounds. Because of the similarity between Cl^- and Br^-, we sought to establish whether the presence of Br^- negatively affects the kinetics of degradation of 2,4-dihydroxybenzoic acid.

In the absence of Br^-, the concentration of 2,4-dihydroxybenzoic acid was seen to decrease at a constant rate in the course of irradiation (Figure 7.5a). The 0th order rate constant for irradiated P25 suspensions was calculated to be $(9.4 \pm 0.3) \times 10^{-7}$ mol L^{-1} (duplicate measurement). In the presence of 3 mg L^{-1} Br^-, 2,4-dihydroxybenzoic acid was degraded at a constant rate, $k_1 = (9.7 \pm 0.3) \times 10^{-7}$ mol L^{-1}, throughout the course of the experiment. Thus, there is no appreciable difference in the reaction kinetics brought about by the presence of 3 mg L^{-1} Br^-.

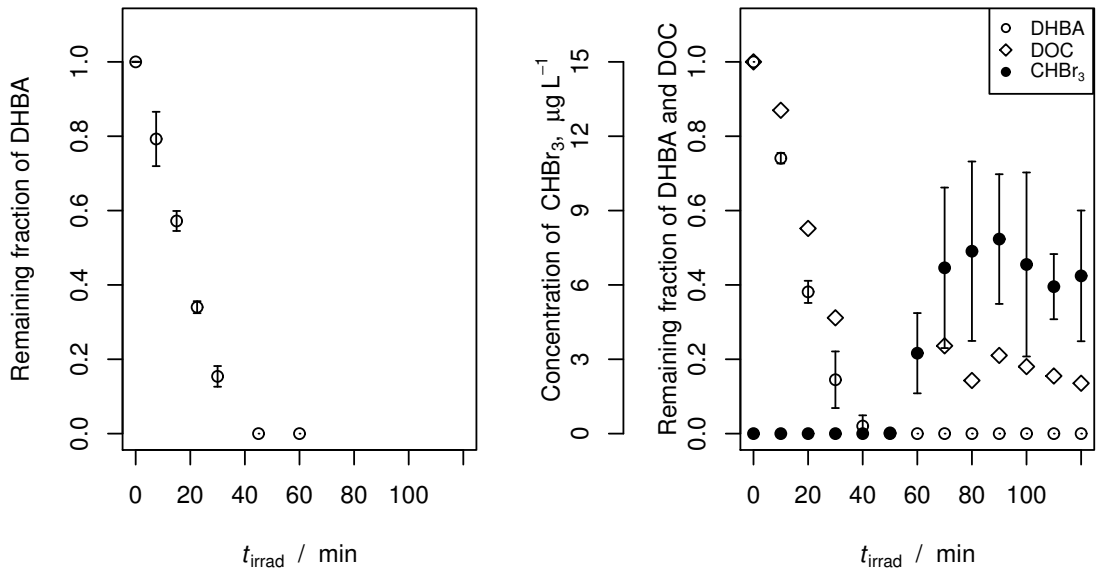

(a) Degradation of 2,4-dihydroxybenzoic acid in the absence of bromide

(b) Degradation of 2,4-dihydroxybenzoic acid and formation of bromoform in the presence of 3 mg L^{-1} Br^-

Figure 7.5: Photocatalysis in the presence and absence of Br^-.

No UV-absorbing intermediates were observed in the HPLC chromatograms of samples taken during the course of the experiments, suggesting that the aromatic ring is

opened at a very early stage in the reaction. This is in agreement with the results of Benoit-Marquié et al. (1997), who propose a ring opening as a first step in the photocatalytic degradation of 2,4-dihydroxybenzoic acid using P25 as a photocatalyst.

We found measurable amounts of bromoform in the irradiation experiments with Br^- starting at approximately 60 min of irradiation, after all the 2,4-dihydroxybenzoic acid had already been degraded. The observed concentration of bromoform increased rapidly and remained approximately constant for $t_{\text{irrad}} > 70$ min.

It is worth noting that the measured concentration of bromoform is the resulting total of bromoform produced by photocatalysis, bromoform *degraded* by photocatalysis (Yoneyama and Torimoto, 2000), and bromoform degraded by photolysis (Legrini et al., 1993). The photolytic degradation of brominated trihalomethanes has been shown to proceed with high quantum yield (0.46) when using a low pressure mercury lamp as a result of the strong absorption of C-Br bonds at about 250 nm (Legrini et al., 1993). The use of other UV-sources (such as black lamps, medium pressure mercury lamps or sunlight), lacking or having only comparatively few photons energetic enough to initiate photolysis of bromoform, could lead to higher concentrations of bromoform than those reported here (Braun et al., 1991; Oppenländer, 2003).

Since bromoform is a very small molecule, it is not surprising to find it at a late stage in the irradiation process, because larger compounds must be broken down to yield it. This finding suggests it may take considerably longer before the appearance of THMs from high molecular weight precursors. This is consistent with our negative finding of THMs in the presence of natural organic matter from Lake Hohloh and salicylic acid: the samples taken in our screening study were likely made too early in the irradiation process (after 45 min) to find any bromoform. Notice that both salicylic acid and 2,4-dihydroxybenzoic acid are C7, aromatic compounds. Because these aromatic compounds are degraded to aliphatic compounds on their way to forming THM (Benoit-Marquié et al., 1997), it is possible that aliphatic precursors give rise to higher THM yields, provided suitable active centers for the addition of bromine are present.

The formation of bromoform after (comparatively long) irradiation of 2,4-dihydroxybenzoic acid indicates that Br^- is oxidized to form Br_2, in agreement with the results of Herrmann and Pichat (1980), though in our case at nearly neutral pH and in a shorter time scale. The amounts of bromoform generated are consistent with the expectation that only a very small fraction of the Br^- is oxidized to Br_2, as shown by Herrmann and Pichat (1980), and is thus able to react with the DOC present in the TiO_2 suspensions. However, the amount of Br^- oxidized in our experiments

in the presence of 2,4-dihydroxybenzoic acid is much larger than that observed by Herrmann and Pichat (1980). In the case of 10 μg L^{-1} of bromoform formed in a suspension initially containing 3.0×10^3 μg L^{-1} Br^-, ≈ 0.3 % of the Br^- ends up bound in the bromoform. This is 100 times the conversion observed by Herrmann and Pichat (1980) in TiO_2 suspensions in the absence of DOC. In addition to this, an unknown amount of Br is bound in precursor compounds and a further amount is released again as Br^- from the photocatalytic degradation of $CHBr_3$ (Yoneyama and Torimoto, 2000). These results indicate that the oxidation of Br^- is favored by the presence of DOC. A reason for this is that the reaction of Br_2 with the DOC removes Br_2 from the system, thus favoring its formation according to Le Châtelier's Principle (Petrucci and Harwood, 1993).

7.4 Interim summary

Our screening experiments with TiO_2 containing different concentrations of Br^- and dissolved organic carbon (DOC) show no formation of BrO_3^- and trihalomethanes (THMs) for up to 45 minutes of irradiation. However, we found an increase in AOBr at short reaction times (15 min) for samples initially containing 3 mg/L Br^-. The AOBr was subsequently degraded as the reaction proceeded. Because the formation of AOBr was dependent only on the initial Br^- concentration and time, the oxidation of Br^- to Br_2 must proceed to a similar extent regardless of the identity and concentration of the photocatalyst, the identity and concentration of dissolved organic carbon, water matrix and temperature in the ranges studied.

When irradiating P25 suspensions containing 10 mg L^{-1} 2,4-dihydroxybenzoic acid and 3 mg L^{-1} Br^-, we observed the formation of bromoform (up to ≈ 10 μg L^{-1}) starting after 60 min of irradiation. The amount of Br bound in bromoform indicates that substantially more Br^- is oxidized to Br_2 in the presence of this highly reactive DOC compared to experiments performed in the absence of DOC.

These results suggest that, in contrast to ozonation and chlorination where the formation of BrO_3^- and brominated organic disinfection byproducts are a known problem, it may be possible to oxidize organic material by photocatalysis in a defined reaction window while incurring a reduced risk of generation of brominated byproducts under conditions relevant for the treatment of drinking water.

Chapter 8

Formation of bromoform in P25 suspensions under simulated solar irradiation*

In the previous Chapter, we showed that bromoform is formed in UV-irradiated P25 suspensions (Figure 7.5b). In this Chapter we systematically explore the influence of variations in the initial concentrations of 2,4-dihydroxybenzoic acid (DHBA) and Br^-, and photocatalyst concentration on the amount and timescale of the production of bromoform.

High concentrations of Br^- (low mg L^{-1} range) in surface waters can be found in arid and coastal areas, for example the Mediterranean basin and the Middle East. Furthermore, these areas often have abundant solar energy at their disposal, rendering them potentially attractive locations for the application of (solar) heterogeneous photocatalysis. To approximate these conditions, the experiments presented in this Chapter were performed using simulated solar UV-radiation.

In order to systematically study the effect of all three variables, we resorted to a Box-Behnken design for three variables (shown in Table 2.5), which consists of experiments at all possible combinations of two levels for two variables at the mean level of the remaining variable, plus repetitions of a "center point" as described in Section 2.5.2 on page 23.

8.1 Adsorption of 2,4-dihydroxybenzoic acid onto TiO_2

Before the samples were irradiated, adsorption was allowed to take place for a period of > 15 min and quantified by the difference method. Although the adsorption

*The findings discussed here were published in *Water Research* by Tercero Espinoza et al. (2009a).

measurements were not conceived with the purpose of building an isotherm (because of the presence of Br^- in varying concentrations and slight variations in room temperature), the adsorption of 2,4-dihydroxybenzoic acid (DHBA) onto the TiO_2 particles $\left(0.5 \frac{\text{mg DOC}}{\text{g TiO}_2} < q < 3.3 \frac{\text{mg DOC}}{\text{g TiO}_2}\right)$ could be described well with the Langmuir equation

$$q = \frac{K_L \, q_{\max} \, \rho_{\text{equil}}}{1 + K_L \, \rho_{\text{equil}}} \tag{8.1}$$

where q is the surface loading ($q \leq q_{\max}$), K_L is the Langmuir adsorption constant and ρ_{equil} is the remaining DOC concentration after adsorption has taken place. The fitted values were $K_L = 0.28 \pm 0.06$ L mg^{-1} and $q_{\max} = 6.2 \pm 0.9 \frac{\text{mg DOC}}{\text{g TiO}_2}$. The resulting fit is shown in Figure 8.1. Fitting the adsorption results with a polynomial approximation (Equation 8.2, below) reveals that the surface loading depends mainly on the concentrations of sorbate (DHBA) and sorbent (TiO_2), with only a small influence of the bromide ion concentration. Samples were then irradiated in the solar UV-simulator.

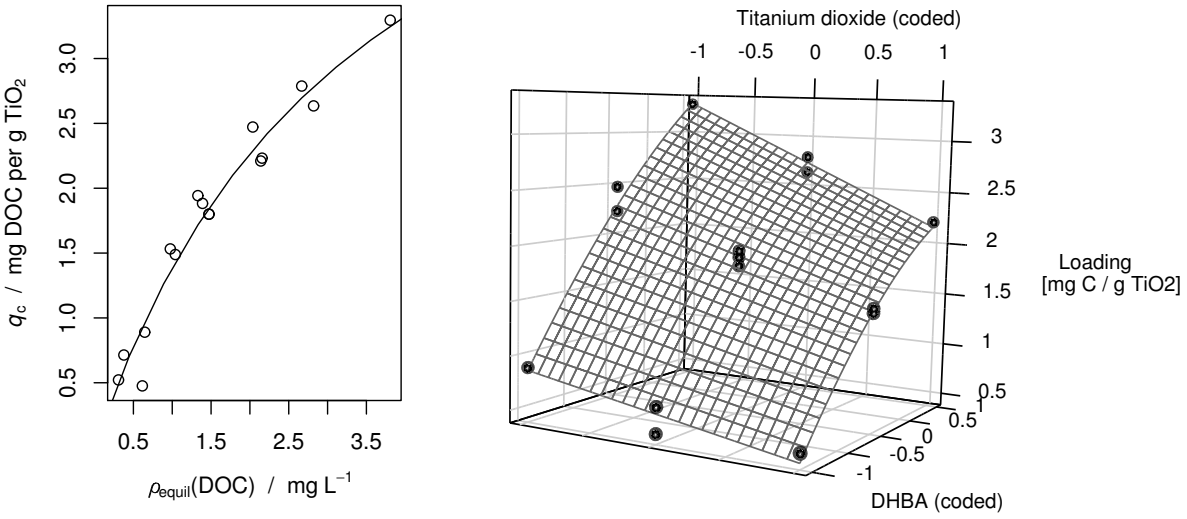

(a) Fitted using the equation for a Langmuir isotherm (8.1).

(b) Fitted with a polynomial approximation ignoring the effect of x_2.

Figure 8.1: Surface loading vs. remaining DOC concentration prior to irradiation of the TiO_2 suspensions.

8.2 A typical set of results

A sample result for the irradiation experiments in presented in Figure 8.2. The three quantities measured as a function of irradiation time, t_{irrad}, were the concentrations of DHBA, of dissolved organic carbon (DOC) and of bromoform. These results are qualitatively representative for all results obtained, namely, they show a very rapid and complete disappearance of DHBA, accompanied by rapid but incomplete degradation of DOC. Bromoform is measured after a certain delay ("lag phase"), after which a rapid increase in its concentration is observed. After this rapid increase, the concentration appears to oscillate as a result of simultaneous formation and degradation in the irradiated TiO_2 suspensions.

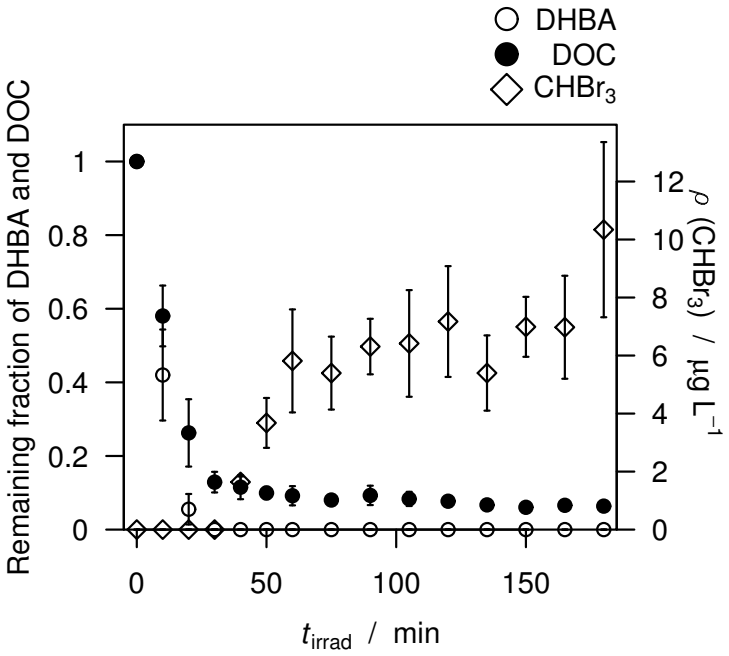

Figure 8.2: Sample data for the degradation of 2,4-dihydroxybenzoic acid and the formation of bromoform in irradiated titanium dioxide suspensions. Conditions: $\rho_0(\mathrm{DHBA}) = 6$ mg L^{-1}, $\rho_0(\mathrm{Br}^-) = 2$ mg L^{-1}, $\rho(\mathrm{TiO_2}) = 1.0$ g L^{-1} (center point).

For further analysis, we defined two quantities to characterize the amount and time scale of the bromoform formation:

1. $max_3(\mathrm{CHBr_3})$: the mean of the highest three bromoform concentrations measured in each irradiation experiment; and

2. t_{lag} or "lag time": the irradiation time, t_{irrad}, when $\rho(CHBr_3) > 0,8$ μg L^{-1} for the first time in each experiment.

The first quantity is a measure of how much bromoform was found in each irradiation experiment, while the second characterizes the time scale of the bromoform formation. For the data shown in Figure 8.2, $max_3(CHBr_3) = 8.6 \pm 1.6$ μg L^{-1} ($n = 4$). We assume this variability to be applicable to the remaining experiments.

8.3 Quantity of bromoform produced

First, we examined the differences in concentration of bromoform as a function of $\rho(TiO_2)$, $\rho_0(Br^-)$, and $\rho_0(DHBA)$ — x_1, x_2 and x_3, respectively (see Table 3.5) in the range

$$\begin{array}{rcccl} 0.5\text{ g L}^{-1} & < & \rho(TiO_2) & < & 1.5\text{ g L}^{-1} \\ 1\text{ mg L}^{-1} & < & \rho_0(Br^-) & < & 3\text{ mg L}^{-1} \\ 2\text{ mg L}^{-1} & < & \rho_0(DHBA) & < & 10\text{ mg L}^{-1} \end{array}$$

These results are shown summarily in Figure 8.3, expressed as $max_3(CHBr_3)$.

Inspection of the results in Figure 8.3 shows that the highest and lowest values of $max_3(CHBr_3)$ differ by approximately a factor of 5 (range 3-17 μg L^{-1} $CHBr_3$). Within this range, "low" values of $max_3(CHBr_3)$ are found at medium to high concentrations of DHBA ($x_3 = 0$ or 1) in combination with low concentrations of TiO_2 ($x_1 = -1$), whereas "high" values of $max_3(CHBr_3)$ are found at low to medium concentrations of DHBA ($x_3 = 0$ or -1) in combination with medium to high concentrations of both TiO_2 and Br^- (x_1 and x_3 equal to 0 or -1). To more formally examine the trends in $max_3(CHBr_3)$, we used the model shown in Equation 8.2 to fit the data (see also Section 2.5.2).

$$\underbrace{y}_{\text{response}} = \underbrace{\beta_0}_{\text{mean response}} + \underbrace{\beta_1 x_1 + \beta_2 x_2 + \beta_3 x_3}_{\text{main effects}} + \underbrace{\beta_{11} x_1^2 + \beta_{22} x_2^2 + \beta_{33} x_3^2}_{\text{quadratic terms}} + \underbrace{\beta_{12} x_1 x_2 + \beta_{13} x_1 x_3 + \beta_{23} x_2 x_3}_{\text{first-order interaction effects}} \tag{8.2}$$

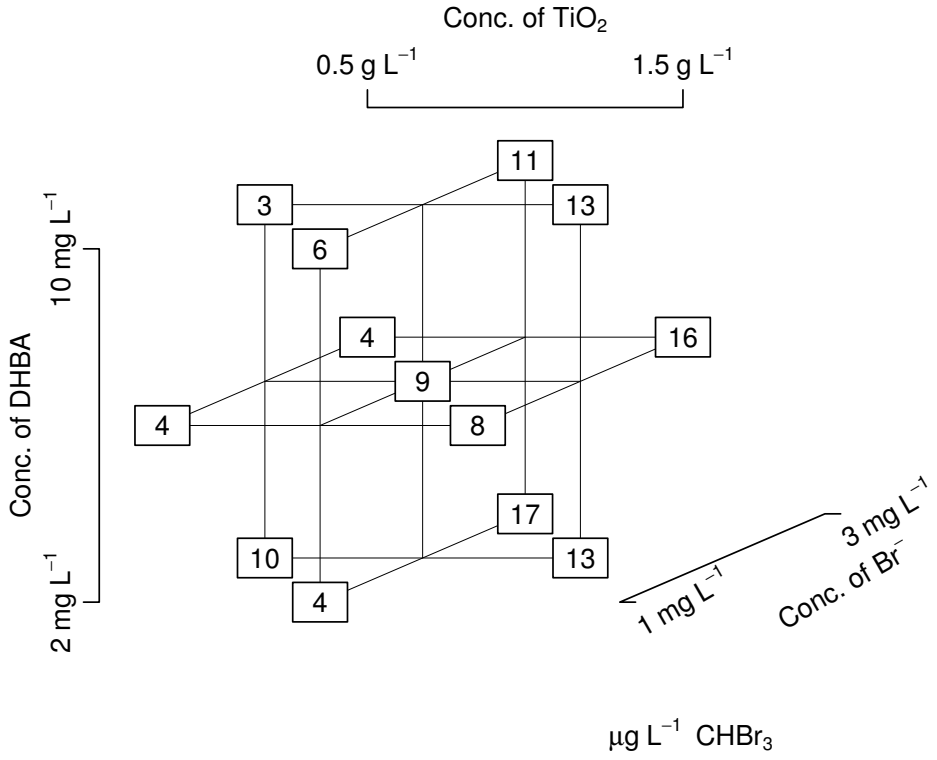

Figure 8.3: Average of the three highest bromoform concentrations found for each experimental run, $max_3(\mathrm{CHBr_3})$. Based on the variability of the center point, the standard deviation of the values is assumed to be ± 1.6 µg L^{-1} $\mathrm{CHBr_3}$.

Discarding coefficients likely to be noise (maximizing R^2_{adj})[†], we arrive at the following approximating polynomial:

$$y = 8.2 + 3.6x_1 + 3.2x_2 - 1.7x_3 + 1.6x_3^2 + 2.2x_1x_2 + 1.8x_1x_3 - 2.1x_2x_3 \tag{8.3}$$

These coefficients imply that:

- the higher the concentration of TiO_2, the more bromoform is produced ($\beta_1 > 0$)
- more bromoform is produced when more bromide is initially present ($\beta_2 > 0$)
- less bromoform is produced when more DHBA is initially present ($\beta_3 < 0$ with minor curvature, $\beta_{33} > 0$)
- the effect of increasing the concentration of TiO_2 is larger when $\rho_0(\mathrm{Br}^-) = 3$ mg L^{-1} than when $\rho_0(\mathrm{Br}^-) = 1$ mg L^{-1} ($\beta_{12} > 0$); and

[†]The value of R^2 increases slightly with every added predictor. The quantity R^2_{adj} takes into account the number of predictors ($R^2_{adj} < R^2$) and is thus useful in making fair comparisons between models with different numbers of independent variables.

- the effect of increasing $\rho_0(Br^-)$ is larger when $\rho_0(\text{DHBA}) = 2$ mg L^{-1} than when $\rho_0(\text{DHBA}) = 10$ mg L^{-1} ($\beta_{23} < 0$).

The relative importance of each effect is given by the magnitude of the corresponding coefficient. Using the model shown in Equation 8.3, it is possible to fit the results in Figure 8.3 well ($R^2 = 0.95$, $R^2_{adj} = 0.89$; 5 degrees of freedom), as shown in Figure 8.4.

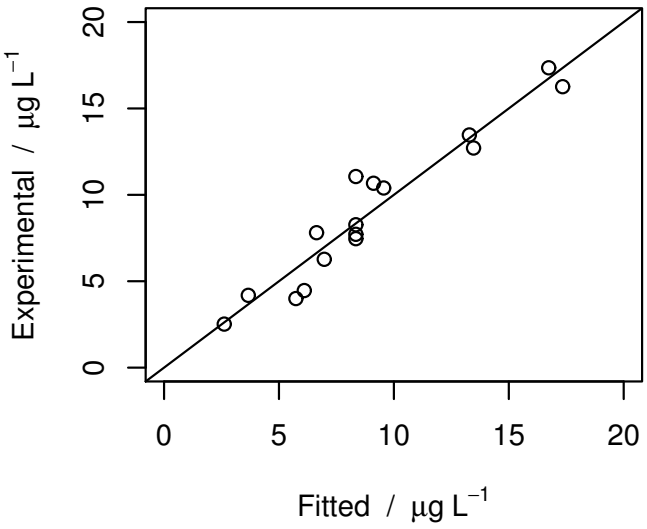

Figure 8.4: Comparison of experimental values (from Figure 8.3) with the values predicted by Equation 8.3. Based on the variability of the center point, the standard deviation of the experimental values is assumed to be ± 1.6 µg L^{-1} $CHBr_3$.

The model shown in Equation 8.3 may be understood in terms of the amount of available Br_2/HOBr compared to the available organic carbon. The results indicate that increasing either $\rho(TiO_2)$ or $\rho_0(Br^-)$ is tantamount to increasing the concentration of Br_2/HOBr in the suspensions, which leads to increased formation of bromoform. This is further supported by the importance of the synergistic interaction of these two variables (β_{12}) and the negative value of β_{23}. On the other hand, increasing ρ_0(DHBA) increases the available organic carbon in relation to Br_2/HOBr, which in turn reduces the probability of forming the triply brominated C present in bromoform (also reflected by the negative value of β_{23}).

8.4 Time scale for the formation of bromoform

The time scale of the bromoform formation was quantified by means of the lag time, t_{lag}. This is the time at the beginning of the irradiation experiments where the concentration of bromoform in the suspensions is < 0.8 µg L^{-1}. The values of t_{lag} are presented summarily in Figure 8.5. Repetitions of the center point showed no variation in t_{lag} ($n = 4$).

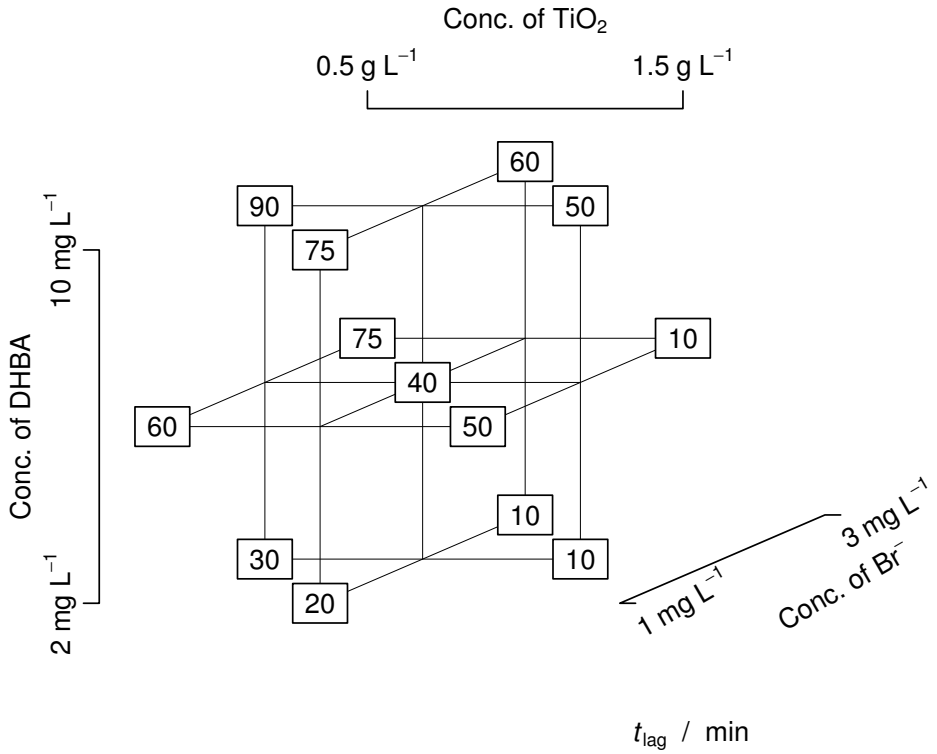

Figure 8.5: Lag time for each experimental run, t_{lag}. The variables x_1, x_2 and x_3 correspond to $\rho(TiO_2)$, $\rho_0(Br^-)$ and $\rho_0(DHBA)$, respectively. The variability of the values of t_{lag} is less than 10 min.

Inspection of Figure 8.5 shows that t_{lag} increases with increasing $\rho_0(DHBA)$ and decreases with increasing $\rho(TiO_2)$. By using regression analysis we arrive at the polynomial approximation:

$$y = 40 - 17x_1 - 6x_2 + 26x_3 + 6x_1^2 - 14x_1x_2 - 5x_1x_3 \tag{8.4}$$

The magnitude of the coefficients reveals that the three main influences affecting t_{lag} are:

- the concentration of photocatalyst (with slight curvature),
- the initial concentration of DHBA, and
- the interaction effect of x_1 with x_2.

These three effects (β_1, β_3, and β_{12}) account for approx. 91% of the variability observed in t_{lag} (see Figure 8.6). Using all coefficients in Equation 8.4 results in an almost perfect fit of the data ($R^2 = 0.99$, $R_{adj} = 0.98$; 6 degrees of freedom).

The largest single effect is that of x_3, indicating that the photocatalytic degradation of the DOC is the main factor influencing the length of the lag phase: the more DOC that must be degraded, the longer the time it takes for bromoform to first appear in measurable concentrations. Increasing the concentration of photocatalyst shortens the lag time, especially at high initial bromide concentrations (β_{12} and modest β_2). Contrary to the results for the amount of bromoform, the interaction effect of x_2 with x_3 did not play an important role in determining the length of the lag phase.

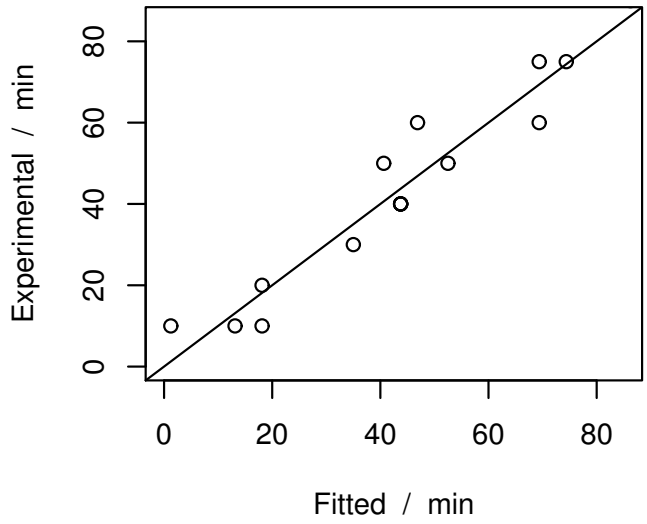

Figure 8.6: Comparison of experimental values (from Figure 8.5) with the values predicted by using only β_1, β_3 and β_{12} in the graduating polynomial. The variability of the experimental values of t_{lag} is less than 10 min.

8.5 Interim conclusions

Taken together, the results presented in this chapter show that there is considerable variability in the extent and time scale of formation of brominated byproducts depending on the specifics of the raw water to be treated (DOC and Br^- concentrations) and on the design parameters, especially the concentration of the photocatalyst. The bromoform levels in irradiated TiO_2 suspensions may be initially considered unobjectionable for conditions similar to those studied here. However, because of the complexity of the process and the many synergistic and antoginistic interactions – some seen here, some which may also occur with other water constituents– and the relatively large variability observed in the results, the formation of brominated byproducts should be tested on a case-by-case basis when applying this technique to bromide-containing waters.

Chapter 9

Other factors affecting the formation of bromoform in irradiated titanium dioxide suspensions*

In the preceeding Chapters, we showed that bromoform can be formed in irradiated titanium dioxide (P25) suspensions in the presence of elevated concentrations of bromide ions. In the following Sections, we compare the formation of bromoform in suspensions of two of the most widely used TiO_2 powders: P25 and Hombikat UV100. Previous comparisons of these two powders regarding the degradation of organic pollutants, for example dichloroacetic acid (Lindner et al., 1997) and x-ray contrast media (Doll and Frimmel, 2004), have found differences in the kinetics of degradation in the presence of the two. Thus, it is to be expected that the formation of bromoform proceeds at different rates when using different TiO_2 materials.

Whereas the results in Chapter 7 showed the formation of bromoform when using 2,4-dihydroxybenzoic acid (DHBA) as a source of dissolved organic carbon (DOC), in this Chapter we also explore bromoform formation using water from a bog lake (Lake Hohloh, Black Forest, Germany) in addition to model solutions of DHBA. With the inclusion of this natural source of DOC, we aimed to achieve a higher level of generality for the results.

Finally, the results in Chapter 6 showed that the degradation of NOM is strongly influenced by the presence of Cu^{2+}. Because the degradation of NOM plays an important role in the formation of bromoform (cf. Figure 7.4), we hypothesized that addition of Cu^{2+} would also show a strong influence on the measured bromoform concentrations after irradiation.

*The findings discussed in this Chapter were published in *Catalysis Today* by Tercero Espinoza et al. (2010).

9.1 Natural versus model sources of dissolved organic carbon

We showed in Chapter 7 that bromoform can be formed in irradiated titanium dioxide suspensions in the presence of both dissolved organic carbon (DOC) and bromide ions. In that case, 2,4-dihydroxybenzoic acid (DHBA) was chosen as a model compound based on results by Boyce and Hornig (1983), which revealed a high yield of bromoform upon bromination of DHBA. Furthermore, the structural features of DHBA make it a good model for humic acids. In order to verify whether this model qualitatively and quantitatively follows the results obtained for a natural water, irradiation experiments were conducted with DHBA and water from lake Hohloh, a bog lake in the northern Black Forest (Germany). Lake Hohloh has been extensively studied and used to characterize the properties of aquatic humic substances (Frimmel et al., 2002).

In good agreement[†] with the results shown in Figure 7.5, we observed the steady formation of bromoform after a lag time of approximately 40 min when irradiating P25 suspensions with DHBA as DOC source. The maximum concentrations were on the order of 15 $\mu g\ L^{-1}$. When using lake Hohloh water as a DOC source, the lag time was approximately 20 min and the maximum bromoform concentrations were close to 20 $\mu g\ L^{-1}$. Both sets of results are shown in Figure 9.1. It should be noted that the plateau in both curves does not indicate the end of bromoform formation, because bromoform can also be degraded in irradiated TiO_2 suspensions (Yoneyama and Torimoto, 2000). Thus, the concentration level of the plateau is the result of the balance between formation and degradation of bromoform in the irradiated TiO_2 suspensions.

We note that both data sets shown in Figure 9.1 are qualitatively and quantitatively similar. Thus, these results indicate that DHBA is an appropriate model compound for characterizing the general behavior of the system, despite the modest quantitative discrepancies.

Further experiments with added chloride ions showed no formation of chlorinated THM for $\rho_0(Cl^-) = 250\ mg\ L^{-1}$, when using DHBA as a DOC source ($\rho_0(DOC) = 1.1\ mg\ L^{-1}$). Thus, it appears that bromoform is the only important THM produced in irradiated TiO_2 suspensions when both chloride and bromide ions are present in the TiO_2 suspensions.

[†]Note that the experimental conditions are different.

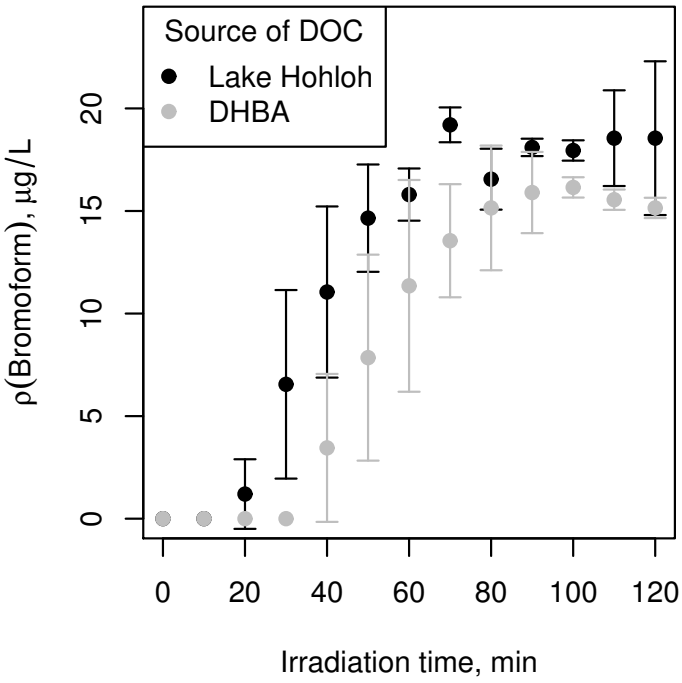

Figure 9.1: Bromoform formation in irradiated titanium dioxide suspensions (P25) with 2,4-dihydroxybenzoic acid and bog lake water as DOC source. $\rho_0(\mathrm{DOC}) = 1.1\ \mathrm{mg\ L^{-1}}$, $\rho_0(\mathrm{Br^-}) = 3\ \mathrm{mg\ L^{-1}}$, $\rho(\mathrm{TiO_2}) = 1.5\ \mathrm{g\ L^{-1}}$.

9.2 Identity of the photocatalyst

We hypothesized that the *formation* of bromoform as a byproduct of the degradation of organic material in the presence of bromide ions proceeds at different rates when using different TiO_2 materials. To test this, we irradiated TiO_2 suspensions of both powders in the presence of a model (DHBA) and a real (water from Lake Hohloh) source of dissolved organic carbon (DOC).

As seen in Figure 9.1, we found up to around 20 $\mu g\ L^{-1}$ bromoform to be formed in irradiation experiments with P25 as the photocatalyst. In contrast, we found almost no formation of bromoform in Hombikat UV100 suspensions. Repeated irradiation experiments led in most cases to bromoform concentrations well below 0.8 $\mu g\ L^{-1}$, and only in one case above but less than 3 $\mu g\ L^{-1}$.

As pointed out above, P25 and Hombikat UV100 have been found to degrade different compounds at different rates. For this reason, we hypothesized that bromoform may also be degraded faster in Hombikat UV100 suspensions, preventing its accumulation in the experiments described above. To support this idea, we measured

the degradation kinetics of bromoform in both P25 and Hombikat UV100 suspensions and found apparent first order kinetic constants of $(8.6 \pm 1.3) \times 10^{-3}$ min^{-1} and $(17.3 \pm 1.3) \times 10^{-3}$ min^{-1}, respectively. Thus, the absence of bromoform in Hombikat UV100 suspensions may be due to a rapid depletion of the bromoform directly after formation. However, it is not possible to claim this conclusively because the rates of *formation* of bromoform with both photocatalysts are unknown.

9.3 Influence of added copper(II) ions

The main natural precursor of bromoform in oxidative water treatment is natural organic matter (NOM). Because bromoform is a C1 compound, it appears as a relatively late product of the oxidation of NOM in the presence of bromide ions (cf. lag time in Figure 9.1). We hypothesized that any factor having an effect on the degradation kinetics of NOM would have an effect on the rate of production of bromoform (cf. Chapter 6 and Figure 7.4).

One such factor is the concentration of copper(II) ions. Addition of Cu^{2+} has been shown to slow down the mineralization of humic acids by $^{\bullet}OH$ (H_2O_2 process, see Liao et al., 2001) and the results in Chapter 6 show that the transformations of NOM reported (experimentally) in Chapter 4 and simulated in Chapter 5 are slowed down in the presence of added Cu^{2+}. Thus, we compared the formation of bromoform with and without added Cu^{2+} (10 µmol L^{-1}). For these experiments, bog lake water served as the DOC source.

While the samples without added Cu^{2+} showed up to approximately 20 µg L^{-1} bromoform (cf. Figure 9.1), the irradiated samples with $c_{\text{added}}(Cu^{2+})$ = 10 µmol L^{-1} showed very little formation of bromoform ($<$ 5 µg L^{-1}). It is attractive to assume that this is due to the changes in transformation of the NOM brought about by the presence of Cu^{2+} as discussed in Chapter 6.

9.4 Interim summary

The amount of bromoform produced in titanium dioxide suspensions containing elevated bromide ion concentrations and dissolved organic carbon is strongly affected by

- the identity of the photocatalyst powder used, and by

- the presence of copper(II) ions

In particular, both the use of Hombikat UV100 as a photocatalyst and the addition of Cu^{2+} led to a large reduction in the observed bromoform concentrations (in all cases < 5 µg L^{-1} compared to up to ≈ 20 µg L^{-1}).

Despite the large differences observed in bromoform formation under different experimental conditions, the absolute amounts were invariably far below the prescribed limit for trihalomethanes (THM) in drinking water, even in the presence of 250 mg L^{-1} of chloride ions. The observation underlines the potential of heterogeneous photocatalysis as an alternative oxidative step in the treatment of water for human consumption, because it can effectively oxidize a large variety of organic pollutants and shows a low potential for THM formation.

Chapter 10

Summary and future directions

The work described in this thesis pertains to the use of heterogeneous photocatalysis for the oxidative treatment of water, especially water containing elevated concentrations of bromide ions. Especially, the formation of byproducts in this process is of particular interest here since byproduct formation has been a largely neglected aspect in the study of heterogeneous photocatalysis to date.

Heterogeneous photocatalysis belongs to a group of oxidation techniques termed "advanced oxidation processes" (AOPs) because their effectiveness is based on the oxidative power of OH radicals. These are able to oxidize almost all organic substances in water. The applicability of AOPs to the degradation of organic pollutants in water has been extensively shown (Fox and Dulay, 1993; Fujishima et al., 1999; Hoffmann et al., 1995; Kabra et al., 2004; Kaneko and Okura, 2002; Legrini et al., 1993; Linsebigler et al., 1995; Malato et al., 2007; Oppenländer, 2003). However, because the reactions of OH radicals are largely unselective, the possibility of forming unwanted byproducts exists and needs to be taken into consideration.

When bromide ions (Br^-) are present in water, they can be oxidized to bromine (Br_2) in TiO_2 suspensions under UV irradiation (Herrmann and Pichat, 1980). Bromine may in turn further react to form bromate or bromoorganic products including bromoform. Bromate is a regulated carcinogen (limit in drinking water: 10 $\mu g\ L^{-1}$) and bromoform (harmful) is one of the four regulated trihalomethanes (THMs) with a limit in drinking water of 50 $\mu g\ L^{-1}$ (sum of THMs).

The goal of the work presented here was to investigate the possible formation of inorganic and organic byproducts in irradiated TiO_2 suspensions containing elevated concentrations of bromide (low mg L^{-1} range). Such bromide concentrations often occur in coastal and arid regions (e.g. around the Mediterranean sea) or inland in the vicinity of mineral salt deposits.

We approached the study of brominated byproduct formation by first examining the degradation of natural organic matter (NOM) in irradiated TiO_2 suspensions. The reason for this is that NOM is ubiquitous in natural waters and is the main natural precursor for halogenated byproducts in water treatment (Frimmel et al., 2002; Zwiener, 2006). Following the experiments with NOM in the absence of bromide ions, studies were performed with irradiated TiO_2 suspensions containing bromide in the presence and absence of dissolved organic carbon (DOC) both from a natural water and from model substances.

10.1 Photocatalytic degradation of natural organic matter

10.1.1 Experimental studies with simulated solar UV radiation

First, we studied the photocatalytic degradation of natural organic matter in TiO_2 suspensions irradiated using a solar UV-simulator. For these experiments, we used water from a bog lake (Lake Hohloh, northern Black Forest) as source of natural organic matter (quantified as dissolved organic carbon, DOC) and followed the degradation process by means of size exclusion chromatography with dissolved organic carbon detection (SEC-DOC). The results showed a progressive breakdown of the natural organic matter (NOM) starting with the larger molecular weight material and proceeding down to lower molecular weight compounds. This progressive breakdown correlated with the preferential adsorption of the higher molecular weight material onto the surface of the TiO_2 particles.

Parallel to the degradation of NOM, the formation of low molecular weight organic acids (formic, oxalic, glutaric and succinic acids) was observed and quantified. The lower molecular weight material generated by the degradation of NOM, and especially the small organic acids, were readily bioavailable such that a biological filter should be applied after oxidation to prevent bacterial regrowth in case the product water was to be stored or distributed over a sizable network.

10.1.2 Simulation of the degradation of natural organic matter in advanced oxidation processes

The claim of sequential degradation of NOM is not unique to heterogeneous photocatalysis but has been also made for homogeneous AOPs (e.g. Sarathy and Mohseni, 2007) for the H_2O_2/UV process. In order to clarify whether the observed sequential degradation of the NOM in irradiated TiO_2 suspensions was the result of a size selective process or simply the result of randomness, both homogeneous and heterogeneous AOPs were simulated as fully unselective degradation processes. By ignoring the chemistry of the NOM molecules, assuming them to be linear chains, and allowing only cleavage reactions, it was possible to simulate both processes fairly well, especially the initial stages of degradation pertaining to the large molecular weight material.

The simulation results showed the initial degradation of the large molecular weight material in both homogeneous and heterogeneous AOPs. However, this degradation was rapid and complete in the case of the heterogeneous process but comparatively slow and incomplete for the case of a homogeneous process. The simulation conditions were identical except for the presence of selective adsorption onto a surface (bias) introduced to the heterogenous case based on experimental measurements. We note that both simulations are in good agreement with the available experimental results (Chapter 4 and Sarathy and Mohseni, 2007).

The good agreement between simulation and experiment indicates, in the case of the heterogeneous system, that there is a degree of selectivity in heterogeneous photocatalysis with TiO_2 suspensions introduced by the size-differentiated adsorption of the NOM onto the surface of the photocatalyst. This is not to say that the large molecular weight material is exclusively degraded in the initial stages of the irradiation experiments in the presence of TiO_2. Rather, a larger fraction of the high molecular weight material reacts compared to the lower molecular material, though the absolute number of reactions is higher for the latter because they are more numerous.

On the other hand, the claim of a selective degradation of the high molecular weight material in a homogeneous AOP is not tenable based on size exclusion chromatograms alone. Our results show that the degradation sequence obtained by Sarathy and Mohseni (2007) and others is congruent with a fully random process.

10.1.3 Effect of metal ions on the photocatalytic degradation of natural organic matter

The presence of metal ions is known to influence the degradation of natural organic matter under direct UV-irradiation (e.g. Brinkmann, 2003; Brinkmann et al., 2003b) as well as in other AOPs (e.g. Liao et al., 2001). We thus sought to quantify the effect of selected metal ions (Cu^{2+}, Fe^{3+}, Mn^{2+} and Zn^{2+}) on the degradation of NOM by means of SEC-DOC measurements.

We found that the addition of metal ions generally slowed down the degradation of NOM in irradiated TiO_2 suspensions. Among the metals studied, addition of Cu^{2+} had by far the largest effect of all. It was observed to slow down the degradation of the large molecular weight material and consequently to slow down the increase in the medium and low molecular weight fractions of the NOM. The production of low molecular weight organic acids was also partly inhibited by addition of Cu^{2+}. Addition of Mn^{2+} resulted in a change in the magnitude of the inhibiting effect of Cu^{2+} (interaction): the effect of Cu^{2+} was smaller in the presence of added Mn^{2+}.

While there are several reports of metal addition affecting reaction kinetics in irradiated TiO_2 suspensions, the metal concentrations used in this study (0-10 μmol L^{-1}) are low compared to those reported previously. Instead, our results suggest a stabilization of the NOM by complexation with Cu^{2+} regarding degradation by $^{\bullet}OH$. We expect the added Cu^{2+} to be fully complexed by the NOM, considering the stability of Cu^{2+}-NOM complexes (Hirata, 1981; Lubal et al., 1998; Prado et al., 2006; Van Dijk, 1971) and the high Cu^{2+} complexing capacity of the water used (Abbt-Braun and Frimmel, 2002).

Examination of the bioavailability of the NOM after irradiation in the presence of the added metals revealed that less organic carbon was assimilated by the bacteria when the concentration of Cu^{2+} increased. This was, however, not the result of toxicity of Cu^{2+} towards the bacteria but rather the result of reduced amounts of bioavailable material as a consequence of the partly inhibited photocatalytic degradation of NOM.

10.2 Formation of brominated byproducts

10.2.1 Screening study: Bromate, bromoorganic compounds and bromoform

As a first step in the search for brominated inorganic and organic byproducts, we performed screening experiments with TiO_2 suspensions containing different concentrations of Br^- and dissolved organic carbon (DOC) following a Plackett-Burman design (Box et al., 2005; Plackett and Burman, 1946). In these experiments, we found no formation of BrO_3^- and trihalomethanes (THMs) for up to 45 minutes of irradiation. However, we found the formation of bromoorganic products in samples initially containing 3 mg L^{-1} Br^-.

Longer irradiation experiments with P25 suspensions containing 10 mg L^{-1} 2,4-dihydroxybenzoic acid (a good model compound for NOM known to give high yields of bromoform upon reaction with bromine, Br_2) and 3 mg L^{-1} Br^- resulted in the formation of measurable amounts of bromoform (up to 10 µg L^{-1}) starting after 60 min of irradiation. The amount of Br bound in bromoform indicates that substantially more Br^- is oxidized to Br_2 in the presence of DOC compared to experiments performed in the absence of DOC (cf. Herrmann and Pichat, 1980). The amounts of bromoform formed during the course of irradiation were much lower than the prescribed (German) limit for THMs in drinking water.

A simplified reaction scheme was proposed based on the competing reactions of DOC degradation and bromination, of which a branch leads to the formation of bromoform. This scheme comprises two competing processes:

1. the degradation of NOM over non-halogenated intermediates and
2. the reaction of Br_2 (from the photocatalytic oxidation of Br^-) with the original organic substances or their degradation intermediates to yield brominated intermediates and eventually bromoform.

10.2.2 Effect of the concentration of photocatalyst, bromide ions and dissolved organic carbon on the formation of bromoform

Based on the scheme described above, we hypothesized that the extent and time scale of bromoform formation would depend on the concentrations of photocatalyst, of

bromide ions and of dissolved organic carbon. To explore this idea, we performed a parameter study following a Box-Behnken experimental design in the range

$$\begin{array}{rcccl} 0.5\ \mathrm{g\ L^{-1}} & < & \rho(\mathrm{TiO_2}) & < & 1.5\ \mathrm{g\ L^{-1}} \\ 1\ \mathrm{mg\ L^{-1}} & < & \rho(\mathrm{Br^-}) & < & 3\ \mathrm{mg\ L^{-1}} \\ 2\ \mathrm{mg\ L^{-1}} & < & \rho(\mathrm{DHBA}) & < & 10\ \mathrm{mg\ L^{-1}} \end{array}$$

The bromoform concentrations observed ranged between 3-17 μg L^{-1} (mean of the three highest measured concentrations in a given irradiation experiment) and did not exceed the limit prescribed for drinking water. The extent of bromoform formation was found to depend on all three variables as follows:

- higher bromoform concentrations were found at higher photocatalyst and bromide concentrations
- lower bromoform concentrations were found at higher initial concentrations of dissolved organic carbon.

In addition, a synergism was observed between the effect of increasing the TiO_2 concentration and that of bromide. These results may be interpreted in terms of the available "active bromine" species (bromine and hypobromous acid) in relation to the available organic carbon: increasing the concentration of either TiO_2 or Br^-, or both, increases the concentration of active bromine species. Increasing the initial concentration of dissolved organic carbon reduces the probability of obtaining a triply-brominated C as is found in bromoform.

The time between the beginning of the irradiation and the appearance of measurable concentrations of bromoform was in the range 10 min $< t_{\mathrm{lag}} <$ 90 min. Most of the variability was found to be explained by

- the initial concentration of DOC, and
- the concentration of the photocatalyst and its interaction with the initial bromide concentration (synergism).

Increasing the DOC concentration increased t_{lag} while increasing the concentration of TiO_2 decreased it, especially at high initial concentrations of bromide ions.

These results show that both the extent and time scale of bromoform formation vary considerably depending on the specifics of the raw water to be treated (DOC and Br^- concentrations) and on the design parameters, especially the concentration of the photocatalyst.

10.2.3 Other factors influencing the formation of bromoform

Finally, using the case of P25 suspensions with

$$\begin{aligned} \rho(TiO_2) &= 1.5\ g\ L^{-1} \\ \rho_0(Br^-) &= 3\ mg\ L^{-1} \\ \rho_0(DHBA) &= 2\ mg\ L^{-1} \end{aligned}$$

as a base of comparison, we explored the influence of the DOC source, the photocatalyst identity and the addition of Cu^{2+} on the extent of bromoform formation.

Comparison of Lake Hohloh water with 2,4-dihydroxybenzoic acid as DOC sources yielded very similar results. Thus, the choice of 2,4-dihydroxybenzoic acid as a model compound (based on the results of Boyce and Hornig, 1983) appears to have been a good one. This suggests that results from the parameter study will be at least qualitatively valid for systems with different DOC sources under otherwise similar conditions.

The amount of bromoform produced was found to be strongly reduced ($< 3\ \mu g\ L^{-1}$) when Hombikat UV100 was used as a photocatalyst instead of P25 ($\approx 20\ \mu g\ L^{-1}$). This difference may be due to the faster degradation of bromoform in Hombikat UV100 suspensions and highlights the role of the photocatalyst material (crystal modification, particle and agglomerate size, etc.).

Addition of 10 $\mu mol\ L^{-1}$ Cu^{2+} to the suspensions (using Lake Hohloh water as DOC source) resulted in the formation of $< 5\ \mu g\ L^{-1}$ bromoform. This may be the result of a slower DOC degradation in the presence of Cu^{2+}, or the consequence of reduced production of active bromine species. The results presented in this thesis regarding the photocatalytic degradation of NOM in the presence of metals support the first possibility. However, the second possibility cannot be ruled out as there are no applicable published results.

Despite the large differences observed in bromoform formation under different experimental conditions, the concentrations observed in all experiments were invariably below the prescribed limit for trihalomethanes (THM) in drinking water, even in the presence of 250 $mg\ L^{-1}$ of chloride ions. The observation underlines the potential of heterogeneous photocatalysis as an alternative oxidative step in the treatment of water for human consumption, because it can effectively oxidize a large variety of organic pollutants and shows a low potential for THM formation.

The main results of this work are summarized graphically in Figure 10.1.

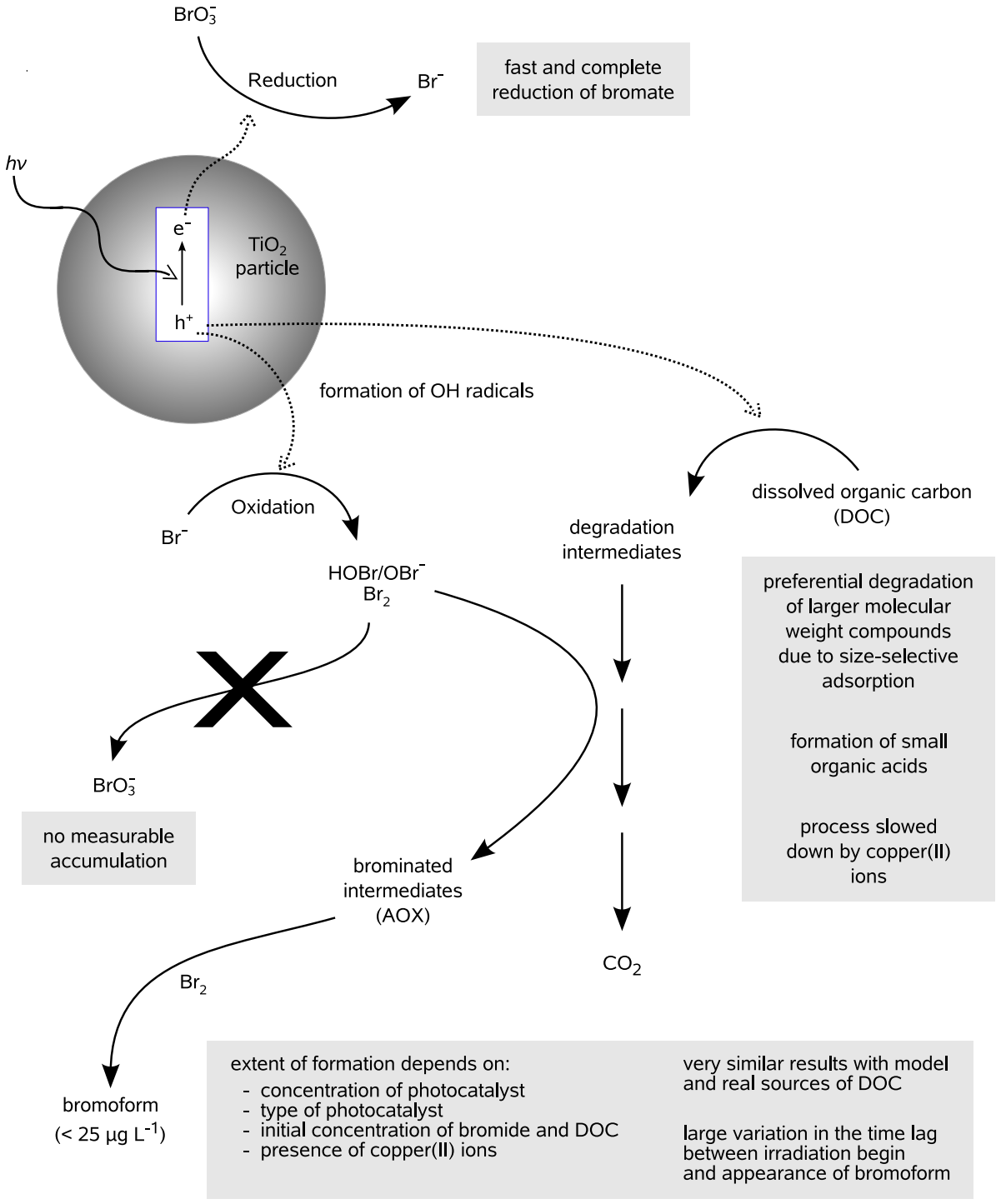

Figure 10.1: Simplified scheme showing the main results presented in this thesis.

10.3 Future directions

We have shown the "sequential" degradation of NOM and its increased bioavailability after irradiation in TiO_2 suspensions using bog lake water as source of NOM. Furthermore, the simulation results and their good agreement with experiment strongly suggest that the photocatalytic degradation of NOM proceeds in a similar manner for other sources, e.g. river water, which are more immediately relevant for water treatment. Thus, a desirable extension of the work presented here would seek to give generality to these results by comparing the photocatalytic degradation of NOM from different source waters. This effort is already underway in our group using water from selected lakes and rivers in Germany and Switzerland. Preliminary results support the generality of the conclusions drawn from our experiments with Lake Hohloh water but point to different reaction velocities.

We also observed that the degradation of natural organic matter and the formation of low molecular weight organic acids are partly inhibited by the addition of copper(II) ions. The evidence at hand points to an increased stability of the Cu^{2+}-NOM complexes towards degradation by OH radicals (see also Liao et al., 2001). However, this hypothesis was not yet tested experimentally. Thus, a systematic study of the stability of Cu^{2+}-NOM complexes to degradation by OH radicals (e.g. by using different model compounds for natural organic matter with different complexation capacity of Cu^{2+} and pertinent controls) would serve to strengthen this hypothesis or reveal the need for an alternative explanation. In either case, such a study would be a valuable addition to the current knowledge of the effect of metal ions in advanced oxidation processes in general.

Regarding the formation of bromate in irradiated TiO_2 suspensions, we do not see an immediate need for any further investigation since our results and those presented in the literature (Mills et al., 1996; Noguchi et al., 2002, 2003), when combined, show that bromate formation is not an issue in heterogeneous photocatalysis. Instead, irradiated TiO_2 suspensions may be used to remove bromate from water.

The formation of bromoform, on the other hand, is an issue that requires further investigation. As a subject of laboratory studies, the most important issue that remains unaddressed is that of temperature. Heterogeneous photocatalysis is likely to be competitive only when using solar energy directly for the otherwise expensive generation of UV photons. Such solar systems, however are not thermostated and can reach temperatures of up to 45 °C (Kositzi et al., 2004; Malato et al., 2007). Preliminary results using the solar simulator suggest an increasing trend in bromoform

formation with increasing temperature. Furthermore, the variability in the results appears to increase at higher temperature. Thus, in the interest of approximating field conditions in the laboratory and giving a better assessment of the formation of bromoform in solar photocatalytic reactors, a study including temperature variations would be desirable. Furthermore, matrix effects were not within the scope of the work presented here and thus have not been sufficiently taken into account.

We note that although knowledge of the general trends in the extent and time scale of bromoform formation as obtained in the laboratory are necessary for the design of real photocatalytic reactors, because of the complexity of the pathways leading to bromoform formation and the many interactions (synergistic and antagonistic) observed in this work, and others that are possible, an assessment of byproduct formation in heterogeneous photocatalysis should be done on a case-by-case basis until a reasonable database of "real world" data is available.

Finally, the formation of iodinated byproducts, especially in coastal areas, should be studied. Although iodide ions are typically present at much lower concentrations than bromide ions, iodide ions are more easily oxidized to iodine (I_2; Herrmann and Pichat, 1980) and may therefore lead to the formation of iodinated byproducts. These in turn are generally more toxic than both brominated and chlorinated compounds and have come into the focus of the research community in recent years (e.g. Hua and Reckhow, 2007; Hua et al., 2006; Krasner et al., 2006; von Gunten, 2003). Thus, an assessment of the formation of iodinated byproducts in heterogeneous photocatalysis would extend and complement the results presented in this thesis.

Bibliography

Aarthi, T., Madras, G., 2007. Photocatalytic degradation of rhodamine dyes with nano-TiO_2. Industrial and Engineering Chemistry Research 46, 7–14.

Abbt-Braun, G., Frimmel, F. H., 2002. Setting the scene. In: Frimmel, F. H., Abbt-Braun, G., Heumann, K. G., Hock, B., Lüdemann, H.-D., Spiteller, M. (Eds.), Refractory Organic Substances (ROS) in the Environment. John Wiley and Sons, New York, pp. 1–38.

Abdullah, M., Low, G. K. C., Matthews, R. W., 1990. Effects of common inorganic anions on rates of photocatalytic oxidation of organic carbon over illuminated titanium dioxide. Journal of Physical Chemistry 94, 6820–6825.

Al-Rasheed, R., Cardin, D. J., 2003. Photocatalytic degradation of humic acid in saline waters. Part 2. Effects of various photocatalytic materials. Applied Catalysis A: General 246, 39–48.

Amy, G., Bull, R., Craun, G. F., Pegram, R. A., Siddiqui, M., 2000. Disinfectants and disinfectant by-products. Vol. 216 of Environmental Health Criteria. World Health Organization, Geneva.

Bailey, J. E., Ollis, D. F., 1986. Biochemical engineering fundamentals, 2nd Edition. McGraw-Hill, New York.

Barrios, E., 2005. BsMD: Bayes Screening and Model Discrimination (based on Daniel Meyer's code). R package version 0.6-5.

Bekbölet, M., Balcioglu, I., 1996. Photocatalytic degradation kinetics of humic acids in aqueous TiO_2 dispersions: The influence of hydrogen peroxide and bicarbonate ion. Water Science and Technology 34, 73–80.

Bekbölet, M., Boyacioglu, Z., Özkaraova, 1998. The influence of solution matrix on the photocatalytic removal of color from natural waters. Water Science and Technology 38, 155–162.

Bekbölet, M., Çeçen, F., Özkösemen, G., 1996. Photocatalytic oxidation and subsequent adsorption characteristics of humic acids. Water Science and Technology 34, 65–72.

Bekbölet, M., Süphandağ, A. S., Uyguner, C. S., 2002. An investigation of the photocatalytic efficiencies of titanium dioxide powders on the decolourisation of humic acids. Journal of Photochemistry and Photobiology A: Chemistry 148, 121–128.

Bekbölet, M., Uyguner, C., Selcuk, H., Rizzo, L., Nikolaou, A. D., Meriç, S., Belgiorno, V., 2005. Application of oxidative removal of NOM to drinking water and formation of disinfection by-products. Desalination 176, 155–166.

Benoit-Marquié, F., Puech-Costes, E., Braun, A. M., Oliveros, E., Maurette, M.-T., 1997. Photocatalytic degradation of 2,4-dihydroxybenzoic acid in water: Efficiency optimization and mechanistic investigations. Journal of Photochemistry and Photobiology A: Chemistry 108, 65–71.

Bideau, M., Claudel, B., Faure, L., Kazouan, H., 1991. The photo-oxidation of acetic acid by oxygen in the presence of titanium dioxide and dissolved copper ions. Journal of Photochemistry and Photobiology A: Chemistry 61, 269–280.

Botsch, W., Höfling, E., Mauch, J., 1977. Chemie in Versuch, Theorie und Übung. Verlag Moritz Diesterweg / Otto Salle Verlag, Frankfurt am Main.

Box, G. E. P., Behnken, D. W., 1960. Some new three level designs for the study of quantitative variables. Technometrics 2, 455–475.

Box, G. E. P., Draper, N. R., 1987. Empirical model-building and response surfaces. Wiley Series in Applied Probability and Mathematical Statistics. John Wiley & Sons, New York.

Box, G. E. P., Hunter, J. S., Hunter, W. G., 2005. Statistics for Experimenters: Design, Innovation, and Discovery, 2nd Edition. Wiley Series in Applied Probability and Mathematical Statistics. Wiley-Interscience, New Jersey.

Box, G. E. P., Meyer, R. D., 1986. An analysis for unreplicated fractional factorials. Technometrics 28, 11–18.

Boyce, S. D., Hornig, J. F., 1983. Reaction pathways of trihalomethane formation from the halogenation of dihydroxyaromatic model compounds for humic acid. Environmental Science and Technology 17, 202–211.

Braun, A. M., Maurette, M.-T., Oliveros, E., 1991. Photochemical technology. Wiley, Chichester.

Brinkmann, T., 2003. Alkalischer und solarinduzierter abbau von natürlicher organischer materie. Ph.D. thesis, Universität Karlsruhe (TH), Karlsruhe, Germany, (in German).

Brinkmann, T., Hörsch, P., Sartorius, D., Frimmel, F., 2003a. Photoformation of low-molecular-weight organic acids from brown water dissolved organic matter. Environmental Science and Technology 37, 4190–4198.

Brinkmann, T., Sartorius, D., Frimmel, F. H., 2003b. Photobleaching of humic rich dissolved organic matter. Aquatic Sciences 65, 415–424.

Buffington, R., Wilson, M. K., 1987. Detectors for gas chromatography – A practical primer. Hewlett Packard, Avondale, PA.

Cai, R., Kubota, Y., Fujishima, A., 2003. Effect of copper ions on the formation of hydrogen peroxide from photocatalytic titanium dioxide species. Journal of Catalysis 219, 214–218.

Callister, J. W. D., 1997. Materials Science and Engineering – An Introduction, 4th Edition. John Wiley & Sons, Inc., New York.

Chen, C., Li, X., Ma, W., Zhao, J., Hidaka, H., Serpone, N., 2002. Effect of transition metal ions on the TiO_2-assisted photodegradation of dyes under visible irradiation: A probe for the interfacial electron transfer process and reaction mechanism. Journal of Physical Chemistry B 106, 318–324.

Daniel, C., 1959. Use of half-normal plots in interpreting factorial two-level experiments. Technometrics 1, 311–341.

Daniel, S. L., Pilsl, C., Drake, H. L., 2004. Oxalate metabolism by the acetogenic bacterium *Moorella thermoacetica*. FEMS Microbiology Letters 231, 39–43.

Defoin, A., Defoin-Straatmann, R., Hildenbrand, K., Bittersmann, E., Kreft, D., Kuhn, H. J., 1986. A new liquid phase actinometer: quantum yield and photo-CIDNP study of phenylglyoxylic acid in aqueous solution. J. Photochem. 33, 237–255.

Doehlert, D. H., 1970. Uniform shell designs. Applied Statistics 19, 231–239.

Doll, T. E., 2004. Photochemischer und photokatalytischer Abbau von Carbamazepin, Clofibrinsäure, Iomeprol und Iopromid. Ph.D. thesis, Universität Karlsruhe (TH), Karlsruhe, Germany, (in German).

Doll, T. E., Frimmel, F. H., 2004. Kinetic study of photocatalytic degradation of carbamazepine, clorfibric acid, iomeprol and iopromide assisted by different titanium dioxide materials - Determination of intermediates and reaction pathways. Water Research 38, 955–964.

Doll, T. E., Frimmel, F. H., 2005. Cross-flow microfiltration with periodical back-washing for photocatalytic degradation of pharmaceutical and diagnostic residues—evaluation of the long term stability of the photocatalytic activity of TiO_2. Water Research 39, 847–854.

Domek, M., LeChevallier, M., Cameron, S., McFeters, G., 1984. Evidence for the role of copper in the injury process of coliform bacteria in drinking water. Applied Environmental Microbiology 48, 289–293.

Eggins, B. R., Palmer, F. L., Byrne, A., 1997. Photocatalytic treatment of humic substances in drinking water. Water Research 31, 1223–1226.

Euroglas Analytical Instruments, 1995. ECS 1200 — Betriebsanleitung.

Fernández-Ibáñez, P., Blanco, J., Malato, S., de las Nieves, F. J., 2003. Application of the colloidal stability of titanium dioxide particles for recovery and reuse in solar photocatalysis. Water Research 37, 3180–3188.

Fox, M. A., Dulay, M. T., 1993. Heterogeneous photocatalysis. Chemical Reviews 93, 341–357.

Fox, M. A., Whitesell, J. K., 1997. Organic Chemitry, 2nd Edition. Jones and Bartlett, Sudbury, MA.

Frim, J. A., Rathman, J. F., Weavers, L. K., Jul. 2003. Sonochemical destruction of free and metal-binding ethylenediaminetetraacetic acid. Water Research 37 (13), 3155–3163.

Frimmel, F. H., 1998. Characterization of natural organic matter as major constituents in aquatic systems. Journal of Contaminant Hydrology 35, 201–216.

Frimmel, F. H., Abbt-Braun, G., Heumann, K. G., Hock, B., Lüdemann, H.-D., Spiteller, M. (Eds.), 2002. Refractory organic substances (ROS) in the environment. Wiley, New York.

Frimmel, F. H., Geywitz, J., 1983. Zur koordinativen Bindung von Metallionen an Gewässerhuminstoffe. Fresenius Zeitschrift für Analytische Chemie 316, 582–588.

Fujishima, A., Hashimoto, K., Watanabe, T., 1999. TiO_2 Photocatalysis – Fundamentals and Applications. Bkc, Inc., Tokyo.

Gjessing, E. T., 1965. Use of "Sephadex" gel for the estimation of molecular weight of humic substances in natural water. Nature 208, 1091–1092.

Gjessing, E. T., Lee, G. F., 1967. Fractionation of organic matter in natural waters on Sephadex columns. Environmental Science and Technology 1, 631–638.

Gräntzdörffer, A., 2000. Formiat-stoffwechsel in *Eubacterium acidaminophilum*: Molekulare und biochemische Charakterisierung der Wolfram- und Selen-haltigen Formiat-Dehydrogenasen sowie einer Eisen-Hydrogenase. Ph.D. thesis, Martin-Luther-Universität Halle-Wittenberg, Halle.

Griffin, M., Trudgill, P. W., 1972. The metabolism of cyclopentanol by *Pseudomonas* N.C.I.B. 9872. Biochemical Journal 129, 595–603.

Gros, N., Camões, M. F., Oliveira, C., Silva, M. C. R., 2008. Ionic composition of seawaters and derived saline solutions determined by ion chromatography and its relation to other quality parameters. Journal of Chromatography A 1210, 92–98.

Hand, D. W., Perram, D. L., Crittenden, J. C., Mullins, M. E., 1991. Destruction of disinfection by-product precursor using photoassisted heterogeneous catalytic oxidation. In: Proceedings – Annual Conference, American Water Works Association. pp. 289–300.

Herrmann, J. M., Pichat, P., 1980. Heterogeneous photocatalysis. Oxidation of halide ions by oxygen in ultraviolet irradiated aqueous suspension of titanium dioxide. Journal of the Chemical Society, Faraday Transactions 1: Physical Chemistry in Condensed Phases 76, 1138–46.

Hesse, S., Balz, A., Frimmel, F. H., 1997. Detailed investigation of the discharge of anthropogenic carbon along the river Forbach/Murg (Black Forest, Southwest Germany). Vom Wasser 88, 110–117.

Hirata, S., 1981. Stability constants for the complexes of transition-metal ions with fulvic and humic acids in sediments measured by gel filtration. Talanta 28 (11), 809–815.

Hoffmann, M. R., Martin, S. T., Choi, W., Bahnemann, D. W., 1995. Environmental applications of semiconductor photocatalysis. Chemical Reviews 95, 69–96.

Hua, G., Reckhow, D. A., 2007. Characterization of disinfection byproduct precursors based on hydrophobicity and molecular size. Environmental Science and Technology 41, 3309–3315.

Hua, G., Reckhow, D. A., Kim, J., 2006. Effect of bromide and iodide ions on the formation and speciation of disinfection byproducts during chlorination. Environmental Science and Technology 40, 3050–3056.

Huber, M. M., Canonica, S., Park, G.-Y., von Gunten, U., 2003. Oxidation of pharmarceuticals during ozonation and advanced oxidation processes. Environmental Science and Technology 37, 1016–1024.

Huber, S. A., Balz, A., Frimmel, F. H., 1994. Identification of diffuse and point sources of dissolved organic carbon (DOC) in a small stream (Alb, Southwest Germany), using gel filtration chromatography with high-sensitivity DOC-detection. Fresenius Journal of Analytical Chemistry 350, 496–503.

Huber, S. A., Frimmel, F. H., 1991. Flow injection analysis for organic and inorganic carbon in the low-ppb range. Analytical Chemistry 63, 2122–2130.

Hufschmidt, D., Liu, L., Selzer, V., Bahnemann, D., 2004. Photocatalytic water treatment: Fundamental knowledge required for its practical application. Water Science and Technology 49, 135–140.

International Humic Substances Society, 2007. What are humic substances? www.ihss.gatech.edu, accessed 13 October 2008.

Kabra, K., Chaudhary, R., Sawhney, R. L., 2004. Treatment of hazardous organic and inorganic compounds through aqueous-phase photocatalysis: A review. Industrial and Engineering Chemistry Research 43, 7683–7696.

Kaneko, M., Okura, I. (Eds.), 2002. Photocatalysis – Science and Technology. Kodansha, Inc., Tokyo.

Kerc, A., Bekbölet, M., Saatci, A. M., 2004. Effects of oxidative treatment techniques on molecular size distribution of humic acids. Water Science and Technology 49, 7–12.

Kleiser, G., 2000. Minimierung der Bildung von Desinfektionsnebenprodukten durch Oxidationsverfahren. Ph.D. thesis, Universität Karlsruhe (TH), Karlsruhe, Germany, (in German).

Kolokassidou, K., Szymczak, W., Wolf, M., Obermeier, C., Buckau, G., Pashalidis, I., 2009. Hydrophilic olive cake extracts: Characterization by physicochemical properties and Cu(II) complexation. Journal of Hazardous Materials 164 (2-3), 442–447.

Kositzi, M., Poulios, I., Malato, S., Caceres, J., Campos, A., 2004. Solar photocatalytic treatment of synthetic municipal wastewater. Water Research 38, 1147–1154.

Krasner, S. W., Weinberg, H. S., Richardson, S. D., Pastor, S. J., Chinn, R., Sclimenti, M. J., Onstad, G. D., Thruston, A. D., 2006. Occurrence of a new generation of disinfection byproducts. Environmental Science and Technology 40, 7175–7185.

Laidler, K. J., Meiser, J. H., 1995. Physical Chemistry, 2nd Edition. Houghton Mifflin, Boston.

Lamb, A., Tollefson, E., 1973. Toxic effects of cupric, chromate and chromic ions on biological oxidation. Water Research 7, 599–613.

Lankes, U., Lüdemann, H.-D., Frimmel, F. H., 2008. Search for basic relationships between "molecular size" and "chemical structure" of aquatic natural organic matter -— answers from ^{13}C and ^{15}N CPMAS NMR spectroscopy. Water Research 42, 1051–1060.

Lankes, U., Müller, M., Weber, M., Frimmel, F. H., 2009. Reconsidering the quantitative analysis of organic carbon concentrations in size exclusion chromatography. Water Research 43, 915–924.

Lapin, L., 1997. Modern Engineering Statistics. Duxbury Press, Belmont, CA.

Legrini, O., Oliveros, E., Braun, A. M., 1993. Photochemical processes for water treatment. Chemical Reviews 93, 671–698.

Lenth, R. V., 1989. Quick and easy analysis of unreplicated factorials. Technometrics 31, 469–473.

Li, X. Z., Fan, C. M., Sun, Y. P., 2002. Enhancement of photocatalytic oxidation of humic acid in TiO_2 suspensions by increasing cationic strength. Chemosphere 48, 453–460.

Liao, C.-H., Lu, M.-C., Su, S.-H., 2001. Role of cupric ions in the H_2O_2 oxidation of humic acids. Chemosphere 44, 913–919.

Lindner, M., Theurich, J., Bahnemann, D. W., 1997. Photocatalytic degradation of organic compounds: Accelerating the process efficiency. Water Science and Technology 35, 79–86.

Linsebigler, A. L., Lu, G., Yates, J. T., 1995. Photocatalysis on TiO_2 surfaces: Principles, mechanisms, and selected results. Chemical Reviews 95, 735–758.

Litter, M. I., Nov. 1999. Heterogeneous photocatalysis: Transition metal ions in photocatalytic systems. Applied Catalysis B: Environmental 23 (2-3), 89–114.

Liu, S., Lim, M., Fabris, R., Chow, C., Chiang, K., Drikas, M., Amal, R., 2008a. Removal of humic acid using TiO_2 photocatalytic process – Fractionation and molecular weight characterisation studies. Chemosphere 72, 263–271.

Liu, S., Lim, M., Fabris, R., Chow, C., Drikas, M., Amal, R., 2008b. TiO_2 photocatalysis of natural organic matter in surface water: Impact on trihalomethane and haloacetic acid formation potential. Environmental Science and Technology 42, 6218–6223.

Lubal, P., Siroký, D., Fetsch, D., Havel, J., 1998. The acidobasic and complexation properties of humic acids: Study of complexation of czech humic acids with metal ions. Talanta 47, 401–412.

Madden, T. H., Datye, A. K., Fulton, M., Prairie, M. R., Majumdar, S. A., Stange, B. M., 1997. Oxidation of metal-EDTA complexes by TiO_2 photocatalysis. Environmental Science and Technology 31 (12), 3475–3481.

Malato, S., Blanco, J., Alarcón, D. C., Maldonado, M. I., Fernández-Ibáñez, P., Gernjak, W., 2007. Photocatalytic decontamination and disinfection of water with solar collectors. Catalysis Today 122, 137–149.

Martyniuk, H., Wieckowska, J., 2003. Adsorption of metal ions on humic acids extracted from brown coals. Fuel Processing Technology 84 (1-3), 23–36.

Metreveli, G., 2008. Kolloidale Wechselwirkungen und kolloidgetragener Transport von Metall(oid)en in porösen Medien. Ph.D. thesis, Universität Karlsruhe (TH), Karlsruhe, Germany, (in German).

Mills, A., Belghazi, A., Rodman, D., 1996. Bromate removal from drinking water by semiconductor photocatalysis. Water Research 30, 1973–1978.

Minero, C., Pelizzetti, E., Sega, M., Friberg, S. E., Sjöblom, J., 1999. The role of humic substances in the photocatalytic degradation of water contaminants. Journal of Dispersion Science and Technology 20, 643–661.

Montgomery, D. C., 1997. Design and analysis of experiments, 5th Edition. John Wiley & Sons, Inc., New York.

Müller, M. B., 2004. Bewertung von Anreicherungs- und Fraktionierungsverfahren für die strukturelle Charakterisierung der gelösten organischen Substanz in Gewässern. Ph.D. thesis, Universität Karlsruhe (TH), Karlsruhe, Germany, (in German).

Noguchi, H., Nakajima, A., Watanabe, T., Hashimoto, K., 2002. Removal of bromate ion from water using TiO_2 and alumina-loaded TiO_2 photocatalysts. Water Science and Technology 46, 27–31.

Noguchi, H., Nakajima, A., Watanabe, T., Hashimoto, K., 2003. Design of a photocatalyst for bromate decomposition: surface modification of TiO_2 by pseudo-boehmite. Environmental Science and Technology 37, 153–157.

Ogawa, S., Tanigawa, M., Fujioka, M., Hanasaki, Y., 1995. Photocatalyzed destruction of humic acid in aqueous semiconductor suspension and diminution of its trihalomethane productivity. Japanese Journal of Toxicology and Environmental Health 41, P–7.

Oppenländer, T., 2003. Photochemical purification of water and air. Wiley VCH, Weinheim.

Palmer, F. L., Eggins, B. R., Coleman, H. M., 2002. The effect of operational parameters on the photocatalytic degradation of humic acid. Journal of Photochemistry and Photobiology A: Chemistry 148, 137–143.

Park, E., Jung, J., Chung, H., Jun. 2006. Simultaneous oxidation of EDTA and reduction of metal ions in mixed Cu(II)/Fe(III)–EDTA system by TiO2 photocatalysis. Chemosphere 64 (3), 432–436.

Petrucci, R. H., Harwood, W. S., 1993. General Chemistry. Principles & Modern Applications, 6th Edition. MacMillan, New York.

Plackett, R. L., Burman, J. P., 1946. The design of optimum multifactor experiments. Biometrika 33, 305–325.

Portjanskaja, E., Preis, S., Kallas, J., 2006. Aqueous photocatalytic oxidation of lignin and humic acids with supported TiO_2. International Journal of Photoenergy 2006 (Article ID 85927), 1–7, doi:10.1155/IJP/2006/85927.

Prado, A. G., Torres, J. D., Martins, P. C., Pertusatti, J., Bolzon, L. B., Faria, E. A., 2006. Studies on copper(II)- and zinc(II)-mixed ligand complexes of humic acid. Journal of Hazardous Materials 136 (3), 585–588.

R Development Core Team, 2007. R: A language and environment for statistical computing. R Foundation for Statistical Computing, Vienna, Austria, ISBN 3-900051-07-0.

R Development Core Team, 2008. R: A language and environment for statistical computing. R Foundation for Statistical Computing, Vienna, Austria, ISBN 3-900051-07-0.

Richardson, S., Thruston, A., Caughran, T., Chen, P., Collette, T., Floyd, T., Schenck, K., Lykins, B., Sun, G.-R., Majetich, G., 1999. Identification of new drinking water disinfection byproducts formed in the presence of bromide. Environmental Science and Technology 33, 3378–3383.

Richardson, S. D., Thruston Jr., A. D., Collette, T. W., Patterson, K. S., Lykins Jr., B. W., Ireland, J. C., 1996. Identification of TiO_2/UV disinfection byproducts in drinking water. Environmental Science and Technology 30, 3327–3334.

Riedel, E., 1990. Anorganische Chemie, 2nd Edition. de Gruyter, Berlin.

Rodriguez, F., 1996. Principles of polymer systems, 4th Edition. Taylor & Francis.

Sarathy, S. R., Mohseni, M., 2007. The impact of UV/H_2O_2 advanced oxidation on molecular size distributioin of chromophoric natural organic matter. Environmental Science and Technology 41, 8315–8320.

Saravia, F., 2009. Entfernung von organischen spurenstoffen und untersuchung von foulingprozessen in getauchten membranen und hybridverfahren. Ph.D. thesis, Universität Karlsruhe (TH), Karlsruhe.

Saravia, F., Zwiener, C., Frimmel, F. H., 2006. Interactions between membrane surface, dissolved organic matter substances and ions in submerged membrane filtration. Desalination 192, 280–287.

Selçuk, H., Sene, J. J., Sarikaya, H. Z., Bekbölet, M., Anderson, M. A., 2004. An innovative photocatalytic technology in the treatment of river water containing humic substances. Water Science and Technology 49, 153–158.

Selcuk, H., Sene, J. J., Zanoni, M. V. B., Sarikaya, H. Z., Anderson, M. A., 2004. Behavior of bromide in the photoelectrocatalytic process and bromine generation using nanoporous titanium dioxide thin-film electrodes. Chemosphere 54, 969–974.

Serway, R. A., 1996. Physics for Scientists and Engineers, 4th Edition. Saunders College Publishing, Philadelphia.

Sievers Instruments, 1999. TOC Analysegerät Modell 800/810/820 — Betriebs- und Wartungshandbuch.

Skoog, D. A., Leary, J. J., 1996. Instrumentelle Analytik: Grundlagen – Geräte - Anwendungen. Springer-Verlag, Berlin.

Specht, C. H., Frimmel, F. H., 2000. Specific interactions of organic substances in size-exclusion chromatography. Environmental Science and Technology 34, 2361–2366.

Tercero Espinoza, L. A., Frimmel, F. H., 2008. Formation of brominated products in irradiated titanium dioxide suspensions containing bromide and dissolved organic carbon. Water Research 42, 1778–1784.

Tercero Espinoza, L. A., Frimmel, F. H., 2009. A simple simulation of the degradation of natural organic matter in homogeneous and heterogeneous advanced oxidation processes. Water Research 43, 3902–3909.

Tercero Espinoza, L. A., Neamtu, M., Frimmel, F. H., 2007. The effect of nitrate, Fe(III) and bicarbonate on the degradation of bisphenol A by simulated solar UV-irradiation. Water Research 41, 4479–4487.

Tercero Espinoza, L. A., Rembor, M., Arribas Matesanz, C., Heidt, A., Frimmel, F. H., 2009a. Formation of bromoform in irradiated titanium dioxide suspensions with varying photocatalyst, dissolved organic carbon and bromide concentrations. Water Research 43, 4143–4148.

Tercero Espinoza, L. A., Rojas Malerba, R., Heidt, A., Frimmel, F. H., 2010. Influence of dissolved organic carbon source, photocatalyst identity and copper(II) ions on the formation of bromoform in irradiated titanium dioxide suspensions. Catalysis Today 151, 84–88.

Tercero Espinoza, L. A., ter Haseborg, E., Weber, M., Frimmel, F. H., 2009b. Investigation of the photocatalytic degradation of brown water natural organic matter by size exclusion chromatography. Applied Catalysis B: Environmental 87, 56–62.

Tercero Espinoza, L. A., ter Haseborg, E., Weber, M., Karle, E., Peschke, R., Frimmel, F. H., 2009c. Effect of selected metal ions on the photocatalytic degradation of bog lake water natural organic matter (submitted).

Ternes, T. A., Hirsch, R., 2000. Occurrence and behavior of X-ray contrast media in sewage facilities and the aquatic environment. Environmental Science and Technology 34, 2741–2748.

Ternes, T. A., Meisenheimer, M., McDowell, D., Sacher, F., Brauch, H.-J., Haist-Gulde, B., Preuss, G., Wilme, U., Zulei-Seibert, N., 2002. Removal of pharmaceuticals during drinking water treatment. est 36, 3855–3863.

Trevors, J., Cotter, C., 1990. Copper toxicity and uptake in microorganisms. Journal of Industrial Microbiology 6, 77–84.

Uyguner, C. S., Bekbölet, M., 2004. Photocatalytic degradation of natural organic matter: Kinetic considerations and light intensity dependence. International Journal of Photoenergy 6, 73–80.

Uyguner, C. S., Bekbölet, M., 2005. Evaluation of humic acid photocatalytic degradation by UV-vis and fluorescence spectroscopy. Catalysis Today 101, 267–274.

Uyguner, C. S., Bekbolet, M., 2007. Contribution of metal species to the heterogeneous photocatalytic degradation of natural organic matter. International Journal of Photoenergy 2007, Article ID 23156.

Van Dijk, H., 1971. Cation binding of humic acids. Geoderma 5, 53–67.

Vermeer, A. W. P., Koopal, L. K., 1998. Adsorption of humic acids to mineral particles. 2. Polydispersity effects with polyelectrolyte adsorption. Langmuir 14, 4210–4216.

Vermeer, A. W. P., van Riemsdijk, W. H., Koopal, L. K., 1998. Adsorption of humic acids to mineral particles. 1. Specific and electrostatic interactions. Langmuir 14, 2810–2819.

Vieno, N. M., Härkki, H., Tuhkanen, T., Kronberg, L., 2007. Occurrence of pharmaceuticals in river water and their elimination in a pilot-scale drinking water treatment plant. est 41, 5077–5084.

Villanueva, C. M., Kogevinasa, M., Grimalt, J. O., 2003. Haloacetic acids and trihalomethanes in finished drinking waters from heterogeneous sources. Water Research 37, 953–958.

von Gunten, U., 2003. Ozonation of drinking water: Part II. Disinfection and by-product formation in presence of bromide, iodide or chloride. Water Research 37, 1469–1487.

von Gunten, U., Oliveras, Y., 1998. Advanced oxidation of bromide-containing waters: bromate formation mechanisms. Environmental Science and Technology 32, 63–70.

Wang, G.-S., Liao, C.-H., Chen, H.-W., Yang, H.-C., 2006. Characteristics of natural organic matter degradation in water by UV/H_2O_2 treatment. Environmental Technology 27, 277–287.

Wang, N., Chen, Z., Zhu, L., Jiang, X., Lv, B., Tang, H., 2007. Synergistic effects of cupric and fluoride ions on photocatalytic degradation of phenol. Journal of Photochemistry and Photobiology A: Chemistry 191 (2-3), 193–200.

Westerhoff, P., Aiken, G., Amy, G., Debroux, J., 1999. Relationships between the structure of natural organic matter and its reactivity towards molecular ozone and hydroxyl radicals. Water Research 33, 2265–2276.

Wingender, J., Neu, T., Flemming, H.-C., 1999. What are bacterial extracellular polymeric substances? In: Wingender, J., Neu, T., Flemming, H.-C. (Eds.), Microbial extracellular polymeric substances: Characterization, structure, and function. Springer-Verlag, p. 258.

Wiszniowski, J., Robert, D., Surmacz-Gorska, J., Miksch, K., Weber, J. V., 2002. Photocatalytic decomposition of humic acids on titanium dioxide Part I: Discussion of adsorption and mechanism. Journal of Photochemistry and Photobiology A: Chemistry 152, 267–273.

Wiszniowski, J., Robert, D., Surmacz-Gorska, J., Miksch, K., Weber, J.-V., 2003. Photocatalytic mineralization of humic acids with TiO_2: Effect of pH, sulfate and chloride ions. International Journal of Photoenergy 5, 69–74.

Yoneyama, H., Torimoto, T., 2000. Titanium dioxide/adsorbent hybrid photocatalysts for photodestruction of organic substances of dilute concentrations. Catalysis Today 58, 133–140.

Zwiener, C., 2006. Trihalomethanes (THMs), haloacetic acids (HAAs), and emerging disinfection by-products in drinking water. In: Reemtsma, T., Jekel, M. (Eds.), Organic pollutants in the water cycle. Wiley-VCH, Weinheim, pp. 251–286.

List of Figures

List of Tables

Appendix A

Acronyms

AOBr	organically-bound Br adsorbable onto activated carbon
AOP	advanced oxidation process
AOX	organically-bound halogens adsorbable onto activated carbon ("adsorbable organic halogens", includes Cl, Br and I but *not* F)
BET	Brenauer-Emmet-Teller method for determining surface area
BOD_5	biological oxygen demand, measured over a 5-day period
CI	confidence interval
COD	chemical oxygen demand
DBP	disinfection by-product
DHBA	2,4-dihydroxybenzoic acid
DOC	dissolved organic carbon
EC	electrical conductivity
F1..F3	fractions 1-3
HAA	haloacetic acids
HPLC	high performance liquid chromatography
IC	in Section 3.2.1, inorganic carbon
	in Section 3.2.5, ion exchange chromatography
ICP-MS	ion coupled plasma-mass spectrometry
ISFET	ion selective field effect transistor
ME	margin of error
MW	molecular weight

NOM	natural organic matter
OC	organic carbon
pH	"hydrogen potential", a measure of acidity and basicity in dilute aqueous solutions
POC	particular organic carbon
PTFE	poly(tetraflouroethylene), Teflon
RP-HPLC	reversed-phase high performance liquid chromatography
SEC	size exclusion chromatography
SEC-DOC	size exclusion chromatography with dissolved organic carbon detection
SEC-UV	size exclusion chromatography with ultraviolet detection
SME	simultaneous margin of error
TEM	transmission electron microscopy
TOC	total organic carbon
TOX	total organic halogen
THM	trihalomethanes (sum of $CHCl_3$, $CHCl_2Br$, $CHClBr_2$ and $CHBr_3$)
THM-FP	THM formation potential
UV	ultraviolet

Appendix B

Nomenclature

B.1 Latin characters

Symbol	Meaning	Value/Units
a	linear fitting constant in Equation 5.1	
b	linear fitting constant in Equation 5.1	min^{-1}
c	in Section 2.1.1, speed of light	3×10^8 m s^{-1}
	otherwise, molar concentration	
c_{added}	molar concentration spiked into water samples	
e^-	electron	
e^-_{cb}	conduction band electron	
E	energy (e.g. of a photon)	
E_g	band gap energy	eV
h	Planck's constant	6.626×10^{-34} J s
h^+	hole	
h^+_{vb}	valence band hole	
k	number of factors in a model	
k_1	first order reaction rate constant	mol L^{-1}
k_b	Boltzmann constant	1.381×10^{-23} J K^{-1}
l	number of subshells in an electron shell (quantum number)	

Symbol	Meaning	Value/Units
m	in Section 2.5.4, median	
m_l	number of states in each subshell (quantum number)	
m_s	electron spin moment (quantum number)	$\pm\frac{1}{2}$
MW_C	molecular weight of carbon	12 Da
MW_{t_r}	apparent molecular weight at elution time t_r	Da
n	in Section 2.1.1, number of electron shells in an atom (quantum number)	
	in Section 2.5.4, number of experimental points	
	otherwise, number of repetitions for one experiment	
nC	apparent chain length (number of C atoms in chain)	
nC_{t_r}	apparent chain length (number of C atoms in chain) at elution time t_r	
n_{molec}	number of molecules	
$n_{\text{molec},nC}$	number of molecules for chain length nC	
$n_{\text{reactions},nC}$	number of reactions for chain length nC	
N	number of atoms in a solid lattice	
OC_{adsorbed}	organic carbon adsorbed onto a surface	
OC_{solution}	organic carbon in solution; $OC_{\text{solution}} \equiv \text{DOC}$	
OC_{total}	total organic carbon in the simulation	
s_0	pseudo standard error	
t	time	s
$t_{\gamma,d}$	t-score for probability level γ with d degrees of freedom	
t_{irrad}	irradiation time	min
t_r	retention time	min

Symbol	Meaning	Value/Units
T	temperature or absolute	°C or K (specified in text)
x_i	coded variable i in a linear model	

B.2 Greek symbols

Symbol	Meaning	Value/Units
β_i	coefficient i in a linear model	
γ	in Section 2.5.4, probability level	
λ	wavelength	nm
ν	frequency	s^{-1}
$\phi_{ads,nC}$	fraction of molecules adsorbed onto the surface for chain length nC	
ρ	mass concentration	mg L^{-1}
ρ_0	initial mass concentration	mg L^{-1}

Appendix C

Additional data for Chapter 5

C.1 Calibration of the size exclusion chromatography column

Table C.1: Molecular weight calibration for TSK HW 50S SEC column with selected substances.

	Sample	MW	$\log MW$	t_r / min
1	Blue Dextran	2000000	6.30	28.73
2	PEG 6000	6000	3.78	39.37
3	PEG 4000	4000	3.60	40.82
4	PEG 1550	1550	3.19	46.47
5	PEG 1000	1000	3.00	49.53
6	Raffinose	504	2.70	54.21
7	Maltose	342	2.53	56.63
8	Glucose	180	2.26	59.21
9	Glycerin	92	1.96	62.27
10	Methanol	32	1.51	67.60
11	D_2O	20	1.30	66.30

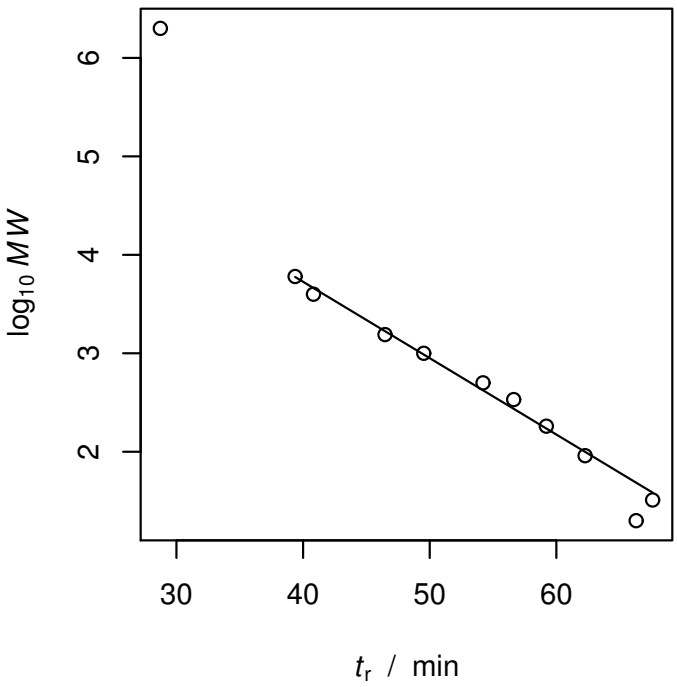

Figure C.1: Molecular weight calibration for TSK HW 50S SEC column with selected substances. Data in Table C.1.

C.2 Simulation code

All simulation code was written in the R language and environment for statistical computing (R Development Core Team, 2008).

C.2.1 Simulation setup and functions

This code is referred to by the name `setup.R` in Sections C.2.2 and C.2.3.

```
rm(list = ls())

## define "global variables"
F1 <- c(28, 45.8)
F2 <- c(45.8, 50.7)
F3 <- c(50.7, 56.5)
mean.c <- 0.45
tot.mol <- 1e6  ## number of molecules to use in simulation
```

```
## assign names to external data
smpl <- data.frame(zeit = c(0, 15, 30, 60, 1140),
                   datei = paste("0304_", 2:6, sep = ""))
smpl

################################################################
## function to read in data from external LC-DOC file
get.data <- function(which.sample,    ## must = one of the elements
                                      ## in the first column of names.df
                     names.df = smpl, ## df with two columns, one giving
                                      ## the sample name and the other
                                      ## the name of the data file
                     which.data = "O",## "O"CD, "U"V, "L"eitfaehigkeit
                     prefix = "data/"){

  which.data <- toupper(which.data)
  file.name <- paste(prefix, which.data,
                     names.df[names.df[ ,1] == which.sample, 2],
                     ".dat", sep = "")
  daten <- read.table(file = file.name, sep = "\t", header = TRUE)[, 1:2]
  return(daten)
} ## end get.data


chr0 <- get.data(0, names.df = smpl, which.data = "o")
chr0
plot(chr0, type = "l")

## substract baseline
baseline <- mean(chr0[chr0$Zeit >= 10 & chr0$Zeit <= 20, "DOC"])
baseline
chr0$DOC <- chr0$DOC - baseline

chr0 <- chr0[chr0$Zeit >= F1[1] & chr0$Zeit <= F3[2], ]
plot(chr0, type = "l")


## calibrate mw with retention time
size.cali <- data.frame(mw = c(6000, 46),
                        ret.t = c(39.37, F3[2])) ## set extremes
```

```
size.cali$log.mw <- log(size.cali$mw)
size.cali

## now calculate intermediate molecular weights
size.lm <- with(size.cali, lm(log.mw~ret.t))
chr0$logmw.calc <- predict(size.lm, data.frame(ret.t = chr0$Zeit))
chr0$mw.calc <- round(exp(chr0$logmw.calc))
chr0

## calculate an estimate number of C
## the signal is proportional to the number of C
## the number of molecules depends on the number of C per molecule
chr0$nC <- floor(chr0$mw.calc*mean.c/12)
#str(chr0)

## now scale signal according to number of C to approximate
## number of molecules
chr0$n.molec <- with(chr0, DOC/nC)
str(chr0)
chr0

## now scale to total number of molecules defined for simulation
chr0$n.molec <- round(chr0$n.molec *
                      (tot.mol / cumsum(chr0$n.molec)[nrow(chr0)]))
tot.mol <- cumsum(chr0$n.molec)[nrow(chr0)]
str(chr0)
chr0

########################
## this is to find out how many points in the chromatogram
## correspond to each nC

temp <- chr0[, c("Zeit", "nC")]
temp$count <- 1
temp <- data.frame(nr = tapply(temp$count, temp$nC, sum),
                   nC = as.numeric(names(tapply(temp$count,
                                                temp$nC, sum))))
str(temp)
with(temp, plot(nC, nr, log = "x"))
abline(h = 1:25, col = "gray")
```

```
abline(v = seq(10, 50, by = 10), col = "gray")

rm(temp)
## end nC thing
###############


## now make data frame to keep all possible number of carbons
## from 1 to c.max => ignore coupling products

chr <- data.frame(nC = 1:max(chr0$nC),
                  n.molec = numeric(max(chr0$nC)))
#str(chr)

for (i in 1:nrow(chr)){
  chr[i, "n.molec"] <- sum(chr0[which(chr0$nC == i), "n.molec"])
}

with(chr, plot(nC, n.molec*nC, log = "x"))
plot(chr0$Zeit, chr0$DOC, type = "l")

## looking better, now do binning
## how many bins?
n.bins <- 25

## first define bin sizes, let them be 1:10 C in size
## getting larger as they go
bin.cali <- data.frame(size = c(2, 625),
                       bin  = c(1, n.bins)) ## set extremes

bin.cali$log.size <- log(bin.cali$size)
bin.cali

## now calculate size of bins
bin.lm <- with(bin.cali, lm(log.size~bin))

bin.sizes <- numeric()
i <- 0
while (sum(bin.sizes) < nrow(chr)){
  bin.sizes <- round(exp(predict(bin.lm,
```

```
                              data.frame(bin = 1:(n.bins + i)))))
  i <- i + 1
  sum(bin.sizes)
}

## now add first five bins
bin.sizes <- c(rep(1, 5), bin.sizes)
bin.sizes

## now chop additional
extra <- sum(bin.sizes) - nrow(chr)
extra

bin.sizes[length(bin.sizes)] <- bin.sizes[length(bin.sizes)] - extra
if (bin.sizes[length(bin.sizes)] < 0)
   bin.sizes[length(bin.sizes)] <- 0

## now have vector of bin sizes which in sum equal length of chr
## assign a bin number to each entry in chr
## create vector of length nrow(chr) containing a bin number
temp <- numeric()
for (i in 1:length(bin.sizes)){
  temp <- c(temp, rep(i, bin.sizes[i]))
}
## add to chr
chr$bin <- temp
rm(temp)
#str(chr)
chr


#################################################################
## set up the fractions

F1.nC <- floor(exp(predict(size.lm, data.frame(ret.t = F1)))
               *mean.c/12)
F1.nC
F2.nC <- floor(exp(predict(size.lm, data.frame(ret.t = F2)))
               *mean.c/12)
F2.nC
```

```
F3.nC <- floor(exp(predict(size.lm, data.frame(ret.t = F3)))
               *mean.c/12)
F3.nC


## now prepare chr for plotting as a chromatogram
plot.chromatogram <- function(chr = NULL, main = NULL, ymax = NULL){
  chr.plot <- data.frame(nC = tapply(chr$nC, chr$bin, mean),
                         n.molec = tapply(chr$n.molec, chr$bin, sum))
  if (is.null(ymax)){
    with(chr.plot, plot(nC, n.molec*nC, log = "x", type = "n",
                        main = main))
  } else{
    with(chr.plot, plot(nC, n.molec*nC, log = "x", type = "n",
                        main = main, ylim = c(0, ymax)))
  }
  abline(v = c(F1.nC, F2.nC, F3.nC), col = "gray", lwd = 2, lty = 3)
  with(chr.plot,
       segments(x0 = nC, y0 = 0, x1 = nC, y1 = n.molec*nC, lwd = 2))
}

plot.chromatogram(chr)

write.table(file = "chr.txt", chr)


#####################################################################
##               now need code to take into account adsorption
##
#####################################################################

## first approach, calculate fraction adsorbed for every point in the
## original chromatograms

chr1 <- get.data(60, names.df = smpl, which.data = "o")
## substract baseline
baseline <- mean(chr1[chr1$Zeit >= 10 & chr1$Zeit <= 20, "DOC"])
baseline
chr1$DOC <- chr1$DOC - baseline
```

```
chr1 <- chr1[chr1$Zeit >= F1[1] & chr1$Zeit <= F3[2], ]
plot(chr0[, 1:2], type = "l")
points(chr1, type = "l")

adsorbed <- chr0 ## initialize as the original chromatogram
adsorbed$ratio <- 1 - chr1$DOC/chr0$DOC
str(adsorbed)

## now assign an "adsorbed fraction" to each nC
chr.heterog <- chr

temp <- tapply(adsorbed$ratio, adsorbed$nC, mean)
temp <- data.frame(nC = as.numeric(row.names(temp)),
                   ratio = temp)
chr.heterog$ratio <- 0

## assign ratio to corresponding nC
for (i in 1:nrow(temp)){
  chr.heterog[which(chr.heterog$nC == temp$nC[i]), "ratio"] <-
    temp$ratio[i]
}
rm(temp)

str(chr.heterog)
chr.heterog[1:5, ]
chr[1:5, ]
chr0[1:5, ]
chr0[nrow(chr0):(nrow(chr0) - 5), ]

## make sure that all nC have an adsorption ratio
for (i in 2:nrow(chr.heterog)){
  if (chr.heterog$ratio[i] == 0){
    chr.heterog$ratio[i] <- chr.heterog$ratio[i-1]
  }
}
## ratio for very small molecules seems/is too high
## it is driving mineralization too quickly
## set to 0.15 -- little lower than nC = 2..3
chr.heterog$ratio[1] <- 0.15
```

```
#########################################################
do.step.heterog <- function(chr = NULL, ## no default, need df
                            reactions.per.step = 100){
  chr$n.reactions <- 0
  sum.molec <- sum(chr$n.molec)
  ## testing if there are molecules left
  ## first, test if the whole thing is still positive
  if (sum.molec <= 0){
    cat("\nNo molecules left!\n")
    return()
  }
  ## now test if any of the bars is negative
  if (min(chr$n.molec) < 0){
    cat(paste("\nNegative n.molec in ",
              chr$nC[which(chr$n.molec == min(chr$n.molec))], "!\n"))
    return()
  }

  sum.ads.molec <- sum(chr$n.molec * chr$ratio)
  ## calculate number of reactions for each nC
  for (i in 1:nrow(chr)){
    chr$n.reactions[i] <-
      ((chr$n.molec[i]*chr$ratio[i])/sum.ads.molec)*reactions.per.step
  }

  ## adjust sum of reactions to the stipulated total number of reactions
  chr$n.reactions <-
    (chr$n.reactions * (reactions.per.step/sum(chr$n.reactions)))

  ## take care of n.reactions between 0 and 1
  for (i in 1:nrow(chr)){
    if (chr$n.reactions[i] < 1){
      chr$n.reactions[i] <-
        sample(x = c(0,1), prob = c(round(1 - chr$n.reactions[i], 2),
          round(chr$n.reactions[i], 2)), size = 1)
    }
  }

  ## now round
```

```
  chr$n.reactions <- round(chr$n.reactions)

  ## now adjust number of molecules according to reactions
  ## assume all reactions for nC = 1 lead to mineralization
  ## make sure no negative molecules appear
  if ((chr[1, "n.molec"] - chr[1, "n.reactions"]) >= 0){
    chr[1, "n.molec"] <- chr[1, "n.molec"] - chr[1, "n.reactions"]
  } else{
    chr[1, "n.molec"] <- 0
  }

  ## now for nC >= 2, perform degradation reaction
  frag1 <- 0
  frag2 <- 0
  ## loop
  for (i in 2:nrow(chr)){ ## go into each nC
    if (chr$n.reactions[i] > 0){ ## only if reaction occurs
      ## make sure not too many reactions occur
      if (chr$n.reactions[i] > chr$n.molec[i]){
        chr$n.reactions[i] <- chr$n.molec[i]
      }
      for (k in 1:chr$n.reactions[i]){ ## perform n.reactions reactions
        frag1 <- sample(1:chr$nC[i], 1) ## never 0
        frag2 <- chr$nC[i] - frag1
        chr[frag1, "n.molec"] <- chr[frag1, "n.molec"] + 1
        chr[frag2, "n.molec"] <- chr[frag2, "n.molec"] + 1
      }
      ## substract degraded molecules
      chr[i, "n.molec"] <- chr[i, "n.molec"] - chr[i, "n.reactions"]
    }
  }
  return(chr)
} ## end function


plot.doc <- function(doc.df = NULL){
  plot(doc.df$run.nr, doc.df$total,
       type = "l", ylim = c(0, max(doc.df$total)))
  points(doc.df$run.nr, doc.df$F1, type = "l", col = 2)
  points(doc.df$run.nr, doc.df$F2, type = "l", col = 3)
```

```
  points(doc.df$run.nr, doc.df$F3, type = "l", col = 4)
}


initialize.doc.heterog <- function(chr = NULL){
  doc <- data.frame(
         F1 = sum(
           chr[chr$nC <= F1.nC[1] & chr$nC >= F1.nC[2], "nC"] *
           chr[chr$nC <= F1.nC[1] & chr$nC >= F1.nC[2], "n.molec"]),
         F2 = sum(
           chr[chr$nC < F2.nC[1] & chr$nC > F2.nC[2], "nC"] *
           chr[chr$nC < F2.nC[1] & chr$nC > F2.nC[2], "n.molec"]),
         F3 = sum(
           chr[chr$nC <= F3.nC[1] & chr$nC >= F3.nC[2], "nC"] *
           chr[chr$nC <= F3.nC[1] & chr$nC >= F3.nC[2], "n.molec"]),
         total = sum(chr$nC * chr$n.molec),
         F1.ads = sum(
           chr[chr$nC <= F1.nC[1] & chr$nC >= F1.nC[2], "nC"] *
           chr[chr$nC <= F1.nC[1] & chr$nC >= F1.nC[2], "n.molec"] *
           chr[chr$nC <= F1.nC[1] & chr$nC >= F1.nC[2], "ratio"]),
         F2.ads = sum(
           chr[chr$nC < F2.nC[1] & chr$nC > F2.nC[2], "nC"] *
           chr[chr$nC < F2.nC[1] & chr$nC > F2.nC[2], "n.molec"] *
           chr[chr$nC < F2.nC[1] & chr$nC > F2.nC[2], "ratio"]),
         F3.ads = sum(
           chr[chr$nC <= F3.nC[1] & chr$nC >= F3.nC[2], "nC"] *
           chr[chr$nC <= F3.nC[1] & chr$nC >= F3.nC[2], "n.molec"] *
           chr[chr$nC <= F3.nC[1] & chr$nC >= F3.nC[2], "ratio"]),
         total.ads = sum(chr$nC * chr$n.molec * chr$ratio),
         run.nr = 0
         )
  return(doc)
}

update.doc.heterog <- function(chr = NULL, doc.df = NULL,
                               run.nr = NULL){
  old.doc <- doc.df
  new.doc <-
    c(sum(chr[chr$nC <= F1.nC[1] & chr$nC >= F1.nC[2], "nC"] *
          chr[chr$nC <= F1.nC[1] & chr$nC >= F1.nC[2], "n.molec"]),
```

```
      sum(chr[chr$nC < F2.nC[1] & chr$nC > F2.nC[2], "nC"] *
          chr[chr$nC < F2.nC[1] & chr$nC > F2.nC[2], "n.molec"]),
      sum(chr[chr$nC <= F3.nC[1] & chr$nC >= F3.nC[2], "nC"] *
          chr[chr$nC <= F3.nC[1] & chr$nC >= F3.nC[2], "n.molec"]),
      sum(chr$nC * chr$n.molec),
      sum(chr[chr$nC <= F1.nC[1] & chr$nC >= F1.nC[2], "nC"] *
          chr[chr$nC <= F1.nC[1] & chr$nC >= F1.nC[2], "n.molec"] *
          chr[chr$nC <= F1.nC[1] & chr$nC >= F1.nC[2], "ratio"]),
      sum(chr[chr$nC < F2.nC[1] & chr$nC > F2.nC[2], "nC"] *
          chr[chr$nC < F2.nC[1] & chr$nC > F2.nC[2], "n.molec"] *
          chr[chr$nC < F2.nC[1] & chr$nC > F2.nC[2], "ratio"]),
      sum(chr[chr$nC <= F3.nC[1] & chr$nC >= F3.nC[2], "nC"] *
          chr[chr$nC <= F3.nC[1] & chr$nC >= F3.nC[2], "n.molec"] *
          chr[chr$nC <= F3.nC[1] & chr$nC >= F3.nC[2], "ratio"]),
      sum(chr$nC * chr$n.molec * chr$ratio),
      run.nr)
  doc.df <- rbind(old.doc, new.doc)
  return(doc.df)
}


plot.doc.heterog <- function(doc.df = NULL){
  plot(doc.df$total  - doc.df$total.ads ,
       type = "l", ylim = c(0, max(doc.df$total)))
  points(doc.df$F1 - doc.df$F1.ads, type = "l", col = 2)
  points(doc.df$F2 - doc.df$F2.ads, type = "l", col = 3)
  points(doc.df$F3 - doc.df$F3.ads, type = "l", col = 4)
}


## plot number of reactions for each bin
plot.rxns <- function(chr = NULL,
                      main = "Reactions per bin",
                      ymax = NULL){
  rxns.plot <-
    data.frame(nC = tapply(chr$nC, chr$bin, mean),
               n.rxns = tapply(chr$n.reactions, chr$bin, sum))
  if (is.null(ymax)){
    with(rxns.plot, plot(nC, n.rxns, log = "xy", type = "h", lwd = 2,
                         main = main))
```

```
  } else{
    with(rxns.plot, plot(nC, n.rxns, log = "xy", type = "h", lwd = 2,
                         main = main, ylim = c(0, ymax)))
  }
  abline(v = c(F1.nC, F2.nC, F3.nC), col = "gray", lwd = 2, lty = 3)
}


## plot number of molecules for each bin
plot.molec <- function(chr = NULL,
                       main = "Molecules per bin",
                       ymax = NULL){
  molec.plot <- data.frame(nC = tapply(chr$nC, chr$bin, mean),
                           n.molec = tapply(chr$n.molec, chr$bin, sum))
  if (is.null(ymax)){
    with(molec.plot, plot(nC, n.molec, log = "xy", type = "h", lwd = 2,
                          main = main))
  } else{
    with(molec.plot, plot(nC, n.molec, log = "xy", type = "h", lwd = 2,
                         main = main, ylim = c(0, ymax)))
  }
  abline(v = c(F1.nC, F2.nC, F3.nC), col = "gray", lwd = 2, lty = 3)
}


## plot number of molecules for each bin
plot.molec.heterog <- function(chr = NULL, main = "Molecules per bin (ads)",
                               ymax = NULL){

  molec.plot <- data.frame(nC = tapply(chr$nC, chr$bin, mean),
                  n.molec = tapply(chr$n.molec, chr$bin, sum),
                  ratio = tapply(chr$ratio, chr$bin, mean))
  if (is.null(ymax)){
    with(molec.plot, plot(nC, n.molec, log = "xy", type = "h",
                          lwd = 2, main = main))
  } else{
    with(molec.plot, plot(nC, n.molec, log = "xy", type = "h",
                          lwd = 2, main = main, ylim = c(0, ymax)))
  }
  abline(v = c(F1.nC, F2.nC, F3.nC), col = "gray", lwd = 2, lty = 3)
```

```
  ## add bars for the fraction of adsorbed molecules
  with(molec.plot,
       points(nC, round(n.molec*ratio), type = "h", lwd = 2,
              col = 2))
}
```

C.2.2 Running the homogeneous case

```
rm(list = ls())
source("setup.R")

pretext <- "simul/heterog-1e6-1e4-s100/"
write.table(file = paste(pretext, "step0.txt", sep = ""),
            chr.heterog)
doc <- initialize.doc.heterog(chr = chr.heterog)
doc.plot <- doc

## set adsorbed amount to 100% (equivalent to homogeneous reaction)
chr.heterog$ratio <- 1
str(chr.heterog)

## export adsorbed amount
write.table(file = paste(pretext, "adsorbed.txt", sep = ""),
            chr.heterog[, c(1,4)])

plot(chr.heterog[, c(1,4)], log = "x")


layout(matrix(1:8, ncol = 4, byrow = TRUE)) ## for follow up
## initial view
plot.chromatogram(chr = chr.heterog)
plot(1,1, type = "n") ## placeholder for molecules plot later
plot(1,1, type = "n") ## placeholder for rxns plot later
plot.doc.heterog(doc.df = doc.plot)

## start loop
for (i in 1:10000){
  if (sum(chr.heterog$n.molec) <= 0){
```

```
    cat("\nNo molecules left!\n")
    break
  }
  chr.heterog <- do.step.heterog(chr = chr.heterog,
                                 reactions.per.step = 10000)
  cat("step ", i, "\n")
  print(chr.heterog[1:5, ])
  print(chr.heterog[(nrow(chr.heterog)-5):nrow(chr.heterog), ])
  cat(sum(chr.heterog$n.reactions), "reactions this step\n\n")

  ## follow up
  if (i <= 25){
      plot.chromatogram(chr = chr.heterog, main = paste("step ", i))
      plot.molec.heterog(chr = chr.heterog)
      plot.rxns(chr = chr.heterog)
      doc.plot <- update.doc.heterog(chr = chr.heterog,
                                     doc.df = doc.plot,
                                     run.nr = i)
      ##      plot.doc.heterog(doc.df = doc.plot)
      plot.doc(doc.df = doc.plot)
  } else{
    if (i %% 10 == 0){ ## update every 10th step
      plot.chromatogram(chr = chr.heterog, main = paste("step ", i))
      plot.rxns(chr = chr.heterog)
      doc.plot <- update.doc.heterog(chr = chr.heterog,
                                     doc.df = doc.plot,
                                     run.nr = i)
#      plot.doc.heterog(doc.df = doc.plot)
      plot.doc(doc.df = doc.plot)
    }
  }
  #print(doc.plot)

  ## export and save information
  if (i %% 100 == 0){ ## save every 100th step
    write.table(file = paste(pretext, "step", i, ".txt", sep = ""),
                chr.heterog[, 1:3])
  }

  ## print out doc table
```

```
  if (i %% 100 == 0){ ## update every 100th step
    doc <- update.doc.heterog(chr = chr.heterog,
                              doc.df = doc,
                              run.nr = i)
    write.table(file = paste(pretext, "doc.txt", sep = ""), doc)
  }

}
```

C.2.3 Running the heterogeneous case

```
rm(list = ls())
source("setup.R")

pretext <- "simul/heterog-1e6-1e4/"
write.table(file = paste(pretext, "step0.txt", sep = ""),
                          chr.heterog)
doc <- initialize.doc.heterog(chr = chr.heterog)
doc.plot <- doc

## using adsorbed amounts from the LC-DOC chromatograms

## export adsorbed amount
write.table(file = paste(pretext, "adsorbed.txt", sep = ""),
            chr.heterog[, c(1,4)])

plot(chr.heterog[, c(1,4)], log = "x")


layout(matrix(1:8, ncol = 4, byrow = TRUE)) ## for follow up
## initial view
plot.chromatogram(chr = chr.heterog)
plot(1,1, type = "n") ## placeholder for molecules plot later
plot(1,1, type = "n") ## placeholder for rxns plot later
plot.doc.heterog(doc.df = doc.plot)

## start loop
for (i in 1:10000){
  if (sum(chr.heterog$n.molec) <= 0){
```

```
    cat("\nNo molecules left!\n")
    break
  }
  chr.heterog <- do.step.heterog(chr = chr.heterog,
                                 reactions.per.step = 10000)
  cat("step ", i, "\n")
  print(chr.heterog[1:5, ])
  cat(sum(chr.heterog$n.reactions), "reactions this step\n\n")

  ## follow up
  if (i <= 25){
      plot.chromatogram(chr = chr.heterog, main = paste("step ", i))
      plot.molec.heterog(chr = chr.heterog)
      plot.rxns(chr = chr.heterog)
      doc.plot <- update.doc.heterog(chr = chr.heterog,
                                     doc.df = doc.plot,
                                     run.nr = i)
      ##      plot.doc.heterog(doc.df = doc.plot)
      plot.doc(doc.df = doc.plot)
  } else{
    if (i %% 10 == 0){ ## update every 10th step
      plot.chromatogram(chr = chr.heterog, main = paste("step ", i))
      plot.molec.heterog(chr = chr.heterog)
      plot.rxns(chr = chr.heterog)
      doc.plot <- update.doc.heterog(chr = chr.heterog,
                                     doc.df = doc.plot,
                                     run.nr = i)
#      plot.doc.heterog(doc.df = doc.plot)
      plot.doc(doc.df = doc.plot)
    }
  }
  #print(doc.plot)

  ## export and save information
  if (i %% 50 == 0){ ## save every XXth step
    ## chromatogram
    write.table(file = paste(pretext, "step", i,
                             ".txt", sep = ""),
                chr.heterog[, 1:3])
    ## DOC
```

```
    doc <- update.doc.heterog(chr = chr.heterog,
                              doc.df = doc,
                              run.nr = i)
    write.table(file = paste(pretext, "doc.txt", sep = ""), doc)
  }
}
```

Appendix D

Additional data for Chapter 6

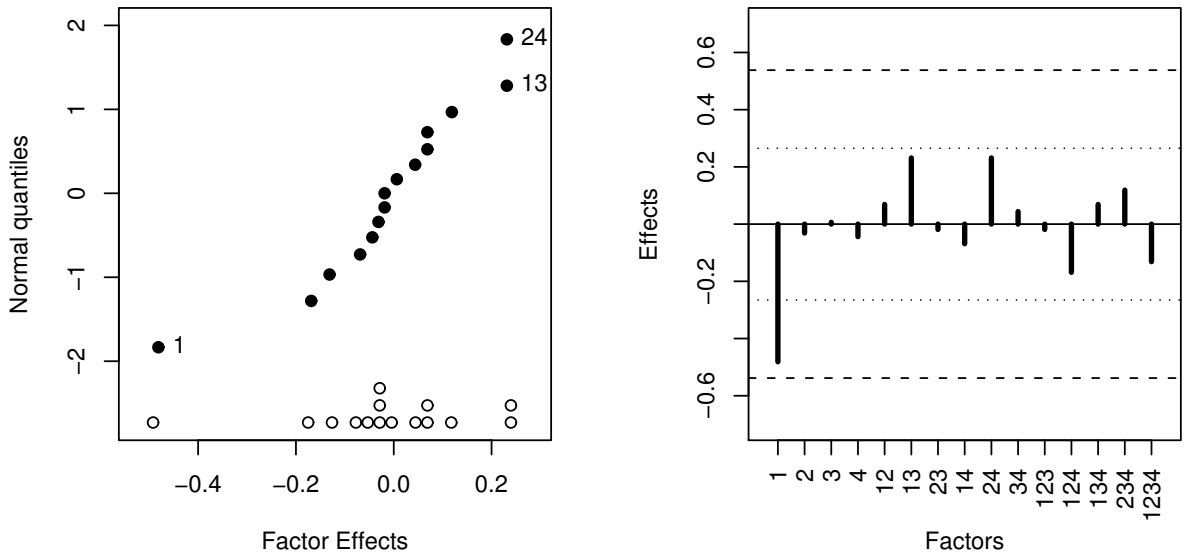

(a) Daniel plot of effects for $\rho(\mathrm{DOC})_{\mathrm{F2}}$.

(b) Corresponding Lenth plot of factor effects.

Figure D.1: Identification of important factors for the DOC content of F2 after $t_{\mathrm{irrad}} = 30$ min. The identifiers correspond to the subscripts given in Equation (6.1) and Table 3.3.

Appendix E

Additional data for Chapter 7

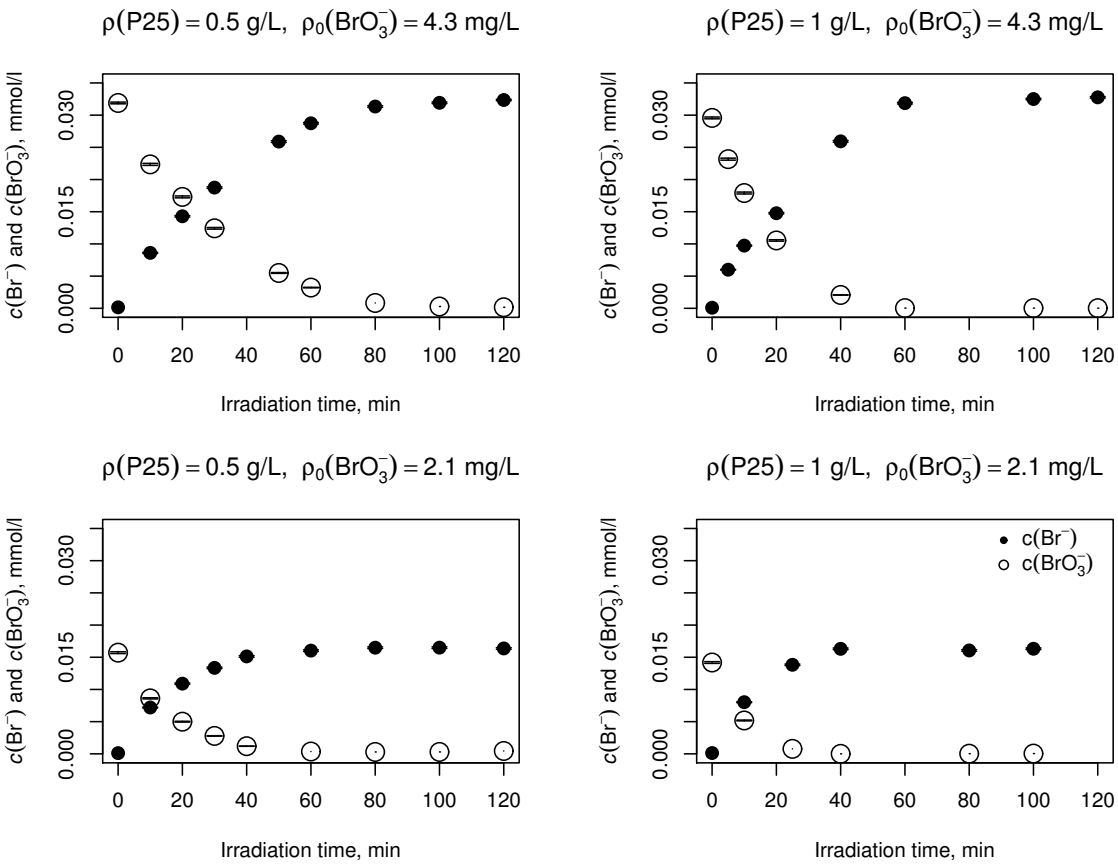

Figure E.1: Reduction of BrO_3^- to Br^- in UV-irradiated P25 suspensions.

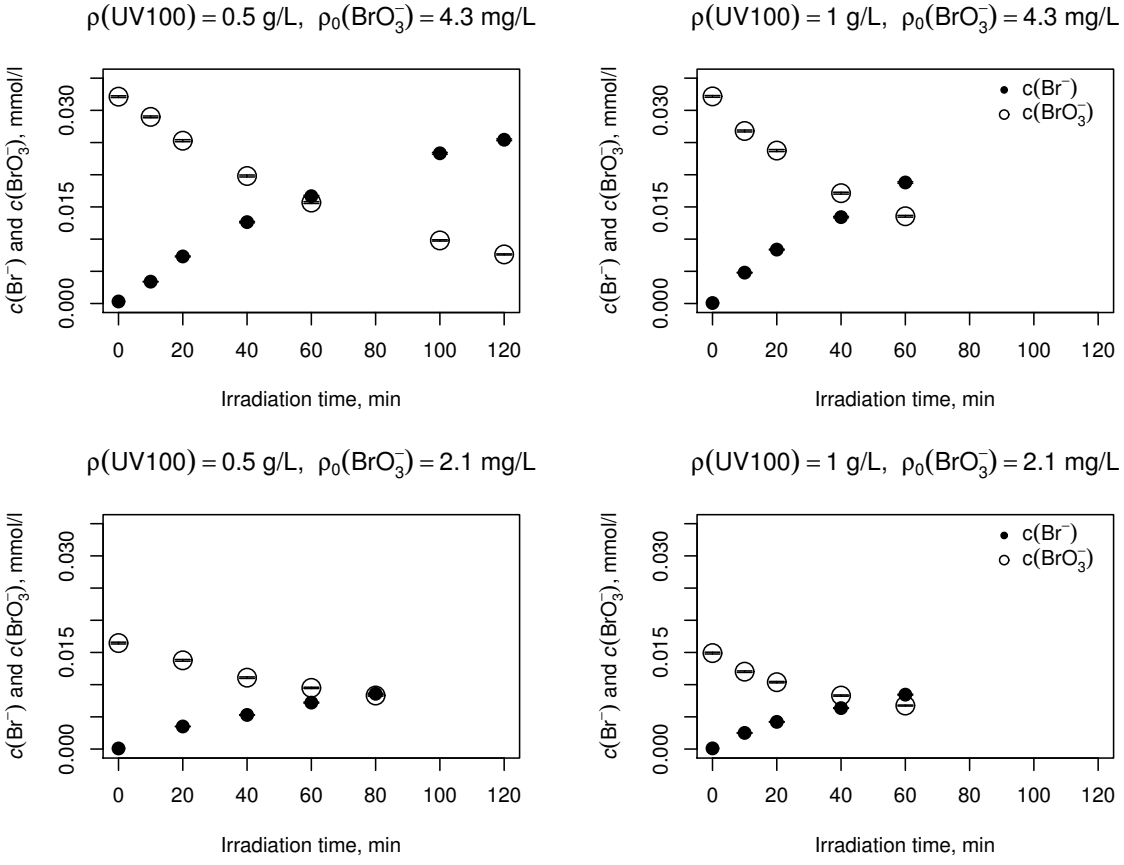

Figure E.2: Reduction of BrO_3^- to Br^- in UV-irradiated Hombikat UV100 suspensions.

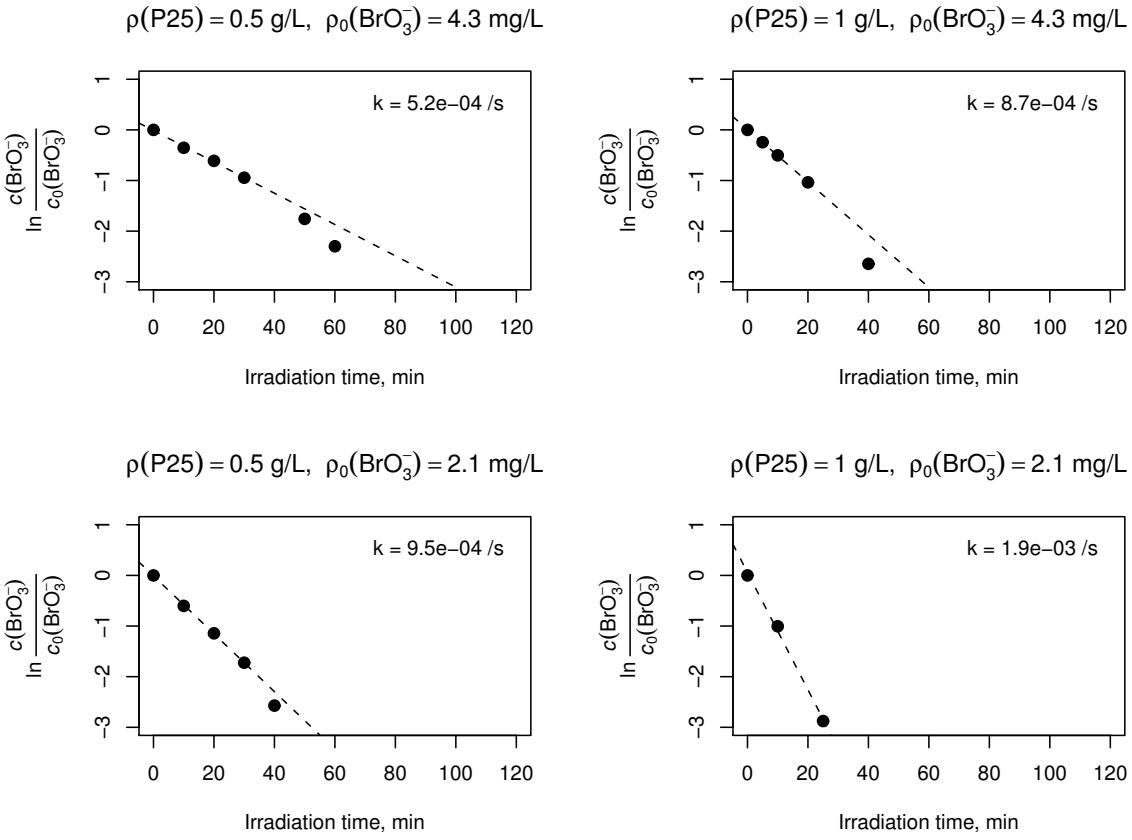

Figure E.3: Reaction rates for the reduction of BrO_3^- to Br^- in UV-irradiated P25 suspensions.

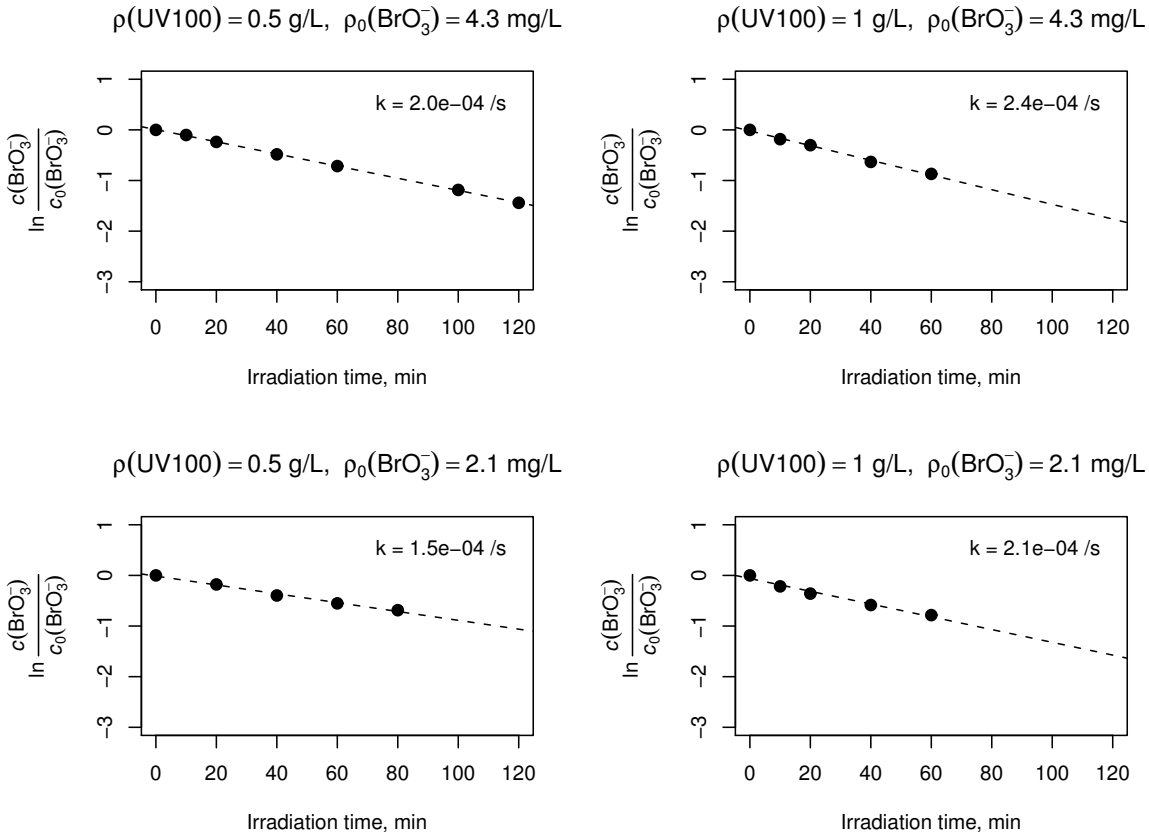

Figure E.4: Reaction rates for the reduction of BrO_3^- to Br^- in UV-irradiated Hombikat UV100 suspensions.

Publications

Many ideas, tables and figures contained in this thesis also appear in the following publications:

- **Tercero Espinoza**, L. A., Frimmel, F. H., 2008.
  Formation of brominated products in irradiated titanium dioxide suspensions containing bromide and dissolved organic carbon.
  Water Research 42, 1778–1784.
- **Tercero Espinoza**, L. A., ter Haseborg, E., Weber, M., Frimmel, F. H., 2009.
  Investigation of the photocatalytic degradation of brown water natural organic matter by size exclusion chromatography.
  Applied Catalysis B: Environmental 87, 56–62.
- **Tercero Espinoza**, L. A., Frimmel, F. H., 2009.
  A simple simulation of the degradation of natural organic matter in homogeneous and heterogeneous advanced oxidation processes.
  Water Research 43, 3902–3909.
- **Tercero Espinoza**, L. A., Rembor, M., Arribas Matesanz, C. Heidt, A., Frimmel, F. H., 2009.
  Formation of bromoform in irradiated titanium dioxide suspensions with varying photocatalyst, dissolved organic carbon and bromide concentrations.
  Water Research 43, 4143–4148.
- **Tercero Espinoza**, L. A., Rojas Malerba, R., Heidt, A., Frimmel, F. H., 2010.
  Influence of dissolved organic carbon source, photocatalyst identity and copper(II) ions on the formation of bromoform in irradiated titanium dioxide suspensions.
  Catalysis Today 151, 84–88.

- Delay, M., **Tercero Espinoza**, L. A., Metreveli, G., Frimmel, F. H., 2010
  Analytical coupling techniques to quantify nanoparticles and to characterize their interactions with water constituents
  In: Frimmel, F. H. and Niessner, R. (Eds.)
  Nanoparticles in the Water Cycle: Properties, Analysis and Environmental Relevance
  Springer-Verlag Berlin Heidelberg, S. 139-163

Other publications

- **Tercero Espinoza**, L. A., Schumann, K., Luk, Y.-Y., Israel, B., Abbott, N., 2004.
  Orientational behavior of thermotropic liquid crystals on surfaces presenting electrostatically bound vesicular stomatitis virus.
  Langmuir 20, 2375–2385.
- Docoslis, A., **Tercero Espinoza**, L. A., Zhang, B., Cheng, L.-L., Israel, B., Alexandridis, P., Abbott, N., 2007.
  Using nonuniform electric fields to accelerate the transport of viruses to surfaces from media of physiological ionic strength.
  Langmuir 23, 3840–3848.
- **Tercero Espinoza**, L. A., Neamţu, M., Frimmel, F. H., 2007.
  The effect of nitrate, Fe(III) and bicarbonate on the degradation of bisphenol A by simulated solar UV-irradiation.
  Water Research 41, 4479–4487.

Luis A. Tercero Espinoza

born 11 May 1979
in León, Nicaragua

married, one child

Education

03/1991 - 12/1995	**Bachiller en Ciencias y Letras** Colegio La Salle, León, Nicaragua *with honors*
01/1996 - 05/2000	**Bachelor of Science (Chemical Engineering)** *Summa Cum Laude*
08/1997 - 05/2000	Christian Brothers University, Memphis, Tennessee, USA
05/1999 - 07/1999	*Research Experiences for Undergraduates*, NSF Center for Advanced Engineering Fabrics and Films, Clemson University, Clemson, South Carolina, USA
01/1996 - 05/1997	University of Mobile, Latin American Branch Campus, San Marcos, Carazo, Nicaragua
08/2000 - 07/2003	**Master of Science (Chemical Engineering)** University of Wisconsin-Madison, Madison, Wisconsin, USA
04/2004 - 05/2010	**Doktor der Ingenieurwissenschaften (Dr.-Ing.)** Lehrstuhl für Wasserchemie, Fakultät für Chemieingenieurwesen und Verfahrenstechnik, Universität Karlsruhe (TH) *Scholarship in the DFG Research Training Group 366*

Selected Awards

2000	The Outstanding School of Engineering Graduate Award, Christian Brothers University, Memphis, Tennessee, USA
2008	Malcolm Award of the International Humic Substances Society, Moscow-St. Petersburg, Russia
2008	"Wissenschaft verstehen" (2nd place), Leipzig, Germany

Certificates

1998 - 1999	*Engineering Futures* Workshop Series – People Skills, Team Building, Analytical Problem Solving. Hosted by Tau Beta Pi National Honor Engineering Society, USA
06/2000	*Engineer Intern*, Tennessee Board of Architectural and Engineering Examiners, USA
07/2002 - 08/2002	*Current Techniques in Protein and Genetic Engineering*, BioPharmaceutical Technology Center Institute, Promega Corporation, Madison, Wisconsin, USA
08/2003 - 11/2003	*German courses*, Goethe Institut, Mannheim, Germany
11/2003	*Zentrale Mittelstufenprüfung*, Mannheim, Germany

Languages

Spanish	Mother tongue
English	fluent
German	fluent

Schriftenreihe des Lehrstuhls für Wasserchemie
und der DVGW-Forschungsstelle am Engler-Bunte-Institut
des Karlsruher Instituts für Technologie (KIT)

Band 35: Symposium on Refractory Organic Substances in the Environment – ROSE, 1997, 248 S., 12,80 €.

Band 36: Symposium on Refractory Organic Substances in the Environment – ROSE II, 2000, 265 S., 12,80 €.

Band 37: Thomas Brinkmann: Alkalischer und solarinduzierter Abbau von natürlicher organischer Materie, 2003, 212 S., 15,00 €.

Band 38: Andreas Gorenflo: Rückhalt und Fouling von natürlichen organischen Substanzen bei der Nano- und Ultrafiltration, 2003, 219 S., 18,00 €.

Band 39: Philip Hörsch: Einfluss der chemischen Oxidation auf das toxische Potenzial und das biologische Abbauverhalten von Industrieabwässern, 2004, 210 S., 20,00 €.

Band 40: Margit B. Müller: Bewertung von Anreicherungs- und Fraktionierungsverfahren für die strukturelle Charakterisierung der gelösten organischen Substanz in Gewässern, 2004, 185 S., 18,00 €.

Band 41: Fritz H. Frimmel, Gudrun Abbt-Braun: Praktikum Allgemeine Chemie und Chemie in wässrigen Lösungen – Qualitative und quantitative Bestimmungen, 2004, 158 S., 18,00 €.

Band 42: Tusnelda E. Doll: Photochemischer und photokatalytischer Abbau von Carbamazepin, Clofibrinsäure, Iomeprol und Iopromid, 2004, 158 S., 18,00 €.

Band 43: Ayşe B. Değer: Entfernung von organischen Schadstoffen aus Wasser mit Hilfe von Poly(ϵ-caprolacton), 2005, 205 S., 18,00 €.

Band 44: Fritz H. Frimmel, Gudrun Abbt-Braun: Wassertechnologisches und wasserchemisches Praktikum, 2005, 201 S., 20,00 €.

Band 45-I, 45-II: Fritz H. Frimmel, Gudrun Abbt-Braun (Eds.): Humic Substances – Linking Structure to Functions. Proceedings of the 13th Meeting of the International Humic Substances Society, July 30 to August 4, 2006, Universität Karlsruhe, 2006, 492 S. (45-I), 623 S. (45-II), 50,00 €.

Band 46: Fritz H. Frimmel, Gudrun Abbt-Braun: Praktikum Allgemeine Chemie und Chemie in wässrigen Lösungen – Qualitative und quantitative Bestimmungen II, 2. verbesserte und ergänzte Neuauflage 2007, 139 S., 20,00 €.

Band 47: Thomas Glauner: Aufbereitung von Schwimmbeckenwasser – Bildung und Nachweis von Desinfektionsnebenprodukten und ihre Minimierung mit Membran- und Oxidationsverfahren, 2007, 233 S., 20,00 €.

Band 48: George Metreveli: Kolloidale Wechselwirkungen und kolloidgetragener Transport von Metall(oid)en in porösen Medien, 2008, 215 S., 20,00 €.

Band 49: Florencia Saravia: Entfernung von organischen Spurenstoffen und Untersuchung von Foulingprozessen in getauchten Membranen und Hybridverfahren, 2009, 213 S., 20,00 €.

Band 50: Markus Delay: Dynamische versus statische Elutionsversuche – Ein Beitrag zur Beurteilung der Wiederverwertbarkeit von Abfallmaterialien, 2010, 206 S., 20 €.

Band 51: Luis A. Tercero Espinoza: Heterogeneous photocatalysis with titanium dioxide suspensions containing bromide and dissolved organic carbon, 2010, 172 S., 20,00 €.

Preise verstehen sich zzgl. der gesetzlichen Mehrwertsteuer und Versandkosten.

Bestellungen über:
Lehrstuhl für Wasserchemie und DVGW-Forschungsstelle
am Engler-Bunte-Institut des Karlsruher Instituts für Technologie (KIT)
Engler-Bunte-Ring 1
D-76131 Karlsruhe
Tel.: +49-(0)721-608-2580
Fax: +49-(0)721-699154
E-mail: fritz.frimmel@kit.edu